THESIS

# THE ROLE OF CACNβ4 IN ZEBRAFISH DEVELOPMENT

Submitted by

Cory Jean Harrell

Department of Biology

In partial fulfillment of the requirements

For the Degree of Master of Science

Colorado State University

Fort Collins, Colorado

Fall 2010

Master's Committee:

Department Head: Daniel Bush

Advisor: Deborah Garrity

Donald Mykles

Jennifer DeLuca

ABSTRACT OF THESIS

THE ROLE OF CACNβ4 IN ZEBRAFISH DEVELOPMENT

The calcium channel β4 subunit (CACNβ4) is an intracellular auxiliary protein of voltage–gated calcium channels. It is a member of the membrane-associated guanylate kinase (MAGUK) family of proteins. Mutations in the CACNβ4 subunit are associated with ataxia and seizures in mice and with epilepsy in humans. Since known mutant alleles of CACNβ4 are not embryonic lethal in mammals, the developmental functions of the protein are unclear. The best characterized role for the β4 subunit is to facilitate the translocation of the calcium channel α subunit to the plasma membrane and the modulation of the channel gating. Recently, additional roles have been proposed for the β subunits including facilitation of vesicle docking, attenuation of gene silencing and transcriptional regulation of calcium channel turnover. In studying the functional roles of the CACNβ4 gene, we unexpectedly discovered that targeted knockdown of CACNβ4 genes in zebrafish led to arrest or delay of epiboly and the subsequent death of the early embryo. Embryonic death can be rescued by co-injection with full-length RNA of human CACNβ4 (homologue). In this study we investigated the sub-cellular localization and critical domains of the β4 proteins. Upon injection of a construct with GFP-tagged β4 gene under the control of the β-actin promoter we observed that the β4 protein is present in the nucleus in higher concentrations than in the rest of the cell. We determined via

rescue experiments with truncated RNA constructs that the N-terminus and the chromoshadow binding element (CBE) are necessary for CACNβ4's function during gastrulation. Our findings suggest that CACNβ4 has a nuclear role, potentially interacting with chromobox family proteins, which is necessary for early zebrafish development.

# ACKNOWLEDGMENTS

I would like to acknowledge my advisor, Deborah Garrity for all of her advice and help with my research and writing. I want to give special thanks to Lindsay Parrie and Yelena Chernyavskaya for all their help, advice and friendship during my two years in the lab. Thanks also to the other members of the Garrity lab including undergraduates, fish room technicians, rotational graduate students and lab volunteers. I want to also acknowledge Eric Wong and Robert Stearman for their critique on my thesis. I would also like to thank Don Mykles and Jennifer DeLuca for being on my graduate committee.

TABLE OF CONTENTS

# Chapter 1: Literature Review

## Literature Review

### *Zebrafish as a Model Organism*

The zebrafish (*Danio rerio*) is a small, freshwater teleost naturally found in warm waters of India that has become an increasingly popular model organism for studying development (Figure 1.1). Charles Kimmel and George Streisinger from the University of Oregon realized that this little fish would be an excellent organism for genetic studies because of its many appealing experimental attributes. Zebrafish have external fertilization, which makes it possible to study early stages of embryonic development, often in live animals, without having to sacrifice the mother. The embryos are transparent until formation of melanocytes at 24 hours post fertilization (hpf) and have clear chorions, which is the outer keratin covering that encases the embryo and embryonic fluid, so the entire developmental process can be easily visualized without manipulating the eggs (Figure 1.2). *Danio rerio* are easy to keep, because as adults they only reach one to two inches long, so many adults can be kept in a small area. Breeding zebrafish is simple, and they can breed a couple times in a week. Each mated female can produce up to 300 eggs per female. Many eggs per clutch allows for consistent data, and enough embryos to produce a significant n value for experiments. The zebrafish develop very quickly, becoming reproductively mature by three months. Many of the genes that regulate the developmental process are conserved throughout vertebrate species, so using zebrafish is a cheaper paradigm for the study of genes that also regulate human development.

**Figure 1.1: *Danio rerio* are a model organism in developmental biology.** These are wild-type WIK line of zebrafish. The male is pictured on the left and the female is on the right. [news.stanford.edu/news/2007/october17/gifs/zebrafish_600.jpg]

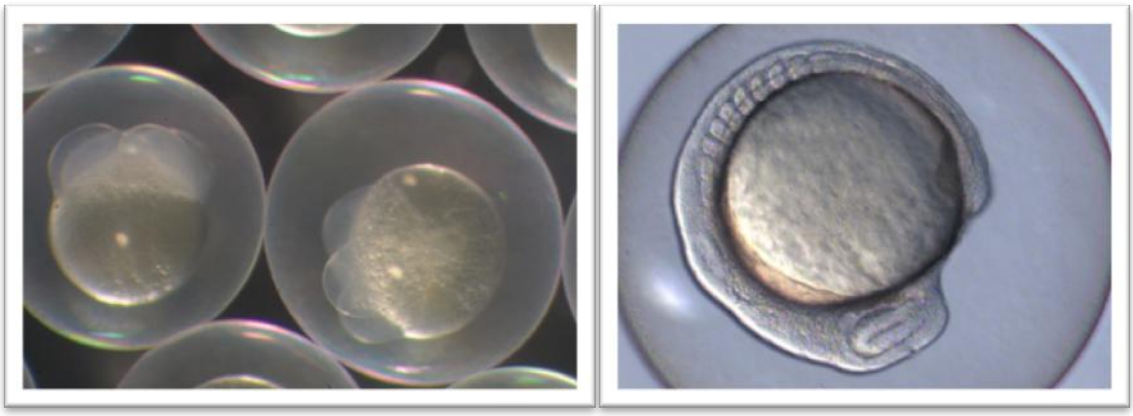

**Figure 1.2: Transparent embryos are useful for observations.** Zebrafish embryos are clear throughout early development, including during (A) cleavage (4-cell stage at 1 hpf) and (B) somitogenesis (10-somite stage at 14 hpf). [www.uq.edu.au/zebrafish/images/zebrafish-embryos-4cell.jpg; http://ihome.ust.hk/~aequorin/images/pic6.jpg]

The zebrafish are also ideal because it is possible to manipulate their genome. Unlike several other teleost species, *Danio rerio* is diploid, making genetic studies easier and applicable for Mendelian inheritance. Today, the zebrafish genome has been nearly sequenced, and many mutant and transgenic zebrafish lines exist. Consistent protocols to develop transgenic lines exist, which make use of specialized vectors and Gateway Cloning (Kwan et al., 2007). The fact that zebrafish undergo external development and the chorions are transparent also makes it straightforward to inject substances into the developing embryo. Morpholino gene knock-down is an experimentally valuable technique performed on zebrafish embryos (Sumanas and Larson, 2002). Morpholinos are synthesized antisense nucleic-acid based oligomers about 25 base pairs long that bind to and inhibit mRNA translation. Injecting the morpholino into the yolk at the 1 cell stage significantly prohibits mRNA translation of a specific gene product, leading to loss-of-function phenotypes at later stages. Early cleavage in the zebrafish embryo is meroblastic, meaning that the dividing cells do not cleave completely due to the presence of highly yolky material (Kane and Kimmel, 1993). Zebrafish blastomeres therefore remain cytoplasically connected and are considered a syncitium. Thus, morpholino injected at the 1-8 cell stage will be dispersed throughout all cells. Morpholino knockdown is an example of a reverse genetics technique, but forward genetic studies are also feasible in zebrafish. For example ENU mutagenesis, retroviral insertional mediated mutagenesis and transgene manipulation using recombinases are useful ways to gain insight into gene function.

Fluorescent analysis is another technique readily used in zebrafish embryos. Fluorescently tagged proteins or plasmids can be injected into the embryo at 1 cell or a

particular time in development to label specific cell types. Cells can be tracked over time using real time imaging. Once again, the clarity of the embryos allows for the fluorescence to be viewed in a live embryo without any invasive means. Green Fluorescent Protein (GFP) can also withstand fixation in paraformaldahyde, so fluorescent embryos can be used in other assays as well.

Zebrafish are a fantastic model for studying genes that affect heart development because they absorb sustenance from the yolk, and gases via diffusion, until they are about six days old (Yelon, 2001). This means that the fish do not need a functioning heart during the first week of development so loss of a gene resulting in a heart defect can be studied without the embryo dying. The genetic studies collectively demonstrate that a variety of gene products, including *casanova*, *bonnie and clyde*, *gata5*, *one-eyed pinhead*, *hand2*, *miles apart*, *heart and soul* and many others are essential for normal morphology, rhythm or contractility in the embryonic heart (Yelon, 2001).

Studying zebrafish development can contribute to understanding of development in other vertebrates. Like heart development, many of the genes that control the first cell movements within a developing embryo are conserved between the zebrafish and human genomes (Yelon, 2001). Gastrulation is the process during early development where the three primary germ layers that compose a vertebrate organism are established via several highly regulated processes (Gilbert and Sarkar, 2000). Understanding the genes involved in these processes gives insight into human early development.

*Voltage Dependant Calcium Channels*

Voltage-dependant calcium channels (VDCCs) are voltage gated ion channels that modulate calcium flux in excitable cells such as nerve and muscle cells(Obermair et al., 2008). These channels modulate cellular responses such as cell excitability, muscle contraction, neuronal transmission and hormonal release. Mutations in the genes that comprise these channels cause a variety of problems related to nerve and muscle function, such as cardiomyopathy, muscular dysgenesis, ataxia, epilepsy, neuropathy, and paralysis. Five main types of VDCCs have been identified: N-type, R-type, P/Q-type, T-type and L-type (Catterall, 2000; Dunlap et al., 1995). N-type calcium channels are found in neuronal cells and are sensitive to conotoxin. R-type and P/Q type channels are found in cerebral granule cells in the brain, involved in poorly understood processes in the brain. R-type channels are resistant to blockers and toxins that affect the other calcium channels. P/Q type channels are sensitive to agatoxin. T-type channels are transient channels found in neurons, bone and pacemaker cells of the heart. L-type calcium channels, named for their long length of activation, are found in skeletal, cardiac and smooth muscle cells, as well as endocrine cells involved in hormone regulation. L-type calcium channels are sensitive to dihydropyridines (hence they are also termed dihydropyridine or DHP receptors) and they also play important roles in pace-making and contractility in the heart, neuronal conduction in the CNS and retinal function in the eye (Obermair et al., 2008).

In smooth muscles, physical stretching, G-protein coupled activation, or neurotransmitter binding can trigger the opening of L-type calcium channels in the membrane. The entry of calcium through the channel leads to increased calcium

concentration inside the cell. Calcium binds calmodulin, which phosphorylates the myosin thick filaments to allow contraction (Dai et al., 2009; Obermair et al., 2008). In skeletal and cardiac muscle VDCCs are very important for excitation-contraction (EC) coupling, as they allow entry of calcium ions as signaling messengers to convert an electrical stimulus into a mechanical reaction (Obermair et al., 2008). In skeletal cells, the L-type channel acts as a voltage sensor. Acetylcholine binding to nicotinic ion channels triggers an action potential that propagates across the membrane, leading to a depolarizing change in membrane potential. Upon membrane depolarization, the dihydropyridine receptor opens, allowing a modest calcium influx which in turn leads to activation (and opening) of the ryanodine receptor on the surface of the sarcoplasmic reticulum. Opening of the ryanodine receptor releases large amounts of calcium from internal stores, leading to a great increase in the cytosolic calcium. Intracellular calcium ions then binds troponin C and triggers muscle contraction (SANDOW, 1952). The ryanodine receptors are mechanically linked to dihdryopyridine receptors in regularly arranged triads, and this structural connection appears to be essential for EC coupling (Franzini-Armstrong et al., 1998). In cardiac muscle, the L-type calcium channel is not physically connected to the ryanodine receptor, and they are not arranged in triads. In cardiac EC coupling, calcium influx through the L-type channel is required for sarcoplasmic calcium release. Pacemaker cells stimulate cardiac action potentials, which are longer than in skeletal muscle and contain a plateau phase during which the calcium channels open. Increase in the cytosolic calcium triggers ryanodine release, calcium binding to troponin C and muscle contraction (SANDOW, 1952).

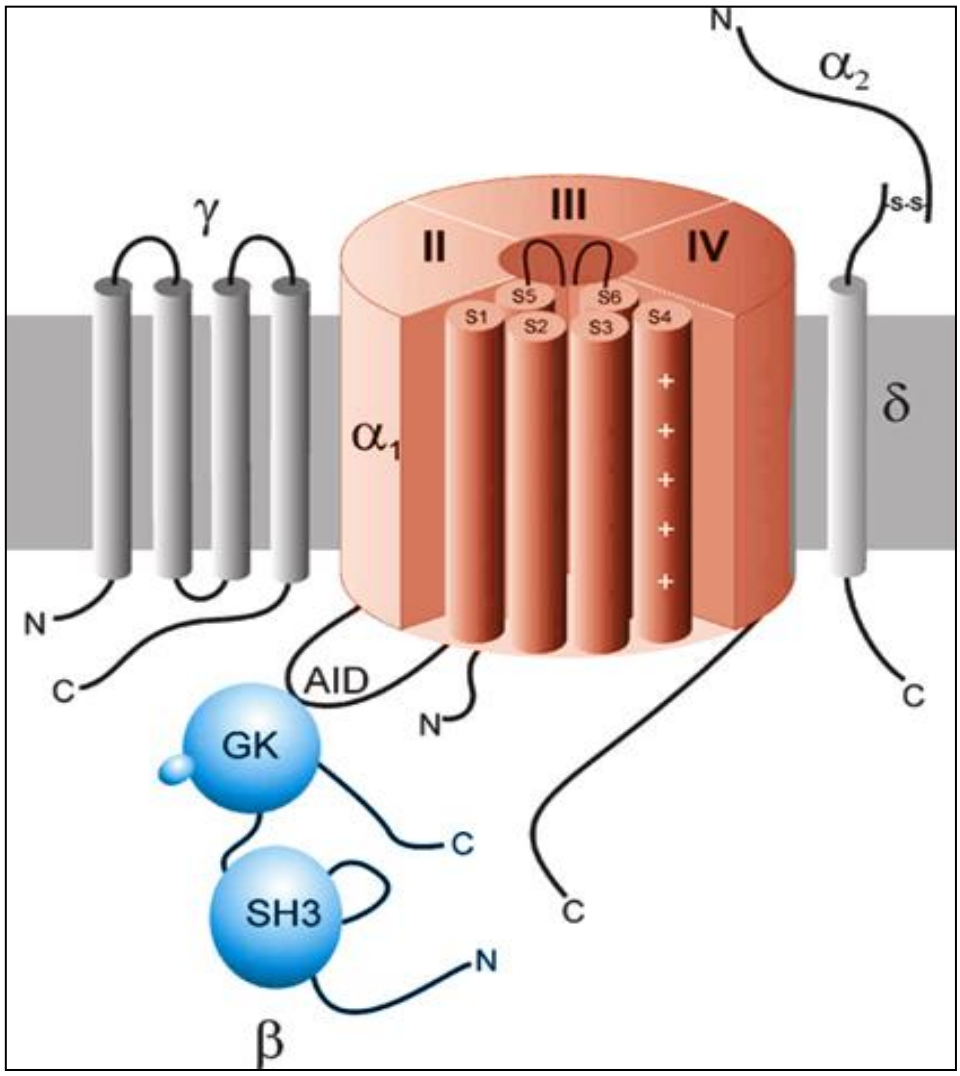


**Figure 1.3: The structural components of VDCCs are defined.** VDCCs contain a pore forming α subunit and β, α2δ and γ auxiliary subunits. The β subunit is entirely cytoplasmic. The β subunit contains conserved SH3 and GK sequences, and interacts with the α subunit via an alpha interacting domain (AID) sequence within the GK domain. [Jeziorski and Greenberg, 2006]

VDCCs are comprised of a pore forming α1 subunit and auxiliary α2δ, β and γ subunits (Figure 1.3 (Jeziorski and Greenberg, 2006)). The α1 subunit contains the voltage sensor, the channel pore and important drug binding sites (Obermair et al., 2008). The α2δ subunit is encoded from a single gene but subsequently cleaved into two peptides that remain associated via disulfide bonds. The mammalian genome encodes four different α2δ genes that have distinct tissue association. Eight different γ genes exist in mammals and these are not required for channel function and are also associated with AMPA glutamate receptors (Dolphin, 2006). The β subunits are the only entirely cytoplasmic calcium channel protein and are responsible for membrane trafficking of the α1 subunit from the Golgi to the plasma membrane, and regulation of the electrophysiological properties of the channel (Castellano et al., 1993). The four mammalian β genes are all members of the membrane associated guanylate kinase (MAGUK) family and contain five modular domains denoted A-E (Figure 1.4). Domains B and D, respectively, are two highly conserved protein domains; the src homology 3 (SH3) adaptor domain and the guanylate kinase-like (GK) domain. Within the GK domain is a region termed the beta interaction domain (BID) where the β subunit binds the α1 subunit (Dolphin, 2003). The SH3 and GK domains are separated by a variable linker HOOK domain that contains a short chromoshadow binding element domain, a sequence recognized by heterochromatin proteins (Ruddock-D'Cruz et al., 2008).

Diseases caused by mutations in L-type calcium channel alpha subunit genes include hypokalemic periodic paralysis, malignant hypothermia, Timothy syndrome, Long QT syndrome and night blindness. These phenotypes include ataxia, muscle weakness, cardiac dysfunction and cognitive impairment. Several mouse models have

enhanced our understanding of the functions of individual calcium channel subunits in the embryo. The mutant mice *totter, leaner, rolling* and *rocker* define four alleles of the α1A subunit and exhibit ataxia and defects in limb coordination (Doyle et al., 1997; Fletcher et al., 1996). The *ducky* mouse has a mutation in an α2δ gene and is used as a model for epilepsy (Barclay et al., 2001). The *lethargic* mouse is a mutant for the β4 gene and exhibits ataxia and seizures (Burgess et al., 1997). Examples of calcium channel mutation phenotypes exist also in the zebrafish, another popular vertebrate model organism. The *island beat* zebrafish has a mutation in the α1C subunit that causes a silent ventricle due to impaired calcium signaling (Rottbauer et al., 2001). The *relaxed* zebrafish is a β1 mutant and has defects involving EC coupling and thus cannot move its trunk muscles (Zhou et al., 2006). These animals represent the importance of L-type calcium channels and their role in excitatory cells.

*CACNβ4 subunits in zebrafish*

The function of the mammalian β genes has been examined in cultured cells and we know little about their role in embryonic development of the heart and other organs. Accordingly, we initiated a study to investigate the role of the calcium channel associated β4 subunit (CACNβ4) in zebrafish development. Like humans, the N-terminus of CACNβ4 is subject to alternative splicing to produce two full-length splice variants. Introduction of an early termination codon at the 212$^{th}$ amino acid gives rise to a third naturally occurring short splice variant (termed β4c), which does not contain the GK domain or the C-terminus (Subramanyam et al., 2009).

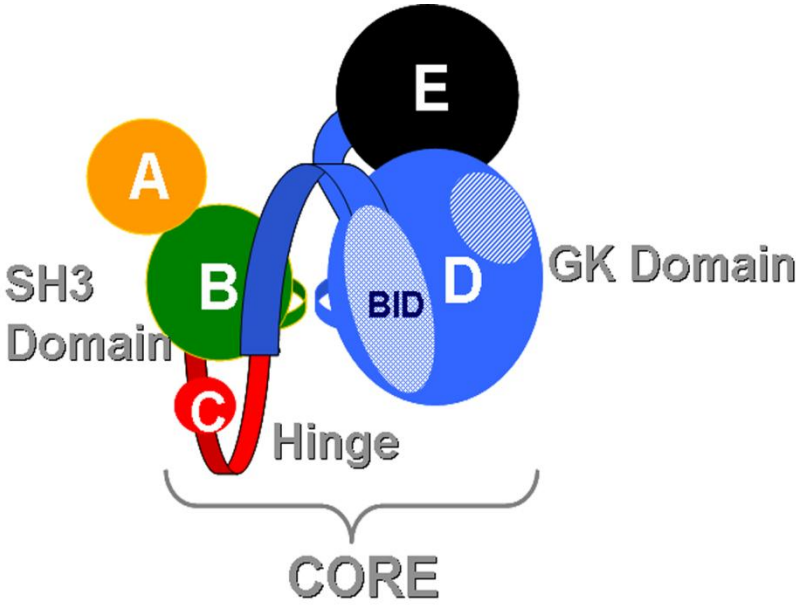


**Figure 1.4: Structural domains of β subunits are termed A-E.** 'A' is the variable N-terminus and 'E' is the C-terminus. Regions B through D make up the core sequence of the β subunits. β interaction domain (BID) is where the β subunit interacts with the alpha subunit.

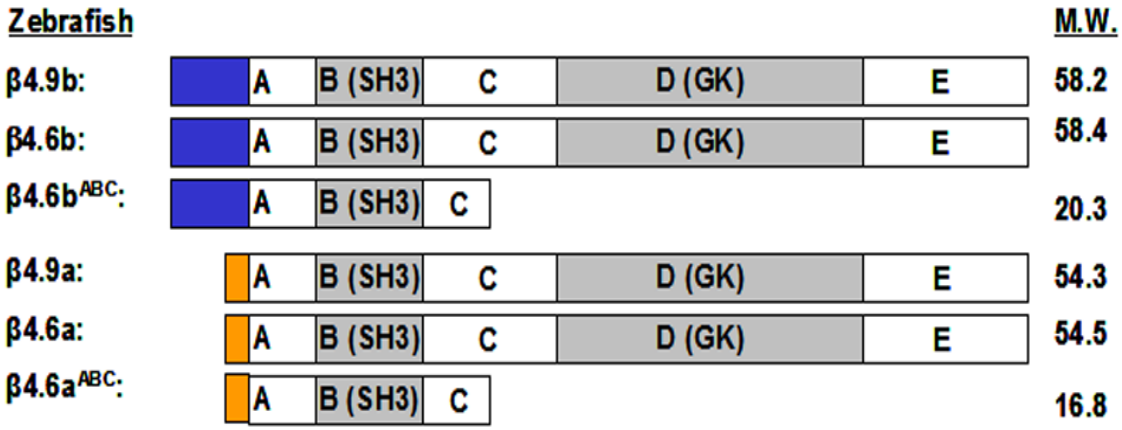


**Figure 1.5: Zebrafish genome encodes six known β4 transcripts.** CACNβ4.1 maps to chromosome 6 (β4.6) and CACNβ4.2 maps to chromosome 9 (β4.9). Both undergo alternative N-terminal splicing to produce longer 'b' variants and shorter 'a' variants. The β4.1 gene also undergoes alternative splicing to produce short transcripts (β4c) that code only for protein domains A-C. [Ebert et al., 2008]

CACNβ4 is highly conserved between humans and zebrafish. Approximately 430 million years ago, teleosts diverged from mammals in the evolutionary tree, and underwent a genomic duplication event resulting in two copies of many genes (Gu et al., 2002). Among the four mammalian β genes, at least three, β2, β3 and β4, have retained duplicate genes and therefore have two zebrafish paralogs (Zhou et al., 2008). CACNβ4.1 codes for 485 amino acids that share 94% homology with human β4 and CACNβ4.2 codes for 489 amino acids that share 88% similarity (Zhou et al., 2008). Each gene undergoes alternative N-terminal splicing to produce 'a' and 'b' variants, and CACNβ4.1 transcripts also produce a shorter 'c' variant, which is truncated within the HOOK domain (Figure 1.5 (Ebert et al., 2008a)). Both genes are expressed widely in the CNS, especially the brain and retina, from 24 to 72 hpf, with slight differences in intensity of expression. CACNβ4.2 is expressed earliest in the developing heart tube and can be detected by the 21-somite stage (19.5 hpf) (Ebert et al., 2008c). Both CACNβ4.2 and CACNβ4.1 are largely expressed in the heart at 48 hpf (Ebert et al., 2008c; Ebert et al., 2008a; Zhou et al., 2008).

Recent studies show that β proteins may exhibit a broader range of functions in the cell beyond their traditional roles involving calcium channel function. Hibino et al. (2003) showed that chick cochlear hair cells, which exhibit L-type calcium current, exclusively express the splice variant β4c (Hibino et al., 2003). Analysis of a GST pulldown and immunoprecipitation assay confirmed that β4c interacts with chromobox protein 2 (CHCB2), which recruits β4c, but not β4a, to the nucleus in transfected tsA201 cells. They used the GAL4-CAT reporter assay to determine that β4c regulates the transcriptional activity of CHCB2, via an unknown mechanism. Also, Colecraft et al.

(2002) noticed the nuclear targeting of β4-GFP fusion protein in cultured adult rat cardiac myocytes (Colecraft et al., 2002). Vendel and Horne (2006) determined via yeast two-hybrid screening that human β4a interacts with synaptotagmin 1 and microtubule associated protein 1A light chain 2 (Vendel et al., 2006). The authors suggest that via protein-protein interaction β4a could regulate cellular responses that affect calcium channels, not by directly regulating calcium flux. Subramanyam et al. (2009) reported nuclear localization of β4 in the granular cells and Purkinje cells in the cerebellar cortex of rat and mouse brains (Subramanyam et al., 2009). Researchers identified β4b as the β gene exclusively expressed in transfected myotubes. In a related topic, Gonzalez-Gutierrez (2007) showed that CACNβ2 regulates endocytic turnover of calcium channels and other membrane proteins via a dynamin-dependant process (Gonzalez-Gutierrez et al., 2007). Dynamin is a molecule that binds to microtubules and regulates stability and intracellular transport. Collectively, these findings all demonstrate that VDCC β subunits can contribute to other cellular functions in addition to their role trafficking α1 subunits to the membrane and modulating calcium flux through LTCC.

*Zebrafish Early Gastrulation*

We analyzed the function of β4 in zebrafish and discovered that these genes are required very early in development. After fertilization, the zebrafish embryo undergoes synchronous cleavage division, once about every thirty minutes. Cleavages in the zebrafish are meroblastic, meaning they do not cleave completely because of the yolk (Kane and Kimmel, 1993; Solnica-Krezel, 2006). The volume of the embryo does not

change so each round of cleavage results in more cells that are smaller, that sit on top of the yolk in a pile called the blastoderm (Figure 1.6, A (Solnica-Krezel, 2006)). After the tenth round of divisions, at 1024 cells (3.3 hpf) the cell divisions have increased the DNA to cytoplasmic ratio to a critical point that triggers the mid-blastula transition (Kane and Kimmel, 1993). The cell divisions become lengthened and asynchronous, and zygotic transcription begins. Also at this time the basal cell layer collapses and deposits the nuclei into the yolk, forming the yolk syncitial layer (YSL). After the mid-blastula transition, the blastoderm cell membranes completely surround the deep cells of the blastoderm and the enveloping layer (EVL), and only the YSL remains as a syncitium. After cell division reaches 1024 cells, the movement of epiboly begins. Epiboly is the first movement of gastrulation and it describes the spreading and rearrangement of the blastoderm cells towards the vegetal pole (Figure 1.6, B and Figure 1.7). Without β4, this first cellular movement of epiboly is not completed and the embryo does not develop.

During epiboly, cells move from the blastoderm down around the yolk until it is covered completely. Epiboly is described in terms of percentage of completion. At 50% epiboly, additional cell movements also begin to take place (Figure 1.6, B). Cells begin migrating inwards and back up towards the animal pole underneath the outer layer of cells, in a movement termed emboly (Figure 1.6, B and Figure 1.8). Cell migration allows internalization of the mesodermal and endodermal precursors (Mizoguchi et al., 2008). Convergence occurs as cells narrow mediolaterally and this movement is essential for the formation of the dorsal shield. Cells extend anterior/posteriorly towards the future head and tail. Mesodermal cells are internalized via synchronized ingression at the dorsal shield, a process requiring E-cadherin (Mizoguchi et al., 2008). The directed cell

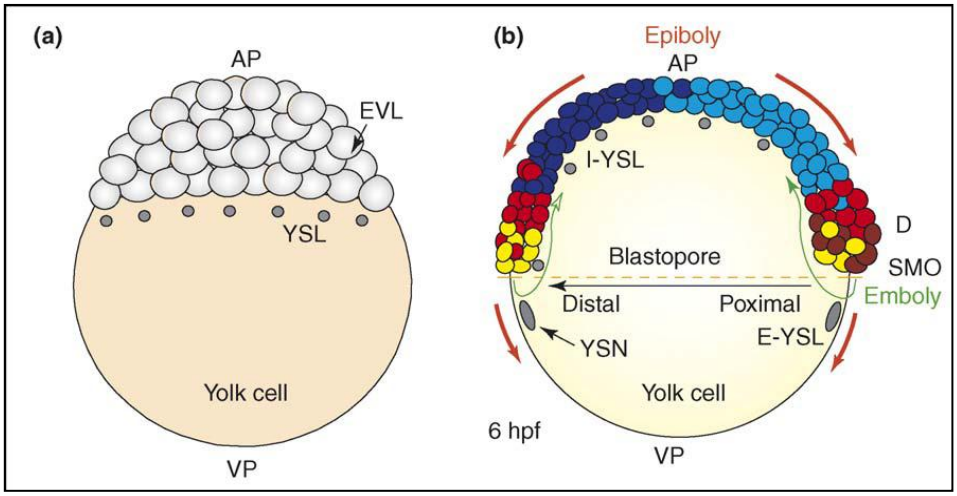


**Figure 1.6: Epiboly is the first movement of gastrulation.** (A) At the MBT, the basal layer of blastoderm cells deposit their nuclei into the yolk to form the YSL. (B) Epiboly is the spreading of cells over the surface of the yolk. The enveloping layer (EVL) is the outermost layer of cells. At 50% epiboly some cells involute back towards the animal pole (AP) in a movement termed emboly that begins at the Spemann-Mangold Organizer (SMO). Epiboly continues towards the vegetal pole (VP) until the yolk is enclosed. [Solnica-Krezel, 2006]

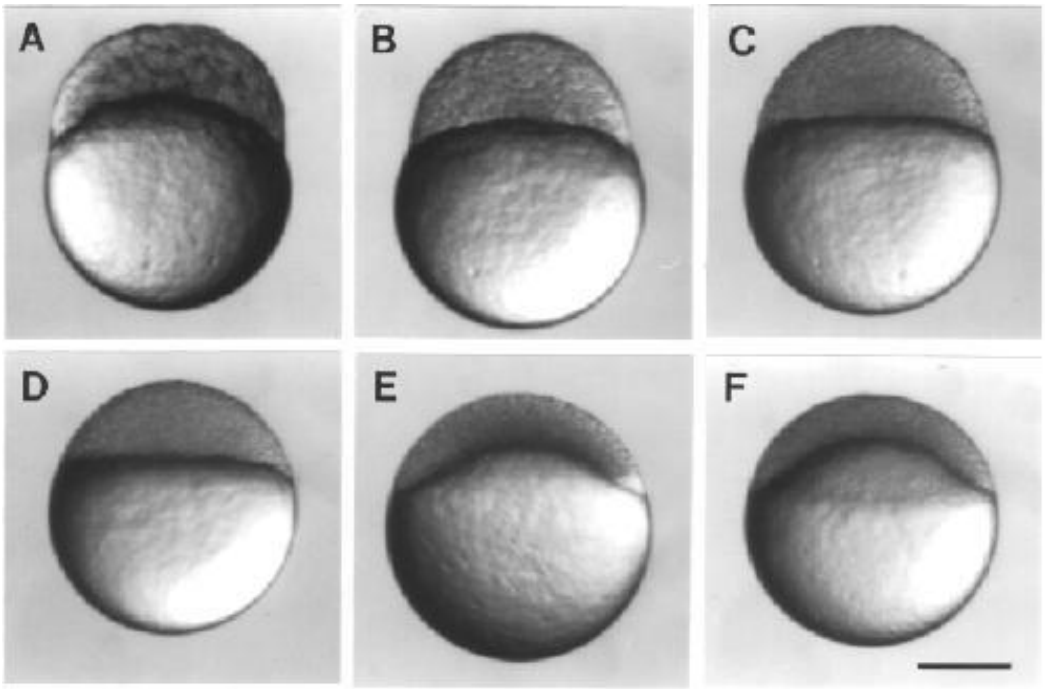


**Figure 1.7: Epiboly in zebrafish initiates after the MBT.** Cell divisions are synchronous at (A) 64-cell stage (2 hpf) and (B) 256-cell stage (2.5 hpf) until the MBT at the (C) 1000-cell stage (3.33 hpf). Blastoderm rounds out to form (D) sphere stage (4 hpf). The (E) dome stage marks epiboly initiation. (F) demonstrates 30% epiboly. [Kimmel, 1995]

movements occur during lateral mesoderm convergence by various signaling pathways, including Wnt signaling and Snail regulation of adhesion (Solnica-Krezel, 2006). Convergence and extension movements after 50% epiboly position precursor cells mediolaterally and then anterior-posteriorly to the animal pole, which will give rise to the head, tail and body of the fish. These movements occur simultaneously with epiboly, which cumulates with the blastoderm cells completely surrounding the yolk (Figure 1.8 and 1.9 (Solnica-Krezel, 2006)).

Several mechanisms contribute to epiboly. Radial intercalation is a process in which blastoderm cells in internal positions move outward and integrate in the more superficial cell layers (Figure 1.10 (Kane et al., 2005)). The integration of additional cells causes the expansion of the layers, and spreads cells around the yolk (Schier and Talbot, 2005). The adhesion molecule E-cadherin is required for epiboly, as E-cadherin mutants have deep cells that do not intercalate with EVL cells (Shimizu et al., 2005). They exhibit a loss of adherens junctions between the deep cell layer (DEL) and the EVL, and deep cells do not complete epiboly. The deep cells require E-cadherin in order to attach to the EVL and use it as a migratory substrate (Shimizu et al., 2005). The mutants *half-baked, weg* and *cdh1rk3* represent allelic mutations for E-cadherin, demonstrating the necessity for the adhesion between the EVL and DEL (Kane et al., 1996; Kane et al., 2005; Shimizu et al., 2005). The dome stage, which marks a rising of the yolk against the blastoderm, is thought to provide a stimulus force on the cells of the DEL that aids radial intercalation and epiboly (Figure 1.7, E). This process may provide a stimulus force to the DEL that drives intercalation and spreading of the cells over the yolk (Solnica-Krezel, 2006; Wilkins et al., 2008).

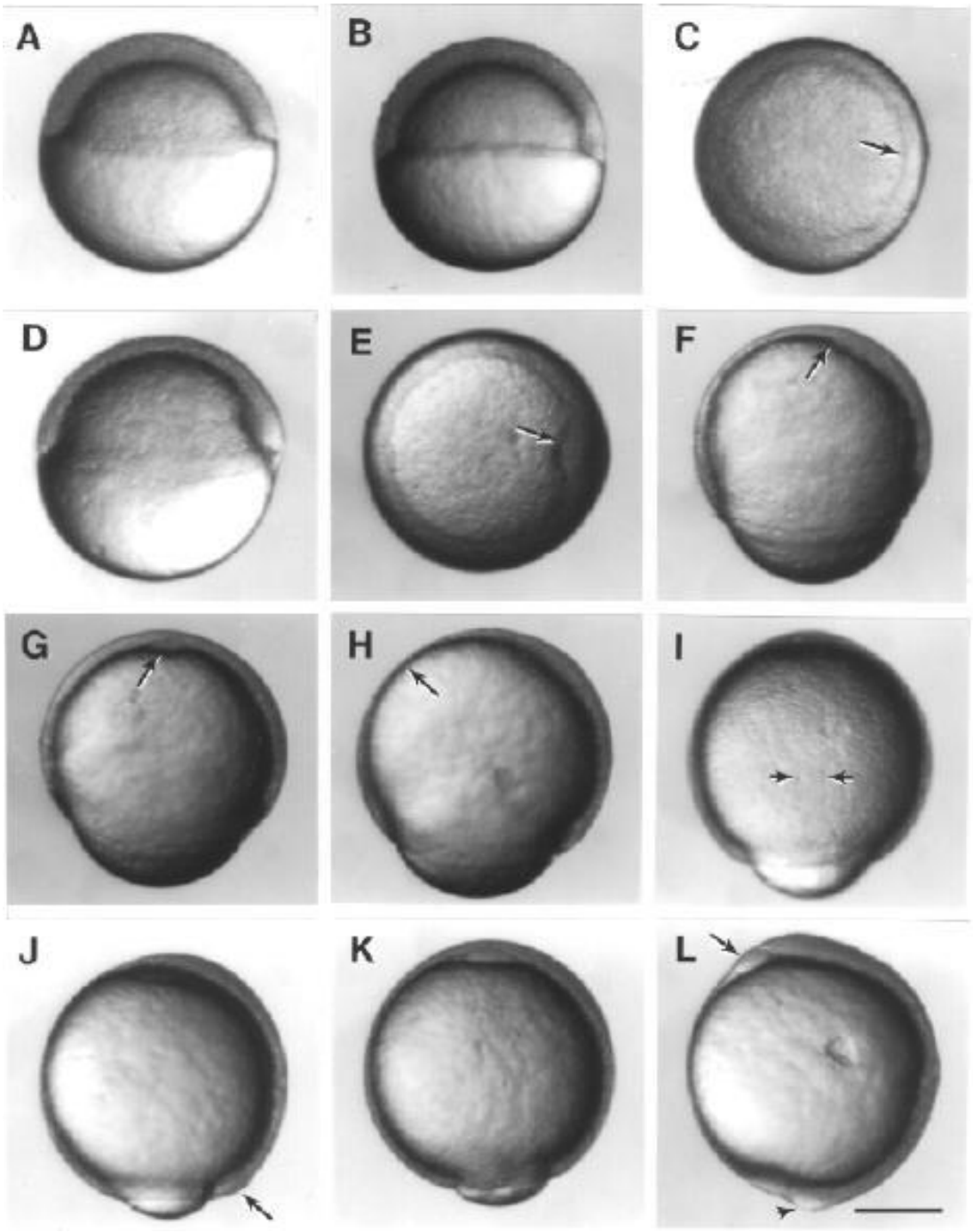


**Figure 1.8: Epiboly progresses until the yolk is enclosed.** (A-C) At 50% epiboly the germ ring forms (arrow indicates future dorsal side). (D and E) The embryonic shield forms as a thickening on the dorsal side at 60% epiboly (arrow). (F-H) Internalization and anterior migration of cells establishes the primitive germ layers of the embryo. (I) The midline of the embryo (paired arrows) condenses as epiboly progresses. (J-K) Epiboly continues, concurrent with internalization, until the blastopore (arrow) closes. (L) At the tailbud stage, the future head (arrow) and tail (arrowhead) are visible. [Kimmel, 1995]

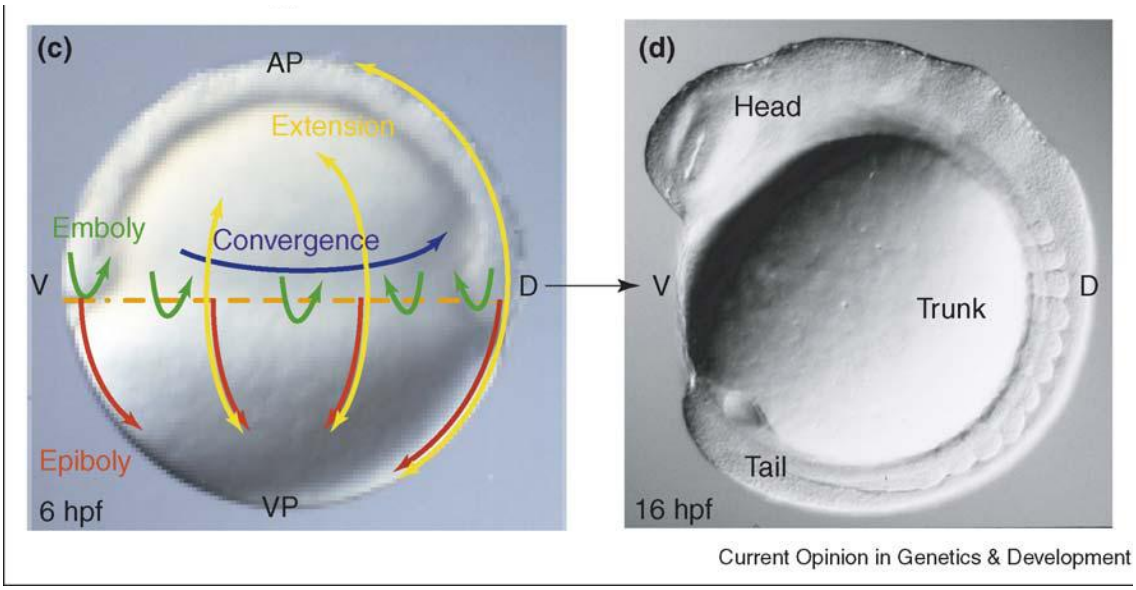


**Figure 1.9: Several cell movements must occur for successful zebrafish gastrulation.** Epiboly, emboly, convergence and extension transform the (C) shield stage (6 hpf) embryo into rudimentary fish at (D) 12-somite stage (15 hpf) with established head, trunk and tail regions. [Solnica-Krezel, 2006]

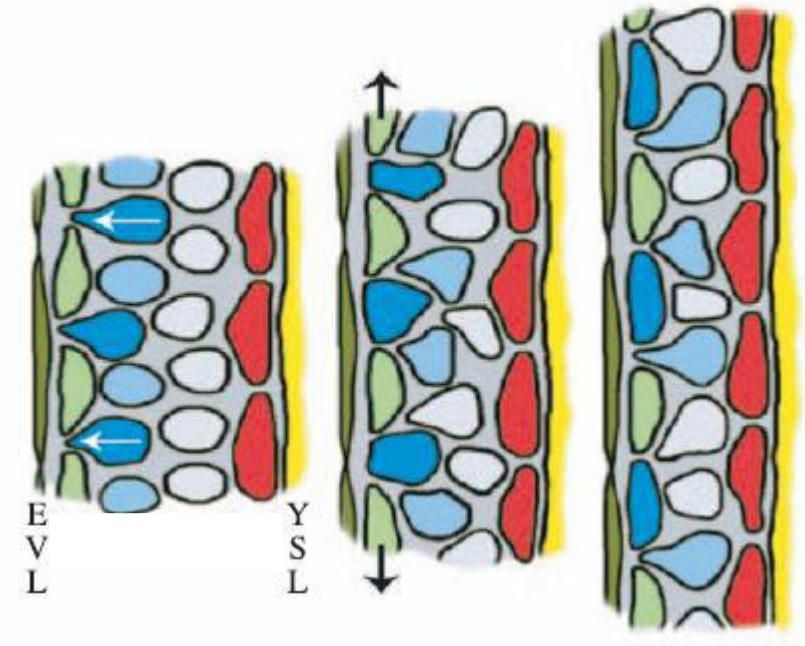


**Figure 1.10: Radial intercalation is essential in epiboly.** This diagram demonstrates the movement of internal cell layers into outer cell layers to spread and thin cells to increase surface area. [Wilson et al., 1995]

The YSL also plays a key role in epiboly. Trinkhaus et al. (1963) demonstrated in classic studies with *Fundulus,* another teleost commonly known as the killifish, that epiboly can occur in the absence of the blastoderm, but the blastoderm cannot complete epiboly without attachment to the YSL (TRINKAUS, 1963). In zebrafish, the YSL secretes Nodal/TGFβ factors that specify the marginal mesodermal and endodermal cell fates (Mizoguchi et al., 2008). Before initiation of epiboly, mesodermal precursor cells induce the migratory movements of the YSL by modulating cortical flow, through a connection involving E-cadherin (Carvalho et al., 2009; Shimizu et al., 2005). It has been proposed that E-cadherin is recycled via endocytosis, but the exact regulation of the process is not well understood. Sakaguchi et al. (2006) proposed that YSL may induce fibronectin expression in the overlying tissue, which is necessary for the migration of heart precursor cells (Sakaguchi et al., 2006). Another protein required for epiboly is the homeobox transcription factor Mtx2, which acts within the YSL to regulate morphogenetic movements of EVL and DEL cells (Bruce et al., 2005; Wilkins et al., 2008). Mtx2 is also required for completion of epiboly, and morpholino knockdown disrupts spatial arrangement of YSL nuclei (Wilkins et al., 2008). The major mechanisms through which the YSL influences epiboly include cytoskeleton components.

*Role of the cytoskeleton*

The cytoskeleton of the yolk plays a major role in epiboly as well. Two distinct types of microtubular (MT) arrays are located in the yolk cytoplasm and are required for

epiboly (Figure 1.11 (Solnica-Krezel and Driever, 1994)). Bundles of MT extend along the animal/vegetal pole, from the base of the blastoderm to the vegetal pole (Solnica-Krezel and Driever, 1994). The second array of microtubules forms a meshwork near the blastoderm margin, interlinking and separating the yolk syncticial nuclei (Solnica-Krezel and Driever, 1994). Prior to the beginning of epiboly, the YSL has nuclei that are regularly arranged in a band around the circumference of the yolk just below the blastoderm cap. At the onset of epiboly the band tightens up and the microtubule network becomes denser which helps regulate the migration of the YSL. Treatment of embryos with microtubule stabilizing drug Taxol or microtubule destabilizing drug Nocodazole blocks YSL migration but only partially inhibits migration of the EVL and DEL (Solnica-Krezel and Driever, 1994). Therefore the epibolic movements of the YSL and blastoderm occur via different mechanisms, and only YSL epiboly is completely dependent on microtubules (Solnica-Krezel and Driever, 1994).

Another essential factor required for the completion of epiboly is F-actin. Before gastrulation, there is a pool of F-actin in the vegetal pole of the yolk (Cheng et al., 2004). After 60% epiboly and formation of the dorsal shield, three regions of F-actin-based structures form (Figure 1.12 (Cheng et al., 2004)). Two circumferential actin rings form at the vegetal margin of the DEL and EVL cells and a punctate F-actin band forms in the external YSL (Cheng et al., 2004). These actin filaments are important for migrating cell layer connection and completion of epiboly (Zalik et al., 1999). Treatment of zebrafish embryos with the drug cytochalasin B, which disrupts all three actin structures, causes epiboly to slow or halt, failure of yolk cell occlusion, and eventual lysis of the embryo (Cheng et al., 2004).

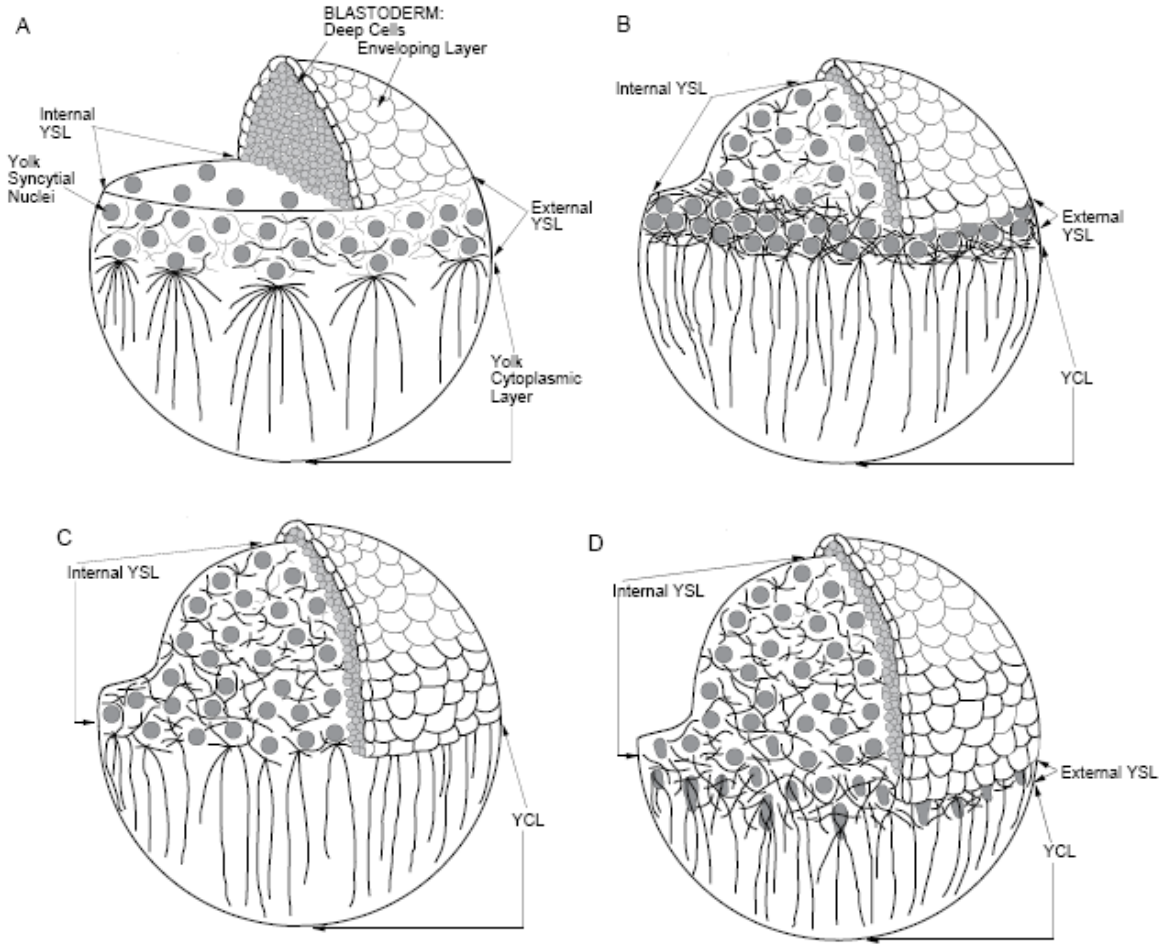


**Figure 1.11: Microtubule arrays are required for epiboly.** This diagrammatic sketch shows microtubules which are located within the yolk syncytial layer (YSL) and in arrays in the yolk cytoplasmic layer (YCL) extending toward the vegetal pole. (A) At sphere stage, the yolk syncytial nuclei (YSN) are loosely packed but condense by (B) 30% epiboly. Some researchers propose that microtubules help "tow" the blastoderm toward the vegetal pole as epiboly progresses through (C) 50% epiboly and (D) 70% epiboly. [Solnica-Krezel and Driever, 1994]

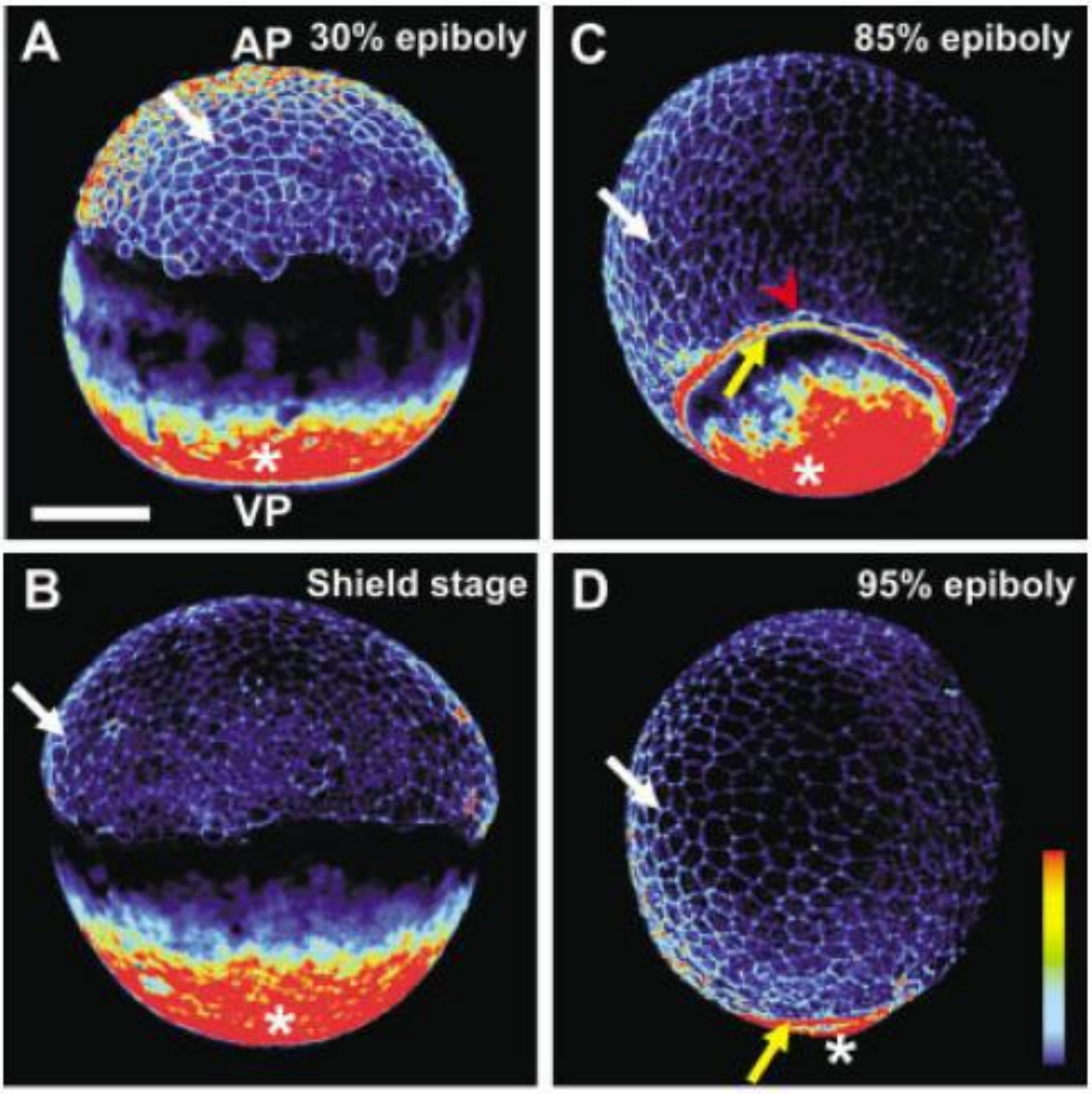


**Figure 1.12: Microfilaments are also required for epiboly completion.** Confocal images show red fluorescently-tagged filamentous actin which form microfilaments. Actin is detected at the periphery of EVL cells at all stages (white arrows). A vegetal (*) pool of actin present at (A) 30% epiboly and (B) shield stage, and is diminished at later stages. Later in epiboly (C and D) two punctate actin rings are detected. These rings of actin at the enveloping layer (EVL) margin (red arrowhead) and the deep cell margin (yellow arrow) are thought to help close the blastoderm pore at the vegetal pole in a "purse-string" fashion. [Cheng et al., 2004]

One proposed mechanism of epiboly involves active endocytosis and coincides with the punctate actin band. In an actin dependant mechanism, the external YSL membrane is moved to the internal YSL membrane via endocytosis/exocytosis, which allows for vegetal movement of the YSL (Holloway et al., 2009). Since the YSL maintains a tight connection with the EVL layer, the EVL is towed along toward the vegetal pole as epiboly proceeds. Endocytosis is still observed after Nocodazole treatment and thus is a microtubule-independent mechanism, but is not sufficient for YSL epiboly without functioning microtubules (Solnica-Krezel and Driever, 1994).

Along with cadherins, actin is responsible for maintaining a tight connection between EVL cells and between the EVL and YSL. The EVL cells maintain a cytoplasmic actin band that coincides with cadherin proteins. At the margins approaching the YSL, EVL cells extend actin-rich filopodia that do not contain cadherins (Zalik et al., 1999). As epiboly approaches completion, the EVL cells change shape by constricting and elongating. This process requires the recruitment of actin and myosin 2 within the yolk cytoplasm and the marginal EVL cells, which is controlled by the kinase Msn1 (Koppen et al., 2006). Presence of active myosin 2 indicates contractility at the YSL margin. The "purse-string" model postulates that after 50% epiboly a circumferential F-actin ring constricts the margin of EVL layer, pulling it closed as cells continue to migrate vegetally around the yolk (Solnica-Krezel and Driever, 1994).

*Other Zebrafish Epiboly Mutants*

Wagner et al. (2004) initiated a maternal-effect zebrafish mutagenesis that yielded mutants with epiboly defects, likely due to the high requirement for maternal gene products during this stage (Wagner et al., 2004). Examiners identified four epiboly mutants: *betty-boop*, *poky*, *slow* and *bedazzled*. The *betty-boop* zebrafish mutant exhibits an epiboly phenotype in which the F-actin ring prematurely constricts, resulting in yolk lysis and embryonic death (Holloway et al., 2009; Wagner et al., 2004). The molecular cloning of this mutant lead to the discovery that the p38 MAPKAPK2 kinase cascade signaling pathway is required to control the contractility of the F-actin band during epiboly (Holloway et al., 2009). The *poky* mutant displayed delayed epiboly in which all three migrating layers were affected, and often the yolk lysed before epiboly completed. This mutation was localized to chromosome 13, but the gene has not been identified molecularly. The *slow* mutant also displayed delayed epiboly, but the DEL was much more affected than the other two layers, similar to the E-cadherin mutant phenotypes. This mutation was mapped to chromosome 7. The *bedazzled* mutant, which has yet to be cloned, also displayed delayed epiboly where the DEL was also more severely affected, but in this mutant EVL cells would slough off the embryo during epiboly, indicating a loss of adhesion. These mutants reflect the persistent effect of maternal influence after the MBT has occurred because initiation of zygotic transcription cannot prevent the phenotypes produced from loss of a maternal gene product.

# Chapter 2: Introduction

## Introduction

To gain insight to the functions of CACNβ4 during early zebrafish development, members of the Garrity lab, primarily Alicia Ebert, cloned the zebrafish homologues of the gene and determined their RNA expression patterns in embryos (Ebert et al., 2008a; Ebert et al., 2008b). The mammalian CACNB4 gene has two paralogs in the zebrafish genome, which we termed CACNβ4.1 and CACNβ4.2. They mapped to chromosome 6 and 9, respectively (Figure 2.1 (Ebert et al., 2008a; Ebert et al., 2008b)). The core region, which includes the SH3 and GK domains, of CACNβ4.1 shares 87% homology to the human gene sequence, and of CACNβ4.2 shares 89% homology (Ebert et al., 2008a). In both humans and zebrafish patterns of alternative splicing at the N-terminus produce the β4a and β4b transcript variants (β4b has a longer N-terminus - Figure 2.1). Mammals also have a short transcript, termed β4c, which is produced by splicing that skips exon six and introduces a stop codon at the 212th amino acid (out of 486 amino acids). Both zebrafish β4 genes also undergo the same alternative splicing to produce short β4c transcripts. The relatively high level of conservation with mammalian genes suggests that biochemical functions or interacting partners may also be similar between mammals and zebrafish.

Maternal genes are required for the early stages of zebrafish development. Until the mid-blastula transition when zygotic transcription begins, the embryo relies on maternally expressed gene products. In zebrafish, the mid-blastula transition occurs at the 512 cell (3 hpf) stage on the $10^{th}$ round of cell division (Kane and Kimmel, 1993). Ebert et al. (2008) examined RNA expression levels during early zebrafish development

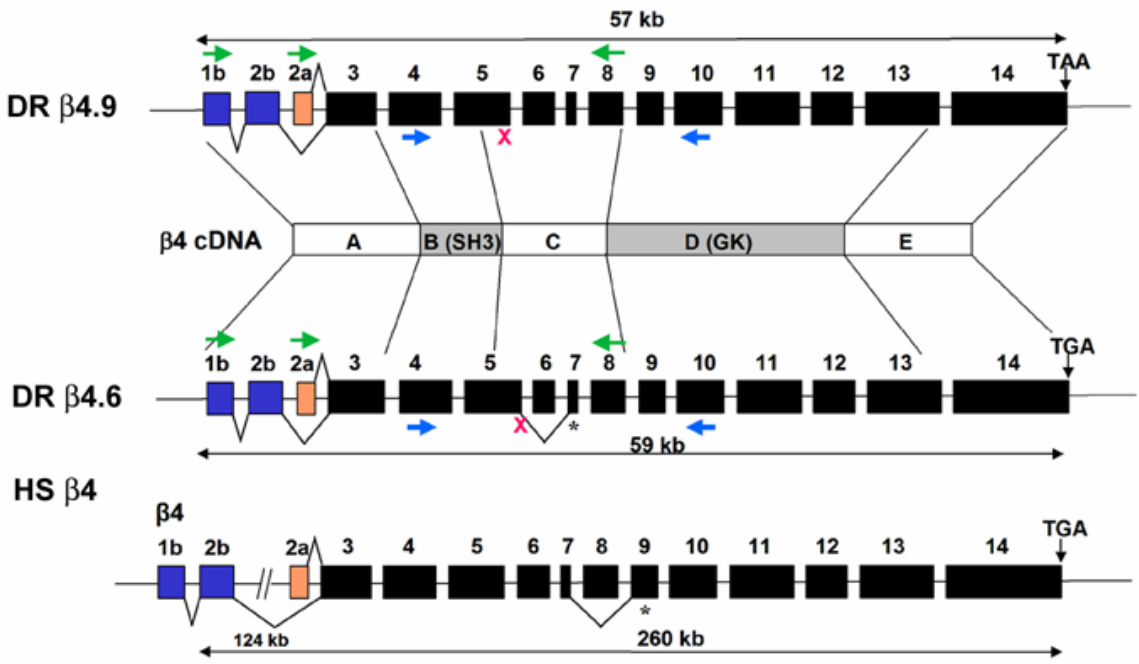


**Figure 2.1: Genomic structure of zebrafish CACNβ4 genes.** We cloned two homologues of the β4 subunits from cDNA via RACE PCR. Both genes are members of the MAGUK family of proteins with conserved SH3, HOOK, and GK domains flanked by variable N- and C-terminal domains. The shorter N-terminal variants (orange) resemble human β4a variants, while longer variants (blue) resemble human β4b variants. All genes show N-terminal splicing and internal splicing similar to human β4 genes. X = MO target sites, blue arrows = internal RT-PCR primers, green arrows = N-terminal RT-PCR primers. [Ebert et al., 2008]

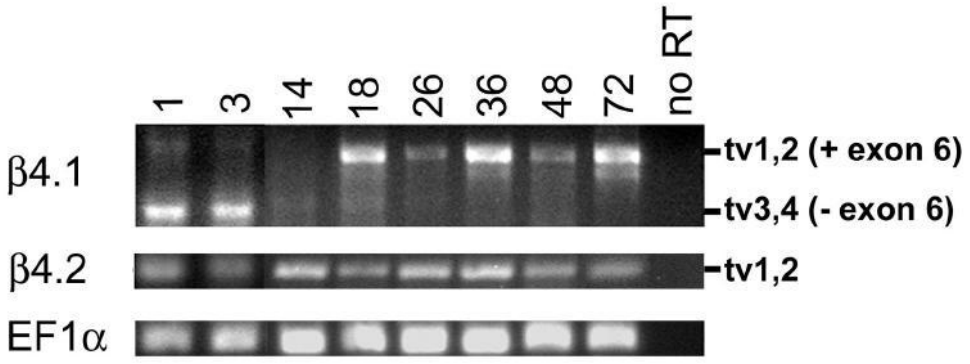


**Figure 2.2: β4 RT-PCR expression profiles.** We performed RT-PCR analysis using variant-specific primers (located in the 5' exons 1 or 2 and exon 10) on RNA samples from whole embryos at various developmental stages. [Ebert et al., 2008]

to determine if CACNβ4.1 and CACNβ4.2 are expressed maternally (Ebert et al., 2008a). They performed RT-PCR from RNA extracted from embryos 1 hpf through 72 hpf (Figure 2.2 (Ebert et al., 2008a)). At both 1 hpf and 3 hpf both β4.1 and β4.2 transcripts are expressed maternally; the shorter splice variants dominate but the longer variants are also expressed. Expression of both β4 genes continues also through epiboly. Using in situ hybridization they determined that both genes are expressed diffusely throughout the blastoderm during epiboly (Figure 2.3, B-E (Ebert et al., 2008b)). Punctate expression of both genes associated with the yolk syncitial nuclei (Figure 2.3, F and G, and data not shown (Ebert et al., 2008b)). Thus, transcripts from both zebrafish CACNβ4 genes are maternally expressed and are associated with YSN during epiboly.

To assess the functionality of the two CACNβ4 genes during epiboly, researchers took a reverse genetics approach. Ebert designed morpholinos targeting each CACNβ4 gene and used them in functional studies to determine the phenotypes associated with loss of gene expression. As occurs for human CACNβ4, both zebrafish CACNβ4.1 and CACNβ4.2 undergo alternative splicing (Zhou et al., 2008). To assure knock down of all splice variants of these genes, morpholinos were designed to target the fifth exon (Figure 2.1 (Ebert et al., 2008a; Ebert et al., 2008b)). The binding of morpholinos to the exon 5 splice acceptor site is predicted to create transcripts lacking exon 5. The direct fusion of exon 4 to exon 6 would alter the protein reading frame, encoding a premature stop codon early in the HOOK domain. Using primers that flank exon 5, Ebert performed RT-PCR to confirm efficient depletion of transcripts containing exon 5 for the specific gene targeted by each morpholino (Figure 2.3, H (Ebert et al., 2008b)).

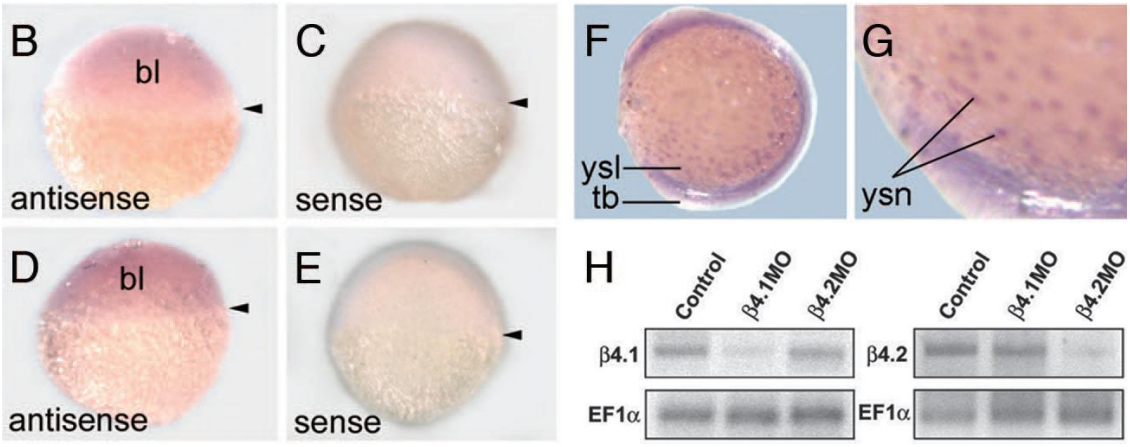


**Figure 2.3:** ***In situ hybridization*** using 3' antisense probes to β4.1 and β4.2. The arrowhead marks the margin between yolk/YSL and the blastoderm. Both (*B* and *C*) β4.1 and (*D* and *E*) β4.2 are expressed at 30% epiboly in the blastoderm (bl). (*F* and *G*) β4.2 and β4.1 (data not shown) are expressed at the five-somite stage (11.7 hpf) in the nuclei of the yolk syncytial layer (ysl). Tailbud (tb) indicates the embryo posterior. (*G*) Nine-fold enlargement of a portion of *F*. We extracted RNA from control or MO-injected embryos at 50% epiboly and (*H*) RT-PCR-amplified β4.1 or β4.2 fragments. [Ebert et al., 2008]

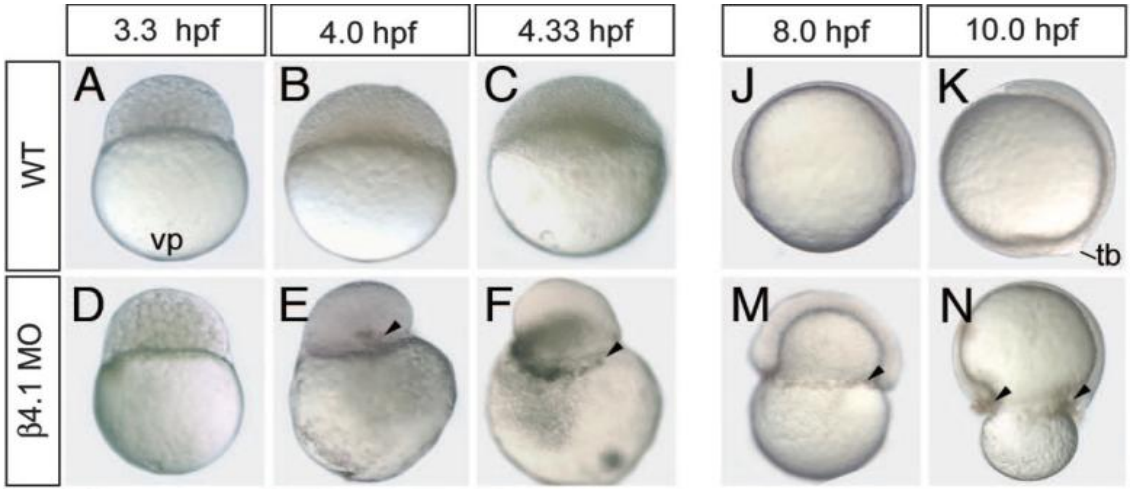


**Figure 2.4: Class I phenotypes of epiboly failure.** (A-C) WT embryos initiated epiboly by 4.33 hpf while (D-F) β4.1 severe morphants underwent blastoderm retraction. Arrowheads show cell death. (J and K) WT embryos completed epiboly by 10 hpf, while (M and N) β4.1 morphants experienced delayed epiboly and pressure on the yolk. [Ebert et al., 2008]

Morpholino knockdown of CACNβ4 resulted in failure of epiboly. In the morphants, cleavage occurred normally, but as soon as epiboly began development was disrupted. Ebert observed a range of phenotypes (Ebert et al., 2008b). The most severely affected embryos did not begin epiboly at all, but instead the blastoderm cap retracted and the embryo died due to rupture of the yolk cell (Figure 2.4, E and F (Ebert et al., 2008b)). Other embryos began epiboly, but it was quite delayed in morphant embryos compared to wild-type. In these embryos, the migrating layers of cells did not migrate all the way down around the yolk, and exerted pressure on the yolk and the embryo died of yolk lysis (Figure 2.4, M and N (Ebert et al., 2008b)). These epiboly phenotypes were collectively called Class I embryos.

If the embryos survived epiboly, they later displayed severe morphological defects, including extensive cell death in the nervous system (Figure 2.5, ClassII (Ebert et al., 2008b)). These embryos had undulating notochords, and were often slightly dorsalized, and lacked proper ventral tissue development. The least severely affected embryos displayed heart defects and died before six days old (Class III, data not shown (Ebert et al., 2008b)).

The failure of epiboly seen in Class I embryos confirms that the CACNβ4 genes are required for epiboly to occur normally. Class I embryos exhibited phenotypes also seen with disruption of microtubules via the use of microtubule stabilizing drug Taxol or microtubule destabilizing drug nocodazole (Solnica-Krezel and Driever, 1994). Therefore Ebert included a nocodazole treatment as a comparative experiment for her morpholino injections (Figure 2.6 (Ebert et al., 2008b)). Nocodazole-treated embryos also exhibited blastoderm retraction, delayed epiboly, and yolk cell lysis. The similarity

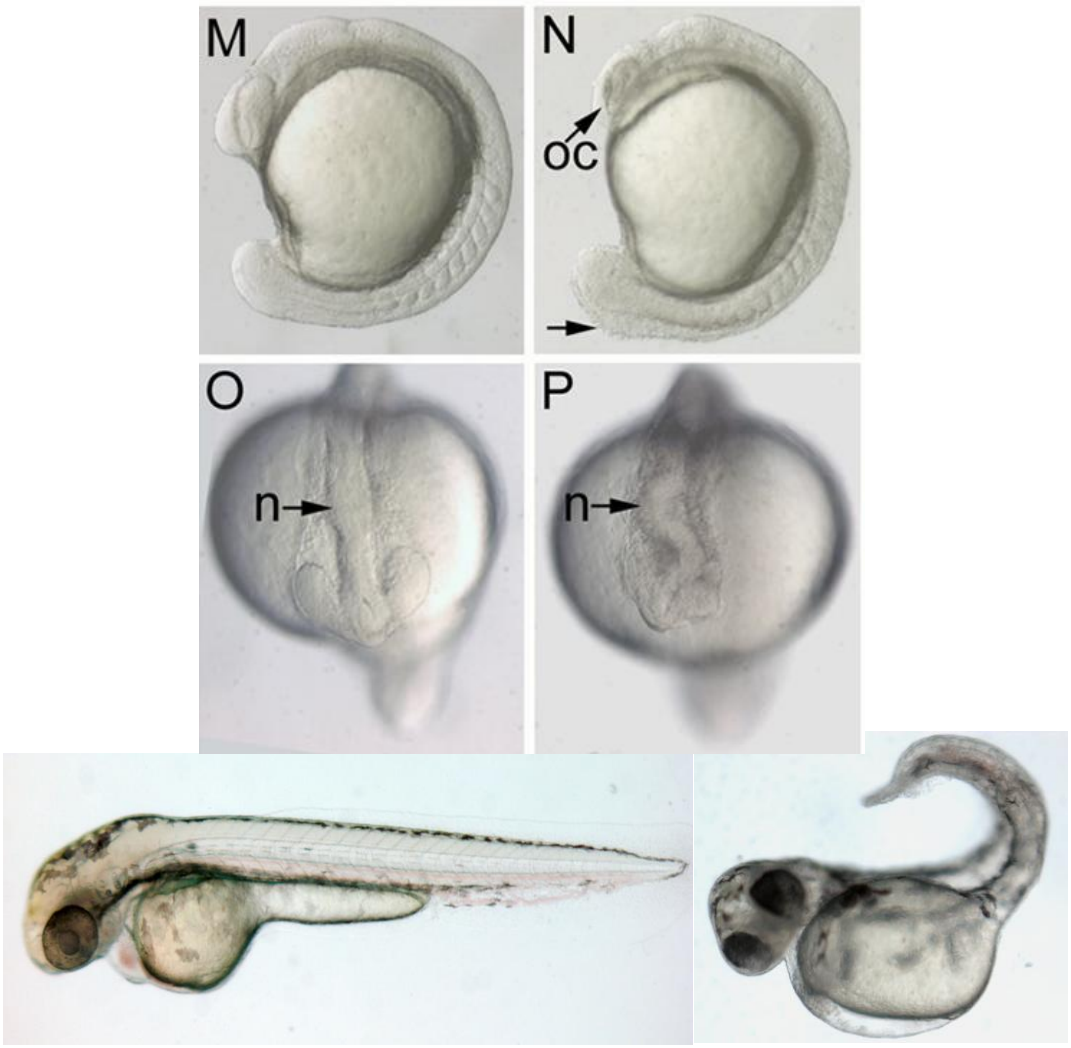


**Figure 2.5: Class II β4 morphant embryos have dorsalized phenotypes.** (M and O) WT embryos at 16 somites exhibited normal development. (N and P) Morphant embryos displayed cell death throughout the central nervous system including the optic cup (OC). Morphants also exhibited an undulating notochord (n). (Q) WTs embryo at 48 hpf looked normal. (R) Morphant embryos that survived to 48 hpf displayed mildly dorsalized phenotypes. Images are of β4.1 morphant embryos; however, β4.2 morphant embryos displayed similar phenotypes. [Ebert et al., 2008]

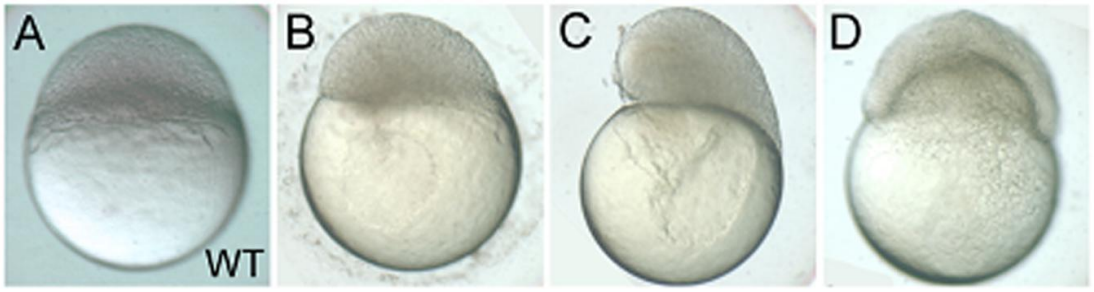


**Figure 2.6: Microtubule disruption causes failure of epiboly.** (A) Wild-type embryos exhibited normal development at the sphere stage. (B-D) Nocodazole treated embryos exhibited (B) cell death, (C) blastoderm retraction and (D) delayed epiboly compared to 50% epiboly wild-type embryos. [Ebert et al., 2008]

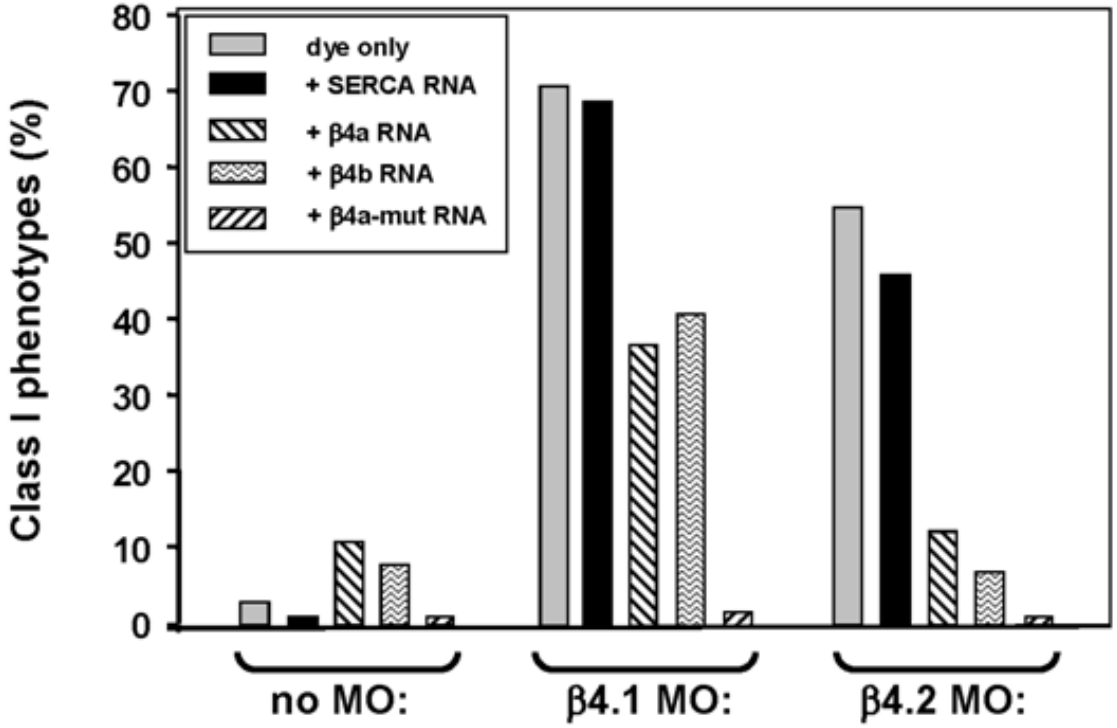


**Figure 2.7: Human β4 cRNA rescues β4 morphants.** We injected β4.1 MO, β4.2 MO or fluorescent tracer alone. We partially rescued Class I phenotypes with addition of 200 ng of human β4a or β4b cRNA. Surprisingly, co-injection with the β4a mutant RNA showed rescue of nearly all embryos. (n= at least 100 embryos per treatment). [Ebert et al., 2008]

between the phenotypes implies that CACNβ4 knockdown could cause a disruption in the microtubule network of the early embryo.

The possibility that the morpholinos bound to multiple genes and caused an off-target effect that resulted in early fatality cannot be excluded. To verify that the observed phenotypes are due to CACNβ4.1 or CACNβ4.2 knockdown specifically, Ebert co-injected human cRNA to rescue the epiboly phenotype. The human CACNβ4 cRNA does not contain the splice donor morpholino target nucleotide sequence present in zebrafish CACNβ4.1 and CACNβ4.2. Injection of CACNβ4.1-specific morpholino resulted in 71% Class I embryos. Co- injection with 40 ng/µl of human CACNβ4 cRNA reduced the lethality to 37% (Figure 2.7 (Ebert et al., 2008b)). Injection of CACNβ4.2-specific morpholino resulted in 55% Class I embryos, which was reduced to 12% with β4a cRNA (Figure 2.7). This data suggests that in wild-type embryos, CACNβ4.1 and CACNβ4.2 both function during epiboly.

As described previously, the best characterized role for the β4 calcium subunit is chaperoning the alpha subunit of the VDCC to the membrane and modulating calcium flux (Obermair et al., 2008). Calcium levels are dynamic during development, and intracellular calcium acts in multiple signaling pathways (Webb and Miller, 2003). The question remained whether failure of epiboly caused by loss of CACNβ4 is due to changes in the calcium dynamics of the embryo. Our collaborator William Horne and his lab created a cRNA construct that contained three point mutations in the GK domain that altered (to alanine) three conserved amino acids required for interaction of the CACNβ4 subunit with the alpha subunit of the voltage-gated calcium channel. If the CACNβ4 gene functioned to regulate calcium channels during epiboly, the mutant construct should

not have rescued the epiboly phenotype since the β subunit should not interact with the α subunit. Co-injection of this mutant construct, termed CACNβ4-3X, surprisingly did rescue epiboly in morpholino-injected embryos. Co-injection of morpholinos with CACNβ4-3X RNA reduced lethality seen in Class I embryos to 2% and 1% (with CACNβ4.1 and β4.2 morpholinos- Figure 2.7). This demonstrates that the CACNβ4 proteins are acting in a calcium channel independent manner during zebrafish epiboly.

Based on the in situ hybridization data, the CACNβ4 proteins might be acting in the YSN. To determine whether loss of CACNβ4 led to any specific phenotypes involving the YSN, wild-type or CACNβ4 morphant embryos were injected with Sytox green dye, which labels nucleic acid, after the 1000-cell stage into the yolk. At this point in development, the blastoderm cells are sealed off from the yolk by their surrounding cell membranes and only the YSN are exposed to the dye. Using fluorescent imagery, members of the Garrity lab observed Sytox-injected embryos at the sphere stage, before the CACNβ4 knockdown epiboly phenotype is observed. By the sphere stage the YSN of morphant embryos already are severely affected by loss of CACNβ4. In wild-type embryos, the YSN are evenly spaced with reference to one another, and they are dispersed in an even band around the circumference of the embryos, just beneath the overlying blastoderm (Figure 2.8 (Ebert et al., 2008b)). In morphant embryos, the YSN are dispersed in a more irregular fashion beneath the blastoderm cap; they are often mislocalized along one side of the embryo towards the vegetal pole, and do not maintain a uniform circumferential ring around the embryo (Figure 2.8). The size of the nuclei in the morphants was also different than wild-type, with some large nuclei and some very

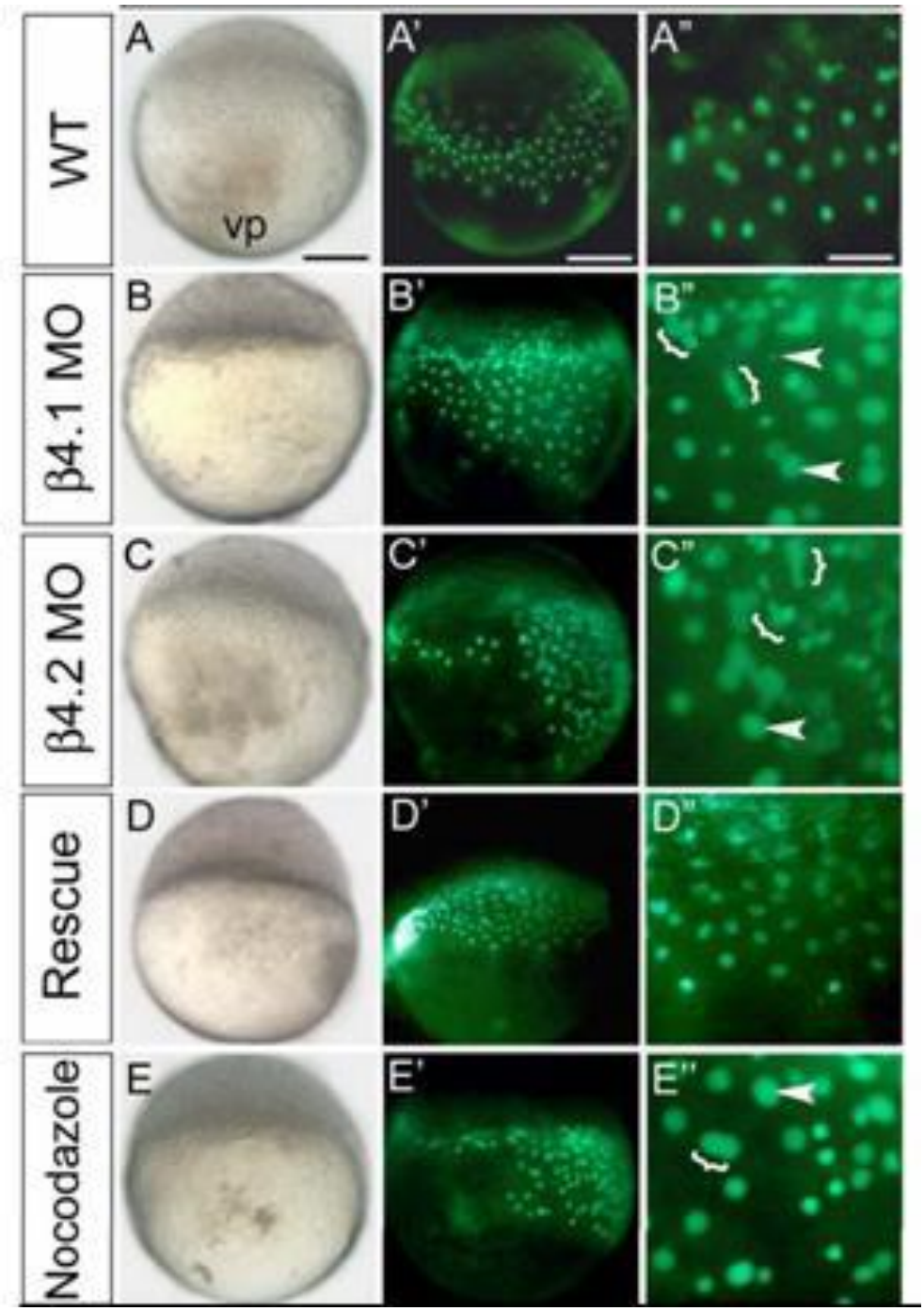


**Figure 2.8: β4 morphants have abnormal YSN.** (A-E) Brightfield or (A'-E') Sytox green fluorescent images of embryos injected at the 1-cell stage with (B) β4.1MO, (C) β4.2MO, (D) β4.1MO plus 200 pg human β4 cRNA. We injected all embryos at the 1000-cell stage with Sytox green into the yolk, with some embryos (E) also receiving nocodazole. To better visualize the YSN, (A"-E") show 9-fold magnification of portions of center panels. Arrowheads indicate nuclei or nuclear fragments. Brackets indicate clumps of nuclei. Scale bar is 200 um for A-E, A'-E', and 600 um for A"-E". [Ebert et al., 2008]

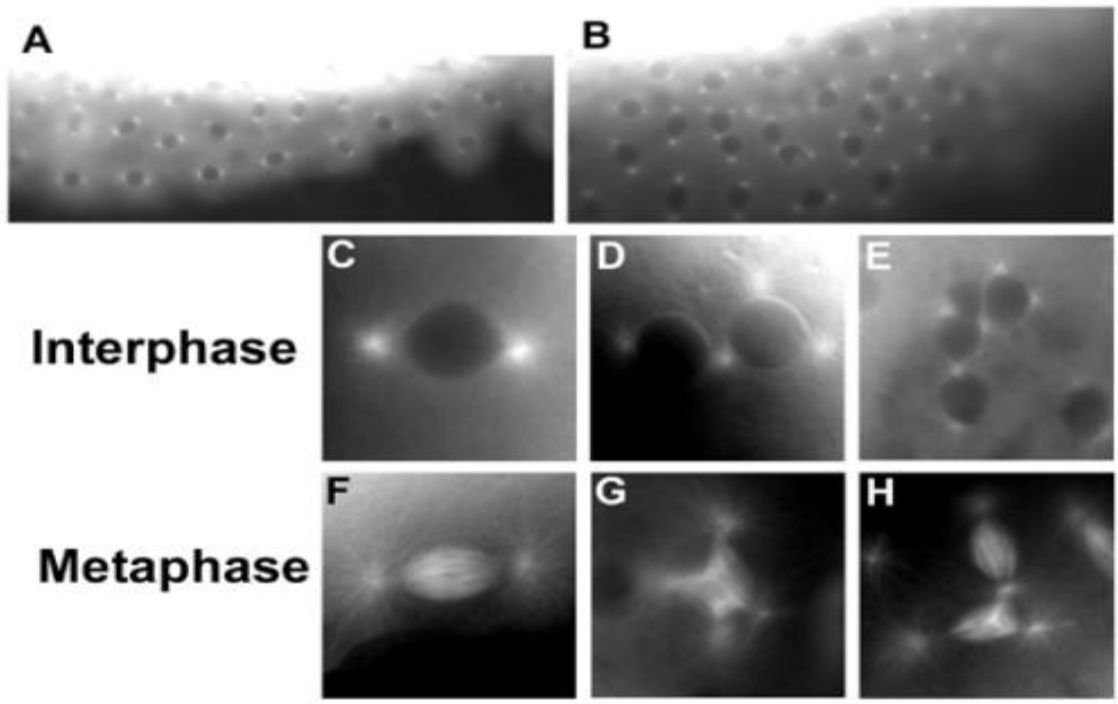


**Figure 2.9: Mitosis of YSN is impaired in CACNβ4 morphants.** Embryos were injected with rhodamine-labeled tubulin subunits ((B) plus or (A) minus morpholino) and mitotic events were visualized using confocal microscopy. (A and C) Wild-type YSL nuclei were separated from one another and (F) correctly underwent mitosis. In (B, D and E) CACNB4 knockdown embryos, YSL nuclei failed to remain separate. As closely-apposed nuclei entered mitosis, they formed (G and H) multipolar spindle arrays, associated with supernumary centrosomes. These nuclei became arrested in mitosis. [Ebert, unpublished data]

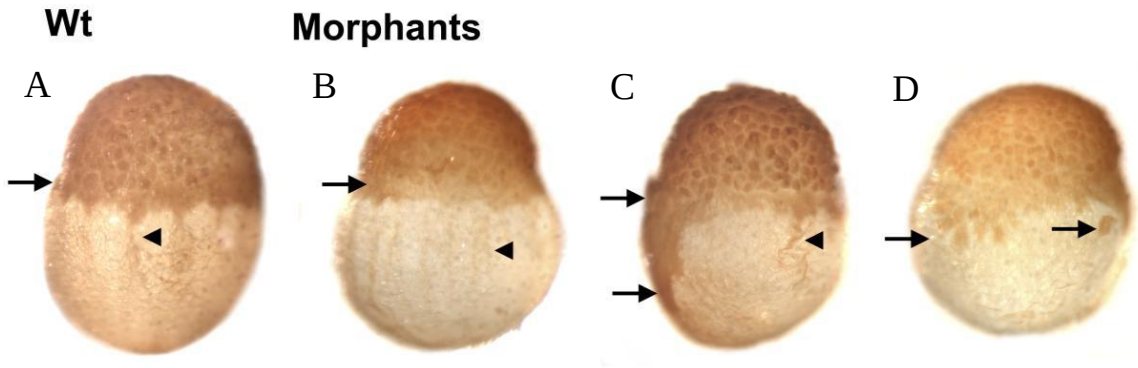


**Figure 2.10: CACNβ4 morphants have abnormal microtubule arrays.** We performed Immunohistochemistry with an acetylated tubulin antibody to detect microtubules in high stage (3.3 hpf) embryos. (A) Control embryos showed long, straight, evenly-spaced microtubule arrays. Microtubule arrays in morphant embryos were (B) thinner and more weakly stained, (C) disorganized, or (D) not detectable. Arrows indicate cortex microtubule network surrounding YSN; arrowheads indicate longitudinal microtubule arrays. [Ebert, unpublished data]

small Sytox-positive fragments (Figure 2.8). The nuclei in CACNβ4 morphants were closely juxtaposed, and were often clumped with two or more nuclei together (Figure 2.8 and 2.9 (Ebert et al., 2008b)). Similar phenotypes are also seen in the nocodazole treated embryos (Figure 2.8). This experiment verifies that the CACNβ4 genes are required for appropriate YSL arrangement.

To obtain a more precise evaluation of the YSL phenotype created by CACNβ4 knockdown, we required real time observation of the YSN in live embryos to observe mitosis. We therefore injected rhodamine-labeled tubulin into 1000-cell wild-type and morphant embryos. The YSL layer is formed at the $10^{th}$ division at the 1000-cell stage and the nuclei undergo only three to five rounds of cell division then cease mitosis by the sphere stage (Carvalho et al., 2009; Kane and Kimmel, 1993). The developing embryo incorporates the labeled tubulin monomers into microtubules and we observed them via confocal microscopy. In the morphants, observed YSN were positioned closely to one another, and they did not have exclusively two centrosomes per nuclei. Instead, some nuclei had three centrosomes and some nuclei were sharing centrosomes (Figure 2.9). The progression of the cell cycle led to mitotic figures with multiple valances, which appeared to arrest without completing anaphase (Figure 2.9). Taken together, these data confirm that CACNβ4 is required for proper division and position of the YSN nuclei during early development.

Based on the phenotypes produced by nocodazole treatment, loss of CACNβ4 may disrupt the microtubule networks that are required for epiboly. To analyze the microtubule arrays in the yolk cell of the morphants, Ebert used an antibody to acetylated tubulin in immunohistochemistry experiments. Wild-type embryos had microtubule

arrays that were dense, evenly spaced, and extended to the vegetal pole (Figure 2.10 (Ebert et al., 2008b), A). The microtubule arrays in the morphant embryos were thin and dispersed in an uneven manner (Figure 2.10, B and C). In some morphant embryos we did not detect microtubule arrays towards the vegetal pole in the yolk cell at all (Figure 2.10, D). This data demonstrates that the microtubule networks are disrupted in CACNβ4 morphants.

Overall, these studies demonstrated a requirement for CACNβ4 during early zebrafish development, specifically for completion of epiboly. Loss of CACNβ4 leads to a disruption of the YSL and microtubule network required for epiboly.

To elucidate the molecular function of this calcium channel auxiliary subunit, we determined the sub-cellular localization of the CACNβ4 proteins. To further understand CACNβ4 we also analyzed the protein domains required for its epiboly function. Our results demonstrate nuclear localization of a calcium channel associated protein, which supports the findings of similar studies in other model organisms. In addition, our studies suggest a role for CACNβ4 in protein interactions with a chromobox protein. The functional consequences of this interaction are still being explored, but potentially involve gene regulation.

# Chapter 3: Results

## Results

*CACNβ4.1knockdown disrupts nuclear distribution in YSN but not DEL or EVL during early epiboly*

We previously showed (using Sytox nuclear labeling dye) that use of an ATG-targeted morpholino to CACNβ4.1 disrupted the cytoskeletal architecture of the YSL and the mitotic divisions of YSN in gastrulating embryos (Ebert et al., 2008b). Although injection of a single morpholino did produce a strong phenotype, RT-PCR indicated some full-length transcript remained (Figure 2.3). We therefore sought to achieve a more complete knockdown by simultaneously injecting two morpholinos against the CACNβ4.1 gene. We introduced a second morpholino that targets the splice donor site of exon five, which would inhibit splicing of exon 5 into mRNA transcripts. The mis-spliced transcripts are predicted to be unstable, or, if translated, would encode a truncated β4.1 protein containing only the N terminus and SH3 domain of CACNβ4.1. Injection of two morpholinos can provide synergistic effects that lead to more efficient loss of full-length transcript (Sumanas and Larson, 2002). Morpholinos designed to independent target sites in the gene also function as additional controls helping to verify the specificity of the phenotype.

To understand the nature of the lethality due to CACNβ4.1 knockdown, we investigated both the structure of the YSL as well as the blastoderm (EVL and DEL) during early gastrulation. In wild-type embryos, the YSL forms prior to epiboly, and resides between the yolk and the blastoderm in a defined layer (Kane and Kimmel, 1993; Solnica-Krezel and Driever, 1994; Zalik et al., 1999). The nuclei of this layer are evenly distributed around the circumference of the yolk, each one spaced evenly away from the

next. Before initiation of epiboly, the YSL band of nuclei is several millimeters wide (on the animal/vegetal axis), and the nuclei are well separated. As epiboly begins and procedes, the band of YSL becomes tightened and narrow, and the nuclei are closer to one another, but still maintain equal space between them (Solnica-Krezel and Driever, 1994). The YSL layer, specifically nuclear arrangement, is disrupted by loss of CACNβ4.1. Knockdown of CACNβ4.1 via the ATG morpholino caused YSN phenotypes, including aggregation and uneven distribution (Ebert et al., 2008b). Since we were using a different morpholino mixture than we had in the past, we first needed to reexamine the YSL in morphant knockdown embryos. After the 1000-cell embryonic stage, the blastoderm cells are surrounded by plasma membrane and are no longer in syncitium and the YSL is created by nuclear release of the basal syncitial cell layer (Kane and Kimmel, 1993; Solnica-Krezel and Driever, 1994; Zalik et al., 1999). To determine whether our morpholinos are specific and result in the same phenotypes as previously described in our lab, we injected Sytox nuclear label into 1000-cell to label only the YSN in wild-type and morphant embryos. By the sphere stage, wild-type un-injected control embryos had YSN that were evenly distributed around the circumference of the yolk (Figure 3.1). The YSL nuclei created a thin band that lay just beneath the blastoderm and at the top of the yolk. The wild-type nuclei were spaced evenly with regards to one another, and mitosis had normal configurations of metaphase, anaphase and telophase. CACNβ4.1 knockdown embryos on the other hand exhibited markedly different results, with unorganized YSLs. The morphant embryos did not maintain the YSL nuclei as a uniform layer. Instead, the YSN were unevenly distributed around the periphery of the morphant embryo, some with more nuclei on one side of the embryo than the other. In

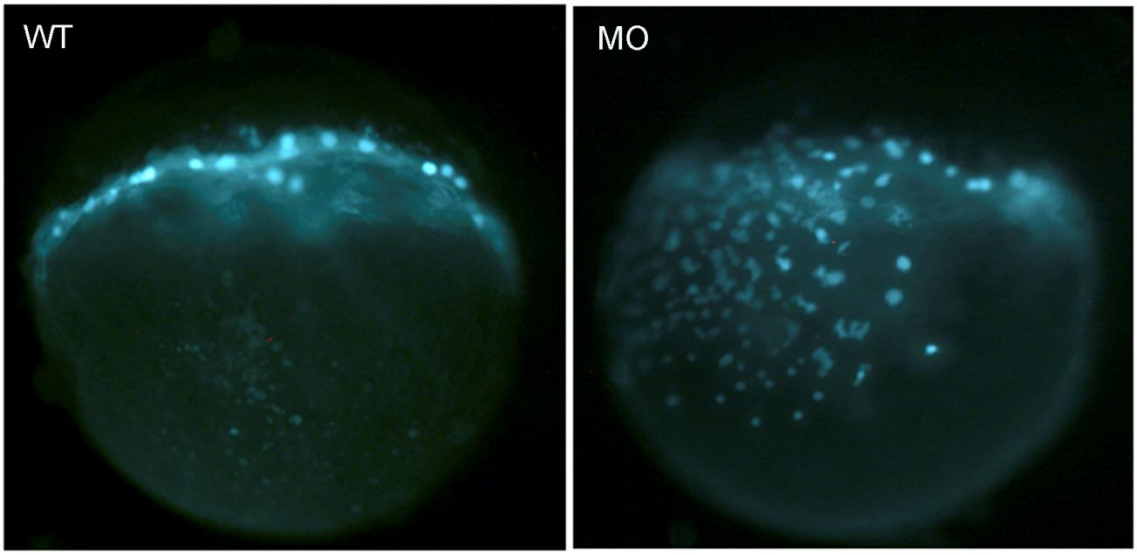


**Figure 3.1: CACNβ4.1 morphants have unorganized YSL nuclei**. Sytox dye was injected at 1000 cell in WT and MO embryos to only label the YSL nuclei. These images (taken at dome stage) demonstrate that CACNβ4.1 knock-down causes the YSL nuclei to lose their association with the migrating margin of blastoderm cells, re-localize dramatically towards the vegetal pole and sometimes aggregate with one another. Images were taken at 144X magnification.

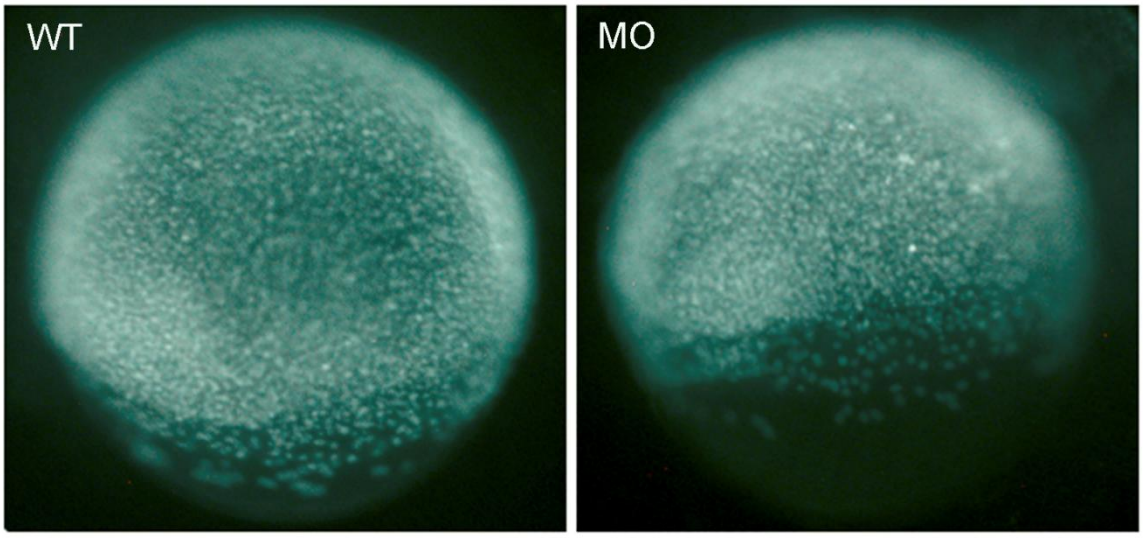


**Figure 3.2: At 50% epiboly, EVL and DEL appear normal in CACNβ4 morphants.** Sytox dye was injected at 1 cell in WT and MO to label all nuclei. Approximate equal number of sytox-positive nuclei suggest rates of cell division are similar. Besides the YSL phenotype, the other layers do not seem to be directly affected in CACNβ4 morphants, as migration of the layers as a whole is similar. Images were taken at 144X magnification.

some morphants, nuclei were only seen in particular regions, and some had YSL in a band, but distribution was not similar to wild-type. In these embryos, as was seen in all the morphants embryos, the YSL was not uniform, instead contained nuclei that had migrated at different distances down the yolk, and did not maintain a tight connection with the developing blastoderm. The most severe morphant embryo phenotype had YSN that were distributed only on one side of the embryo all the way down to the vegetal pole (Figure 3.1). As previously noted (Ebert et al., 2008b), CACNβ4.1 morphants had YSN that aggregated in groups of 2-4 nuclei. The identical knockdown phenotypes found with two different morpholinos against CACNβ4.1 confirmed that disruption of the YSL is a specific effect.

We described that blocking translation of the CACNβ4.1 protein caused disruption of the YSL in the gastrulating embryo. We wished to address the behavior of the other two important migrating cell layers at this stage; the DEL and the EVL. In wild-type embryos, the outer EVL and the inner DEL undergo epiboly, and these layers maintain association with the YSL during migration. The EVL is attached to the yolk membrane via adherins connections, and actin microfilaments are enriched at the marginal EVL/YSL junction, which may aid in towing the EVL down over the yolk as the YSL undergoes vegetal movement (Cheng et al., 2004; Holloway et al., 2009; Lachnit et al., 2008; Shimizu et al., 2005). The DEL is not physically attached to the other two layers, but uses the EVL as a migration surface, and is associated with the EVL via E-cadherin. Since we knew that loss of CACNβ4.1 protein disrupts the YSL, we wondered if the movements of the EVL and DEL also required presence of CACNβ4.1 during epiboly. To examine this, we simultaneously injected wild-type embryos at the 1 cell

stage with both the two CACNβ4.1 morpholinos and also Sytox nuclear label, which marked all nuclei in the developing embryos (Figure 3.2). We injected a control group at the 1 cell stage with just Sytox dye so wild-type nuclear distribution could be observed. As epiboly progressed, in the wild-type embryos we observed the band of YSN at the leading edge of the migrating cells, consistent with the previous experiment (Figure 3.2). The EVL and DEL nuclei of the wild-type embryos were evenly distributed over the blastoderm, bordered by the YSL. These nuclei were spaced out so that none were directly adjacent to one another (Figure 3.2). In the CACNβ4.1 morphant embryos, the YSL was disrupted but the other two cell layers were comparable to wild-type at this stage (Figure 3.2). We observed that nuclei appeared to be evenly distributed, without aggregation, and appeared to move towards the vegetal pole at similar rates throughout early epiboly in CACNβ4.1 morphants. Therefore during early epiboly, nuclear distribution and layer maintenance was disrupted in CACNβ4.1 morphants, but this was not apparent in the DEL and EVL. We concluded that CACNβ4 is not required for efficient cell division in the DEL or EVL during early epiboly.

As an additional test of the hypothesis that disruption of CACNβ4.1 translation in zebrafish embryos via morpholino knockdown results in specific disruption of the YSL which eventually leads to failure of epiboly (Figure 3.1), we examined YSN in CACNβ4.1 transgenic animals. We created transgenic embryos (described later) expressing CACNβ4b-GFP fusion protein. As these germline transgenic embryos expressed GFP endogenously in all nuclei before the MBT, we injected transgenic CACNβ4b embryos with our morpholinos and observed the phenotype (Figure 3.3). Even in wild-type embryos the leading edge of the migrating cells in the EVL was not

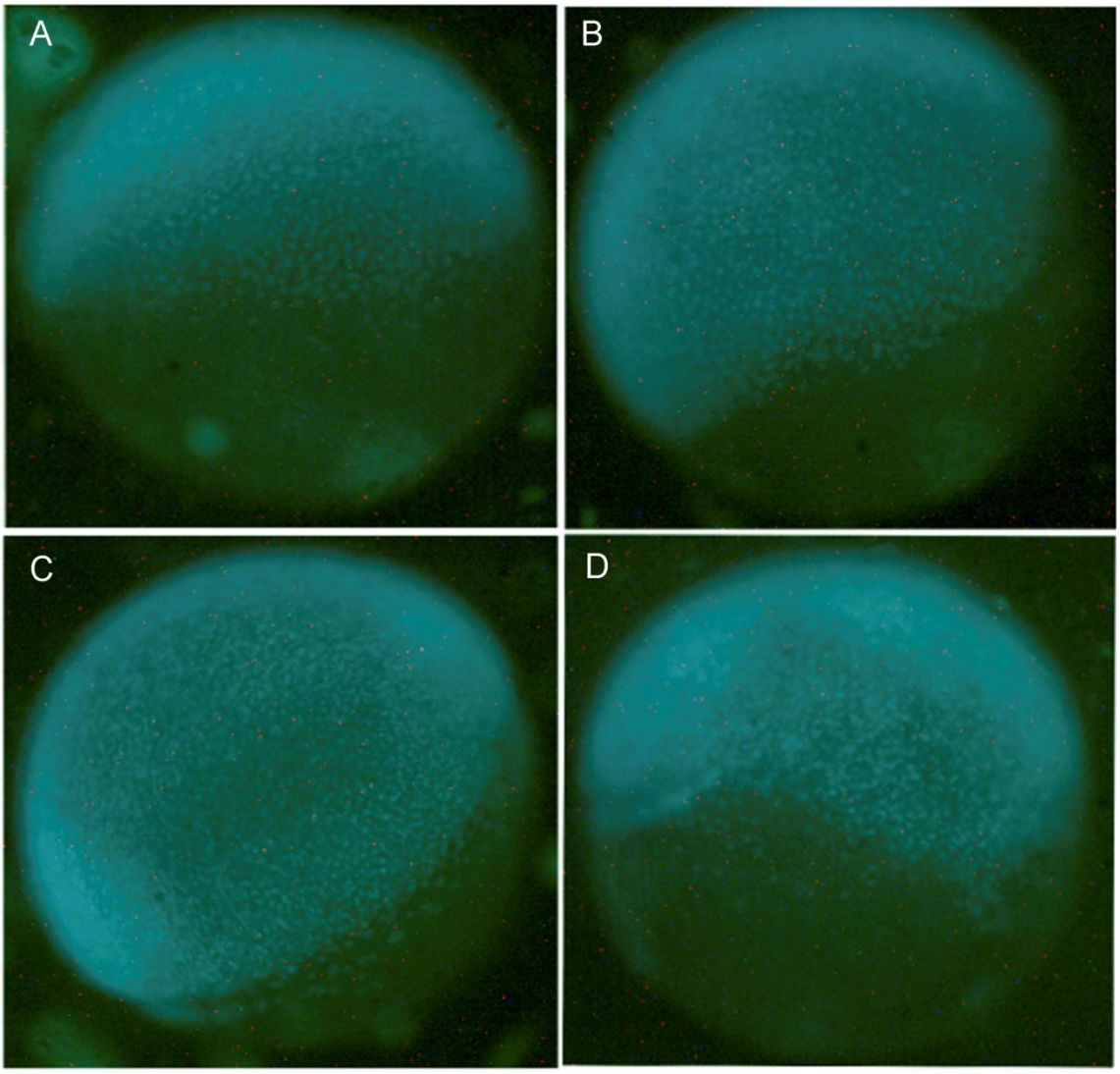


**Figure 3.3: *Tg[β-actin:β4b-GFP]* embryos injected with MO have YSL phenotype**. *Tg[β-actin:β4b-GFP]* embryos were injected with morpholinos targeting CACNβ4.1. At 30% epiboly, (A) transgenic un-injected embryos and (B) MO-injected transgenic embryos collectively have a similar, somewhat wavy margin. However at 50% epiboly, (C) transgenic un-injected embryos and (D) MO-injected transgenic embryos look very different. In (C) the leading margin has now flattened; YSN are migrating toward the vegetal pole slightly ahead of the DEL and EVL. In (D) the blastoderm margin is uneven, and the YSL nuclei are distributed much more randomly. Images were taken at 144X magnification.

perfectly uniform. However, blastoderm cells did migrate at an overall similar rate, resulting in defined margin of the blastoderm cap although the migrating edge itself is not perfectly flat. We observed the marginal EVL cell layer in our wild-type embryos at 30% and 50% epiboly, respectively. At 30% epiboly, the morpholino-injected embryos phenotypically resembled the un-injected transgenic control embryos. They both had a wavy but regular distribution of migrating cells. Nuclei were evenly spaced and cell division appeared normal. However, by 50% epiboly, these morphant embryos displayed YSL phenotypes that were consistent with our previous data of CACNβ4.1 morpholino injected embryos stained with Sytox at the 1000 cell stage (Figure 3.1 and 3.3). Morphant embryos exhibited nuclear aggregation, distribution to the vegetal pole, and did not maintain a connected layer. Due to the YSL defect, the migrating cell layers appeared that they were not uniform compared to the wild-type distribution of cells shown in the *Tg[β-actin:β4b-GFP]* embryo. However, the EVL and DEL nuclei still maintained good spatial distribution, and they continued to be associated with the leading YSL. These results are consistent with our previously described data, and demonstrated that the disruption of CACNβ4.1 results in YSN that are aggregated and unevenly distributed around the circumference of the embryo during early epiboly.

*During late epiboly, migration of all cell layers is disrupted in CACNβ4.1 morphants*

We performed fluorescence-labeling of actin on wild-type and CACNβ4.1 morphant embryos prior to 12 hpf to further examine the patterns cell migration that are exhibited by cells of the blastoderm margin in the absence of CACNβ4.1. Although the YSL nuclei were disorganized in the morphants, as described in the previous section,

nuclear staining techniques did not allow us to adequately assess whether DEL migration was normal throughout epiboly due to interference of background fluorescence from Sytox dye in the EVL and YSL layers. When these Sytox-injected morphant and wild-type embryos were fixed and stained with Alexa488-phalloidin, which labels peripheral actin, we observed abnormal cell shape in the marginal EVL of morphants at later stages of epiboly. To assess the changes in cell shape of these marginal EVL cells as epiboly progresses, we labeled embryos with Alexa488-phalloidin alone as to diminish interference from the Sytox nuclear label (Figures 3.4 and 3.6). Previous studies showed that as epiboly approached 75%, marginal EVL cells lengthen along the anterior/posterior axis and become constricted at their width (Lachnit et al., 2008). To quantify the differences in cell shape as epiboly progressed, we imaged ≥10 embryos each of morphant and wild-type embryos at several stages of epiboly (30%, 40%, 50%, 60%, 70% and 80%). Using ImageJ, we measured the width and length of ~9 individual marginal EVL cells per embryo, and determined the length/width ratio for each cell as a way to evaluate how columnar the cells were (Figure 3.5). Up until 60% epiboly, we found no significant difference in the wild-type and morphant marginal EVL cell shape. However at 70% epiboly, by which time the morphants exhibited slowed epiboly, we found that the marginal cells did not become columnar as do wild-type embryos (Figure 3.4). Based on the length/width ratio, wild-type marginal cells showed a significant difference in cell shape from 60% to 70% epiboly (ANOVA of wt embryos, $p<<0.001$). This result reflected a gradual elongation of marginal cells along the animal/vegetal axis during the latter third of epiboly. In morphant embryos, the rounder morphology of cells at 30% epiboly was maintained through 70% epiboly. A gradual elongation began in the

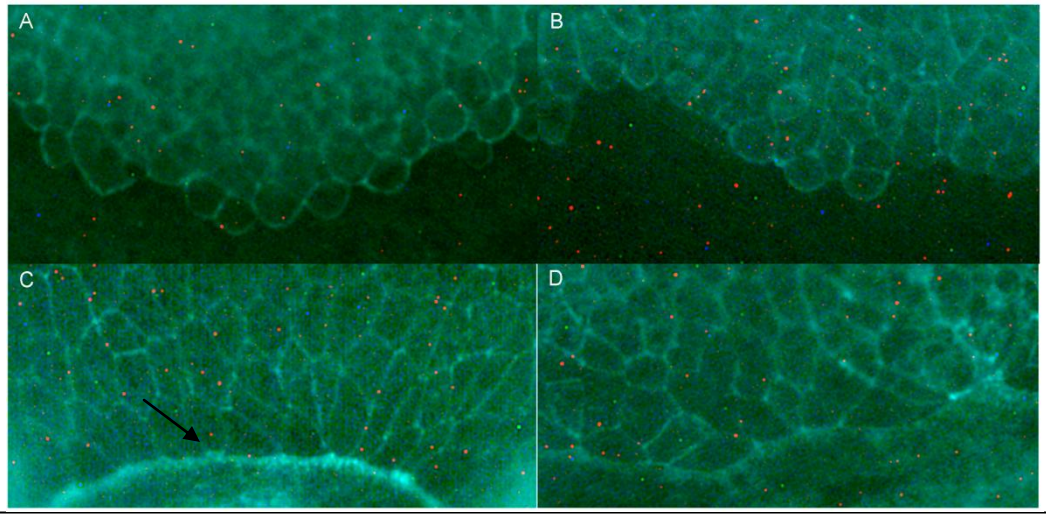


**Figure 3.4: Marginal EVL cells do not change shape normally as epiboly progresses in β4.1 morphants.** Embryos were visualized with Alexa488-phalloidin to mark cell margins. At the blastoderm margin, (A) wild-type and (B) CACNβ4.1 morphant cells at 30% epiboly have similar round cell shapes, and collectively the margin of migrating tissue is uneven. (C) wild-type embryos at 70% epiboly have marginal EVL cells that elongate, and have an evenly circular actin ring (arrow) at the rim, while (D) CACNβ4.1 morphant embryos at 70% epiboly have cells at the margin that do not elongate and actin ring is present but not evenly circular. Images were taken at 144X.

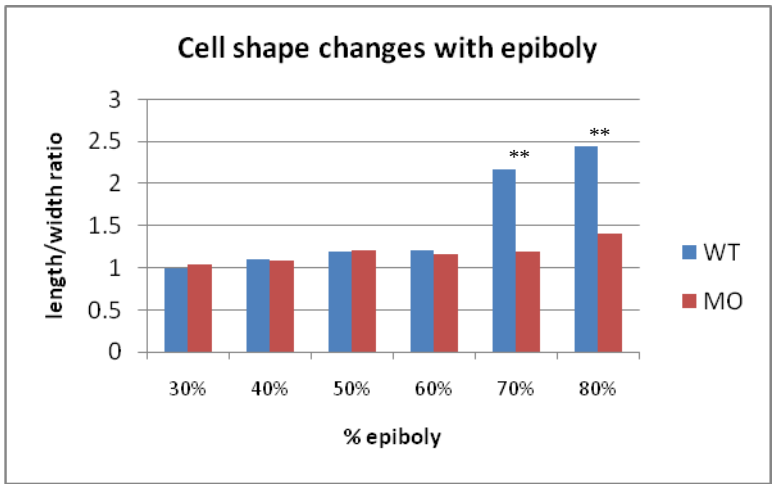


**Figure 3.5: Quantitative analysis of changes in cell shape of the marginal EVL cells**. Embryos were stained with Alexa488-phalloidin to visualize cell margins. For each stage in epiboly progression (30%-80%) we measured width and length for ≥83 marginal EVL cells using the ImageJ program (measurements in pixels), and determined the length/width ratio for each cell, for both un-injected embryos [WT] and CACNβ4.1 morpholino-injected [MO] embryos. This graph represents the average ratio for each stage with the standard error shown. ANOVA analysis reveals significant difference among groups for both WT and MO with p-values of 3.54021E-57 and 0.000223, respectively. Student's t-tests comparing WT and MO gave a p-value of 3.04127E-12 at 70% epiboly and 1.69348E-11 at 80% epiboly, verifying a significant difference between the two groups at these stages.

morphants by 80% epiboly (ANOVA of morphant embryos, $p<0.001$). We observed highly significant differences in wild-type and morphant embryo marginal cell shape at 70 and 80% epiboly (student's t-tests with p values $<< 0.001$). We conclude that CACNβ4.1 is required for the marginal EVL cells to elongate and constrict appropriately in the latter third of epiboly.

We next investigated the uniformity of blastoderm migration in early epiboly and the subsequent migration of the EVL and DEL at later stages of epiboly. In wild-type embryos, the migrating cell margin appeared wavy as the cells were not migrating exactly uniformly down the yolk (Figure 3.6), but by 70% epiboly actin had accumulated at the margin in cooperation with the YSL (Carvalho et al., 2009; Cheng et al., 2004; Hsu et al., 2006; Koppen et al., 2006; Solnica-Krezel and Driever, 1994; Zalik et al., 1999). Cheng et al. (2004) proposed that once they form at 50% epiboly, actin structures help drive the completion of epiboly by constricting the border of migrating cells in a purse-string fashion (Cheng et al., 2004). The underlying DEL maintains a connection with the EVL so that both layers complete the migration to the vegetal pole evenly and together (Schier and Talbot, 2005). In the CACNB4.1 morphants, we observed a broad, uneven gap between the phalloidin-labeled leading edges of the EVL and the DEL at late stages in epiboly (Figure 3.7). In the morphants, the cell margin was comparable to wild-type up to 60% epiboly, but at later stages epiboly slowed relative to wild-type. The shape of EVL cells at this stage did not change, as just described. The actin ring was present in the morphants but had not formed evenly around the circumference of the embryo, presenting a wavy look (Figures 3.6 and 3.7). Actin rings were detectable in some morphants but missing in others. In addition, CACNβ4.1 morphant embryos had a wider

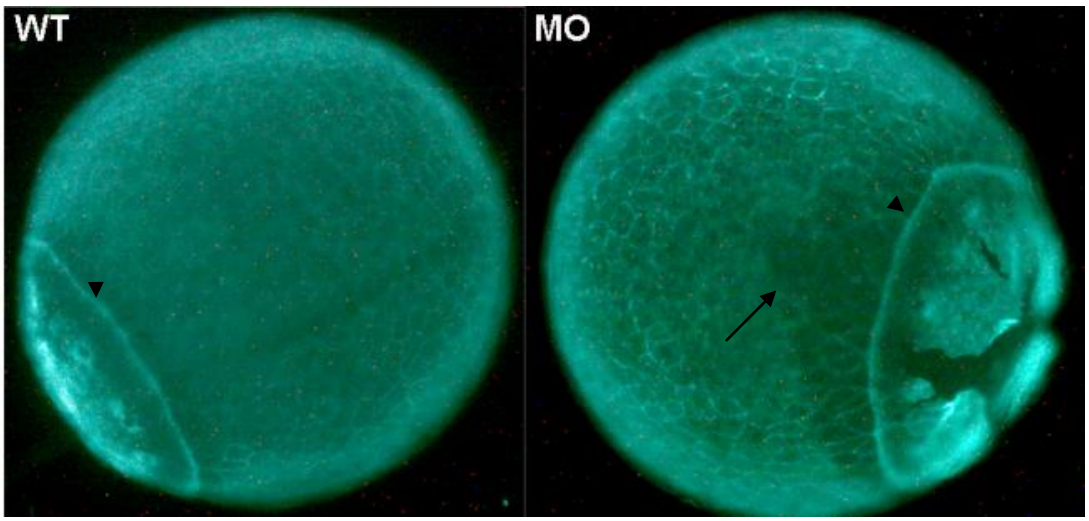


**Figure 3.6: β4.1 morphants display a wide gap between migrating cell layers.** Embryos were labeled with Alexa488-phalloidin. The WT image was taken at 70% epiboly, whereas MO image was taken at 80% epiboly for age-matched comparison. The marginal edge of the EVL is at the bright actin band (arrowheads), and the above area of less intense staining marks the edge of the DEL (arrow). Images were taken at 144X.

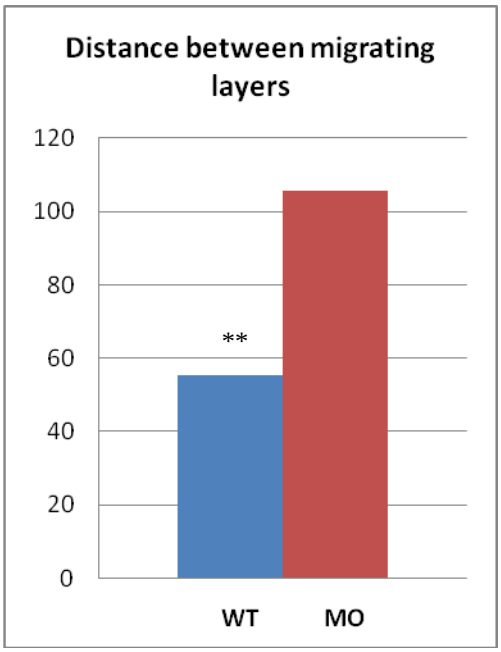


**Figure 3.7: β4.1 morphants have a wider gap, on average, between the migrating EVL and the migrating DEL than wild-type embryos**. Un-injected WT embryos and CACNβ4.1 morpholino-injected embryos were visualized with Alexa488-phalloidin to analyze cell margins. Using ImageJ, we measured the distance (in pixels) between the edge of the EVL and the edge of the DEL at five different points for each embryo to find the average. We measured 10 WT embryos at 70% epiboly and 10 MO embryos at 80% epiboly in order to age match the delay in epiboly seen in the MO embryos, and this graph represents the average with standard error shown. A t-test confirms a significant difference between the two groups with a p-value of 0.000107.

and less uniform gap between the migrating EVL and the migrating DEL when compared with wild-type embryos (Figure 3.7). To quantify the differences between morphant and wild-type embryos in regards to the distance between the two migrating layers, we used ImageJ to measure the EVL:DEL gap at 5 places along the margin and averaged this distance (Figure 3.7). We compared wild-type and morphant embryos at stage-matched 70% epiboly (morphant embryos were 1 hpf older than wild-type embryos to stage-match, due to the delay in epiboly seen in the morphants). We found that as epiboly progressed, the EVL and DEL margins were statistically more widely separated in morphant embryos compared to wild-type embryos. Thus both EVL and DEL migration was slowed in CACNβ4.1 morphants, and the layers became inappropriately separated over time.

Lachnit et al. (2008) recently showed that zebrafish embryos mutant for transcription factor *pou5f1* displayed severe gastrulation defects due to an epiboly delay phenotype (Lachnit et al., 2008). Homozygous mutant *pou5f1* embryos displayed slowed deep cell migration, which contributed to a subtle gap between the migrating EVL and deep cell layers that widened as epiboly progressed. Furthermore, the marginal EVL cells of the morphants had delayed cell elongation as compared with wild-type at the later stages of epiboly. CACNβ4.1 morphants showed a similar phenotype to *pou5f1* mutant embryos. Lacnhit et al (2008) proposed that a lack of *pou5f1* results in changes in adhesive properties of the cells that may account for the slowed migration of DEL on EVL and YSL substrates (Lachnit et al., 2008). Likewise, the role of CACNβ4.1 in completion of epiboly could involve the interactions between the EVL and the DEL.

*CACNβ4.1 localizes to the nucleus in mosaic transgenic embryos*

To further characterize the role of CACNβ4.1 in zebrafish epiboly, we wanted to determine the sub-cellular localization of the β4.1 protein. In order to accomplish this, we created mosaic transgenic embryos expressing GFP-tagged β4.1 constructs in several cells all throughout the body of the developing fish. Using the Gateway Cloning technique, we created four different plasmid constructs containing all or part of the CACNβ4.1 gene fused in frame with the GFP coding sequence, under the control of the ubiquitously expressed β-actin promoter. These constructs promote GFP-tagged CACNβ4.1 expression in all types of cells. In order to examine the sub-cellular localization of both isoforms of the CACNβ4.1 gene, we used injection constructs containing the full length β4a or β4b gene (Figure 3.8). Wild-type embryos were injected with the construct of choice along with RNA encoding the enzyme transposase in order to randomly incorporate the transgene into the genome. After injection at the 1 cell stage, in cells that had incorporated the construct, we observed GFP signal in the cell nucleus by 50% epiboly (Figure 3.9), as well as cytoplasmic GFP signal in EVL cells. Nuclear expression was not expected because the best characterized role for CACNβ4 is as an auxiliary subunit found in L-type calcium channels, which would predict expression associated with the cell membrane (Colecraft et al., 2002; Dai et al., 2009; Dolphin, 2006; Obermair et al., 2008). Nevertheless, our nuclear localization data is consistent with other recently published articles showing that CACNβ4 localizes to the nucleus in cultured cells from other model organisms in development.

The function for CACNβ4.1 is best characterized as an intracellular adaptor protein for voltage gated calcium channels (Colecraft et al., 2002; Dai et al., 2009;

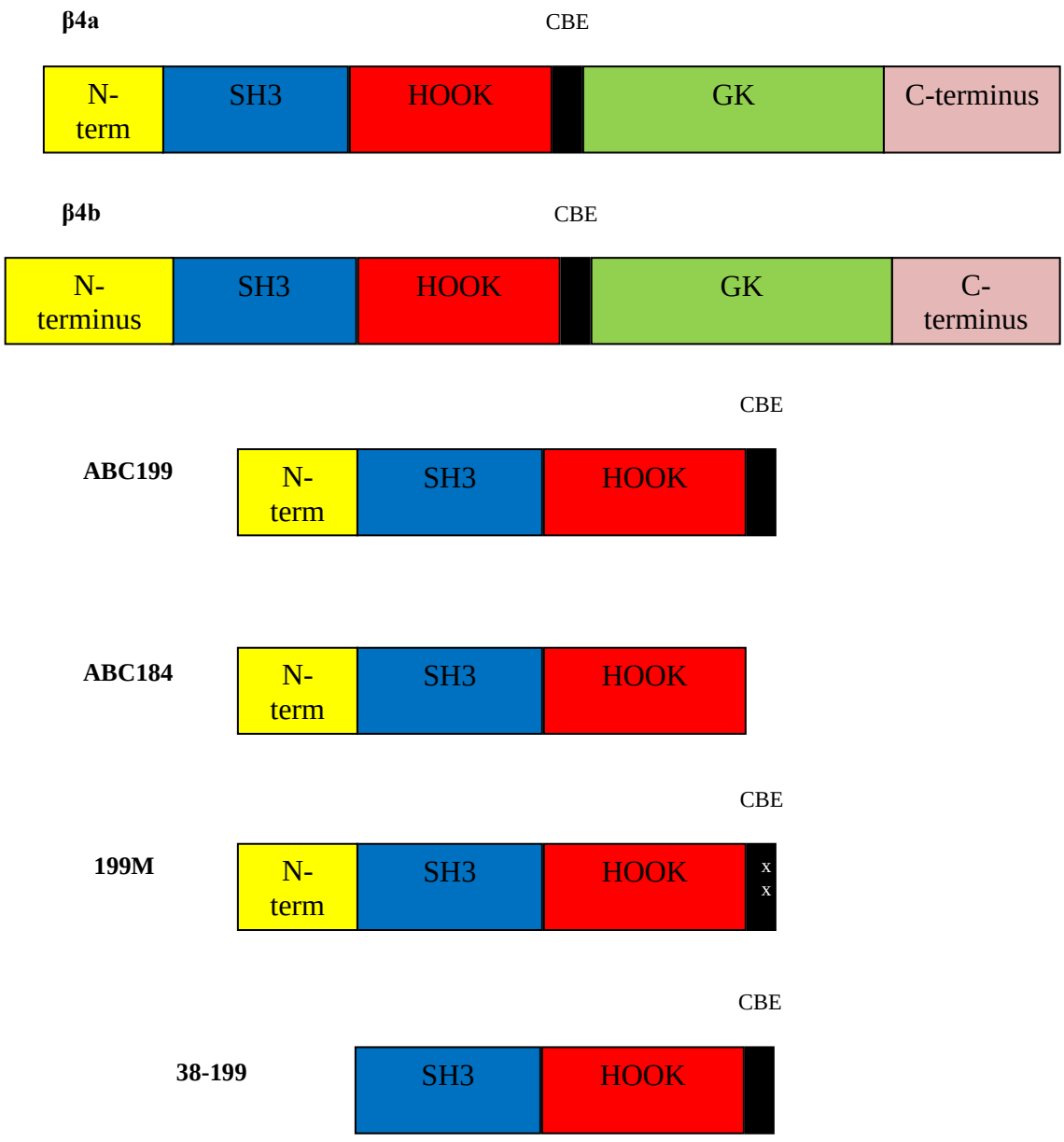


**Figure 3.8: Full-length β4 proteins contain five modular domains.** The core domain includes the SH3, HOOK (CBE) and GK domains. The domains included in the truncated β4 constructs are shown above. The 199M construct contains two point mutations in the CBE domain, indicated as xx.

Dolphin, 2006; Obermair et al., 2008). At 24 hpf in our mosaic transgenic embryos, we observed GFP expression of β4.1 constructs (Figure 3.8, described below) in the nucleus as well as the cell membranes in peridermal cells surrounding the yolk, which are large flat cells convenient for imaging (Figure 3.10). However, we observed similar nuclear expression in multiple types of differentiated cells such as myocytes, peridermal, neuronal and cardiac cells. After creation of the mosaic transgenics, we confirmed nuclear localization of the β4.1-GFP signal by co-labeling the nuclei (DNA) with Hoechst stain, and confirming that these signals overlap (Figure 3.11).

We next analyzed which protein domains of the β4 protein are necessary for nuclear localization. The wild-type CACNβ4.1 contains a variable N-terminus, a conserved SH3 adaptor domain, a linker HOOK domain followed by a conserved GK domain and a variable C-terminus (Figure 3.8). The beta subunit interacts with the alpha subunit via the GK domain. Between the HOOK and GK domains is a small region called the chromoshadow binding element (CBE). The CBE would bind chromobox family proteins, which have proposed functions in transcriptional repression, cell cycle regulation and chromatin remodeling (Ruddock-D'Cruz et al., 2008). We desired to know which of these domains are required for CACNβ4.1 nuclear targeting.

To determine which protein domains are necessary for CACNβ4.1 nuclear localization, we created plasmids containing GFP coding sequence fused to truncated versions of CACNβ4.1 coding sequence. 'ABC184' spans amino acids 1-184 and contains the N-terminus, the SH3 domain and the HOOK domain. 'ABC199' spans amino acids 1-199 and contains the N-terminus, the SH3 domain, the HOOK domain and the CBE. Mosaic transgenic animals injected with either construct demonstrated that the

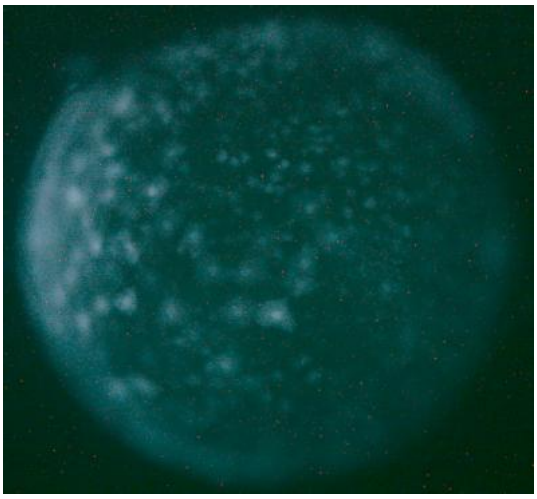

**Figure 3.9: Nuclear GFP expression of β4 constructs is observed by 50% epiboly.** Mosaic transgenic embryos at 50% epiboly injected with β-actin: β4-GFP constructs (β4a, β4b, ABC199 and ABC184) displayed nuclear localization in DEL, and nuclear and cytoplasmic localization in EVL cells. Image is of a β4a-injected embryo, but other constructs result in similar expression. Image was taken at 200X magnification.

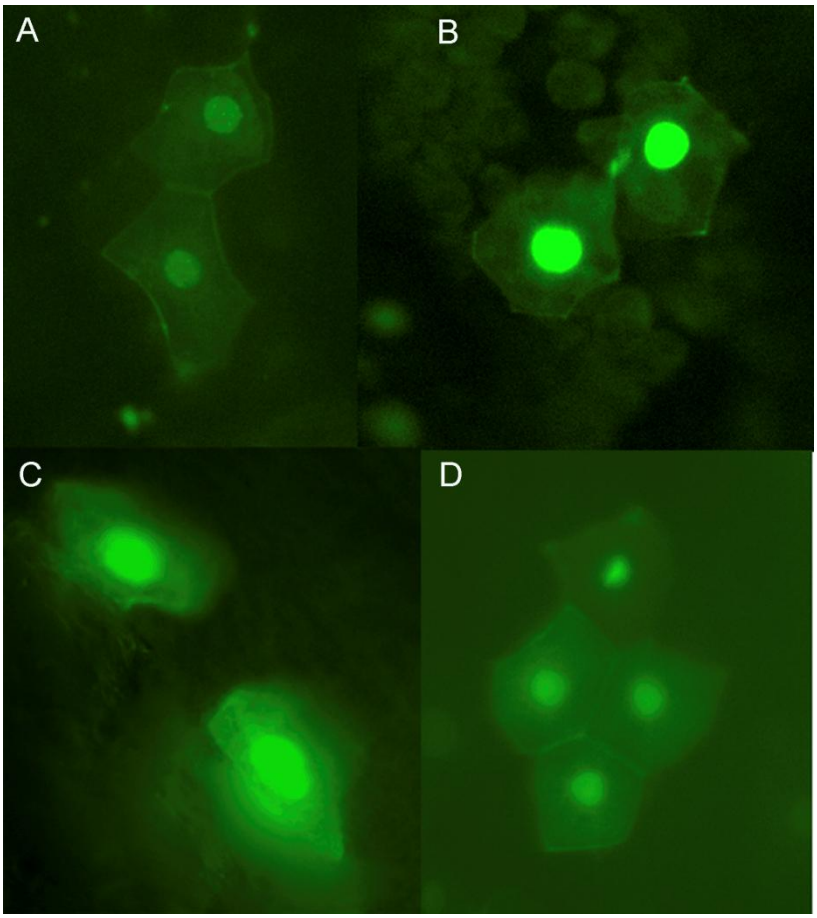


**Figure 3.10: β4.1 mosaic transgenics show that β4.1 constructs localize to the nucleus and the membrane at 24 hpf**. Four constructs of β4.1; two full length constructs of (A) β4a and (B) β4b, and two truncated constructs (C) ABC184 and (D) ABC199; show nuclear and membrane localization at 24 hpf. Images are of peridermal cells and were taken at 400X.

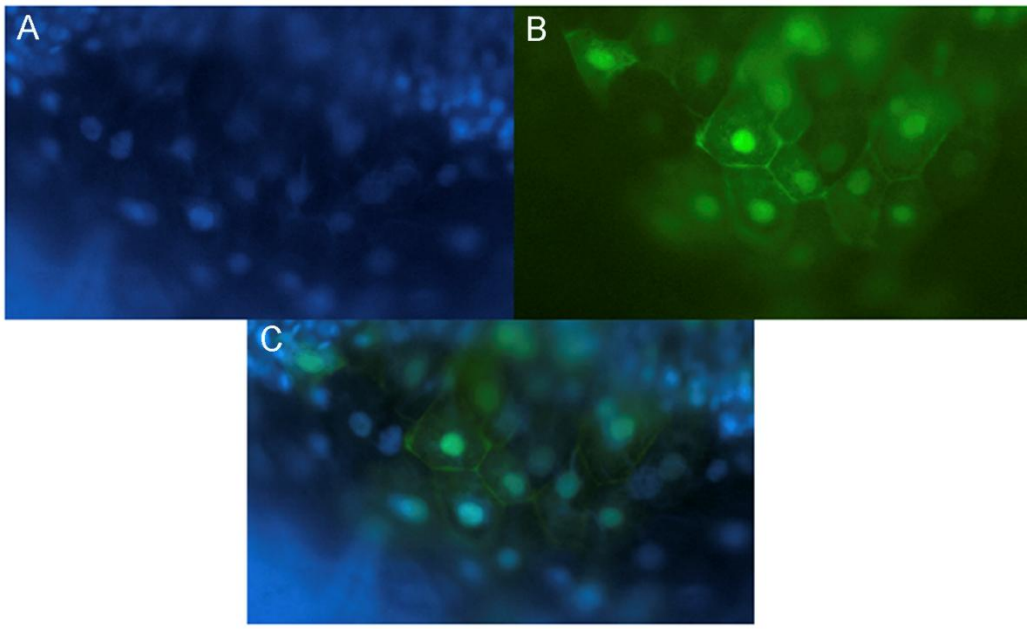


**Figure 3.11: CACNβ4.1 localizes to the nucleus and the membrane in 24 hpf zebrafish embryos.** Mosaic embryos injected with β4.1-GFP construct (B) were stained with Hoechst stain to label the nuclei blue (A). The merged image confirms the nuclear overlap of Hochst and GFP signal. Images were captured at 400X magnification and overlays (C) were made in Adobe Photoshop.

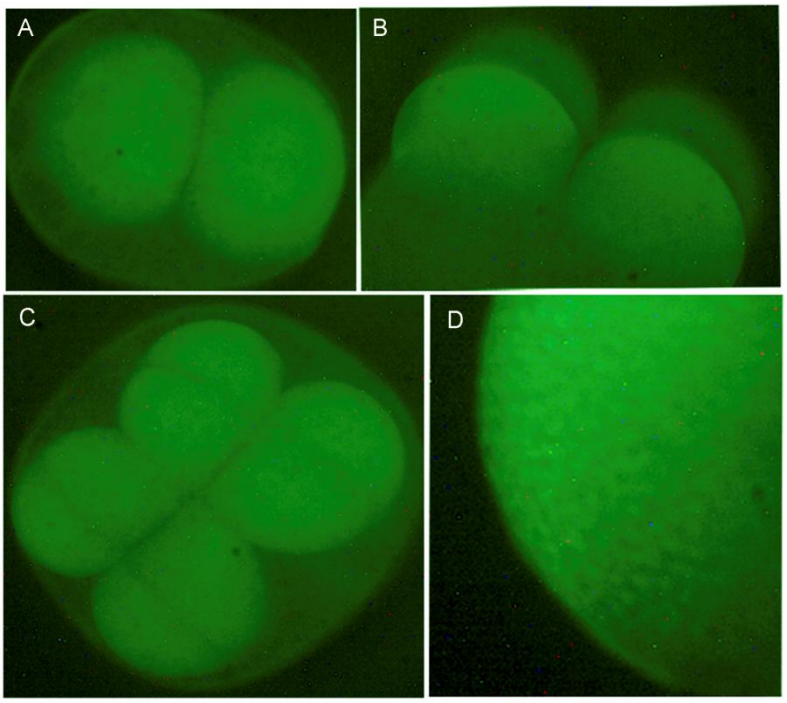


**Figure 3.12: CACNβ4 does not localize to the nucleus during the first few embryonic cleavages, prior to the MBT**. Embryos transgenic for β4b-GFP display diffuse cytoplasmic GFP expression at the (A) 2 cell and (B) 4 cell stages, as well as in cells undergoing cleavage, such as (C) the transition from 4 cells to 8 cells. In contrast, the punctuate nuclear localization occurs by (D) sphere stage. Images were taken at 144X magnification.

fusion proteins localized to the nucleus in all GFP-positive cells (Figure 3.10). In rat and mouse, the N-terminus of β4 is necessary and sufficient for nuclear targeting in nerve and muscle cells (Subramanyam et al., 2009). We observed that all four β4.1-GFP fusion proteins contain an N-terminus and all localize to the nucleus. The CBE domain and/or the GK domain and the C-terminus are dispensable for nuclear localization. Taken together, these data indicate that sequences within the first 184 amino acids of CACNβ4.1 are sufficient for nuclear localization of the β4-GFP fusion protein.

*Germline transgenic expression of CACNβ4.1 reveals further localization data*

We screened for the germline transmission of the transgene from mosaic fish to F1 offspring. We recovered first one β4b transgenic [Tg(β-actin:CACNβ4.1b,EGFP)] female adult and later (on a second generation of fish) obtained one β4a transgenic female adult [Tg(β-actin:CACNβ4.1a,EGFP)].

During cleavage, in both transgenic lines GFP is localized diffusely throughout the syncitial cells and specific sub-cellular localization cannot be determined (Figure 3.12). Expression of the β4-GFP fusion protein was detectable in the nucleus at the dome stage (Figure 3.12). This change in cellular localization after the MBT suggests that zygotically encoded proteins could assist the transport of CACNβ4 to the nucleus.

During epiboly, we observed that the β4b germline transgenic embryos had more intensity in GFP expression than did β4a germline transgenic embryos (Figure 3.13). Confocal microscopy revealed stronger nuclear GFP expression in β4b embryos verse β4a embryos, in DEL, EVL and YSL (Figure 3.14). Although they have these

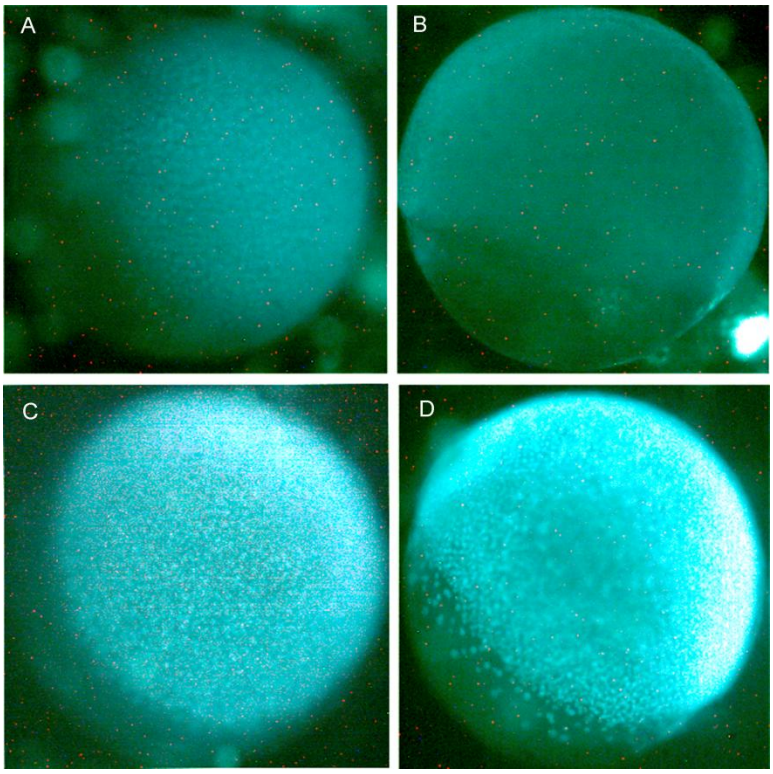


**Figure 3.13: *Tg[β-actin:β4b-GFP]* show markedly more intensity in expression than *Tg[β-actin:β4a-GFP]***. Images at equal magnification of β4a (A,B) and β4b (C,D) transgenics show GFP localization at dome and shield stages of early zebrafish gastrulation. This shows that GFP localization in the β4b stable transgenic line is more intense than the β4a stable transgenic line. Nuclear localization is evident in both. Images were taken at 144X.

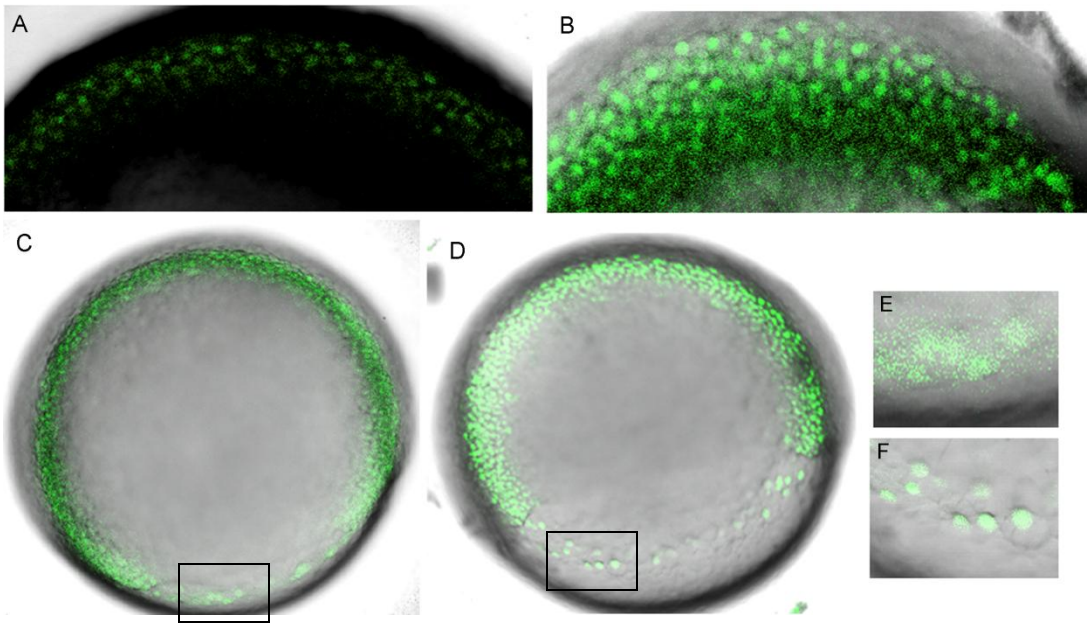


**Figure 3.14: *Tg[β-actin:β4b-GFP]* embryos show strong nuclear localization, whereas *Tg[β-actin:β4a-GFP]* embryos show more diffuse expression**. Confocal microscopy images at 200X magnification show a comparison of β4a (A,C,E) with β4b (B,D,F) at dome (A,B) and shield (D,E) stages of development. Figures E and F show a magnified view (400X magnification) of the YSL layer of nuclei (boxes) at the shield stage, and β4b has more defined and fluorescent GFP localization in the nucleus.

differences, both transgenic lines showed clear nuclear localization during zebrafish gastrulation in the EVL, the DEL and the YSL (Figures 3.13 and 3.14).

Interestingly, by 24 hpf, the β4a transgenic line showed more diffuse GFP expression within the cell compared to β4b transgenic embryos (Figure 3.15). Expression was primarily nuclear but appeared to extend into the cytoplasm as well. Therefore we performed experiments requiring 24 hpf or older embryos on the *Tg[β-actin:β4b-GFP]* line. In mosaic embryos we were able to examine isolated cells making it easier to detect localization near periphery without interference from underlying cells. In the stable transgenics we found that the fusion protein localized to the nucleus of embryonic and non-embryonic cells, as well as in pluripotent vs. differentiated cells of several types, and that expression persists through gastrulation (data not shown).

Since β4.1 localized to the nucleus, we next asked whether it was associated with chromatin specifically. In fluorescently labeled proteins that localize to chromatin, their association can be seen readily during mitosis, when the chromosomes are condensed (Ruddock-D'Cruz et al., 2008). We compared β4b-GFP expression with Tg(H2A:GFP) expression. This line expresses a histone-GFP fusion protein tightly associated with other histone proteins within chromatin structure. Therefore if β4.1 is similarly associated with chromatin, we might expect to see a similarity between GFP expression patterns in these two lines. We examined embryos before the beginning of epiboly when the rate of mitosis is high and there are many cells with punctate GFP expression. H2A-GFP could be seen clearly associating with chromatin present in the metaphase plate. In contrast, β4b-GFP was consistently broadly localized within all nuclei and not restricted

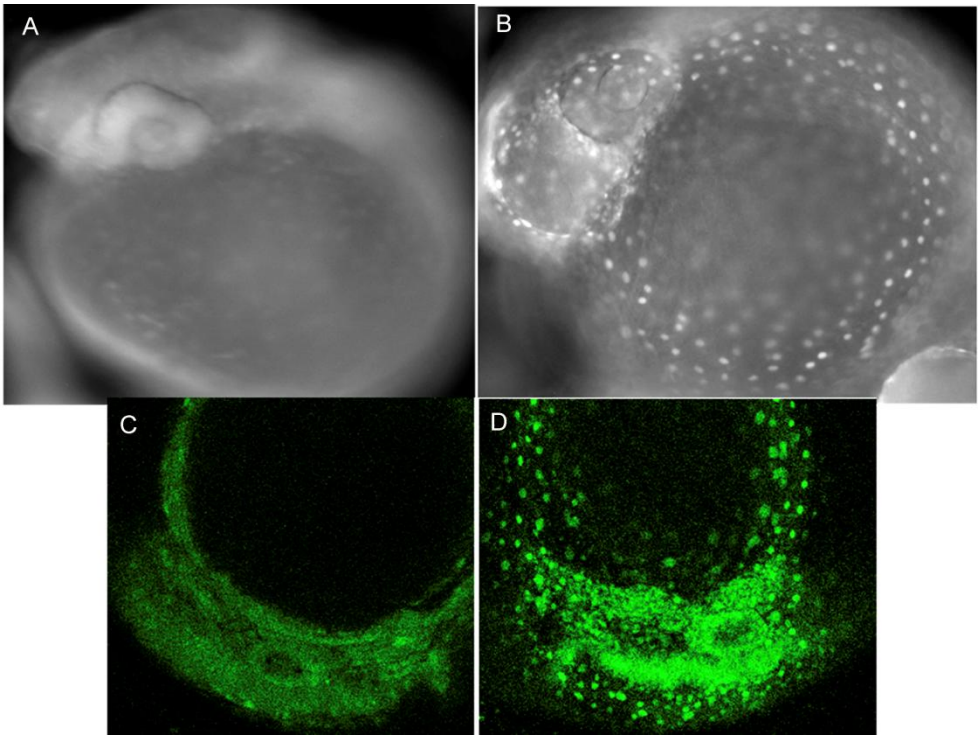


**Figure 3.15: *Tg[β-actin:β4a-GFP]* embryos had GFP localization to the nucleus and the cytoplasm at 24 hpf, whereas *Tg[β-actin:β4b-GFP]* embryos maintain strong localization to the nucleus.** Images taken at 200X on the Leica (A,B) and on the confocal (C,D) show β4b (B,D) maintains strong nuclear localization in all cells while β4a (A,C) has decreased intensity and nuclear localization is not apparent.

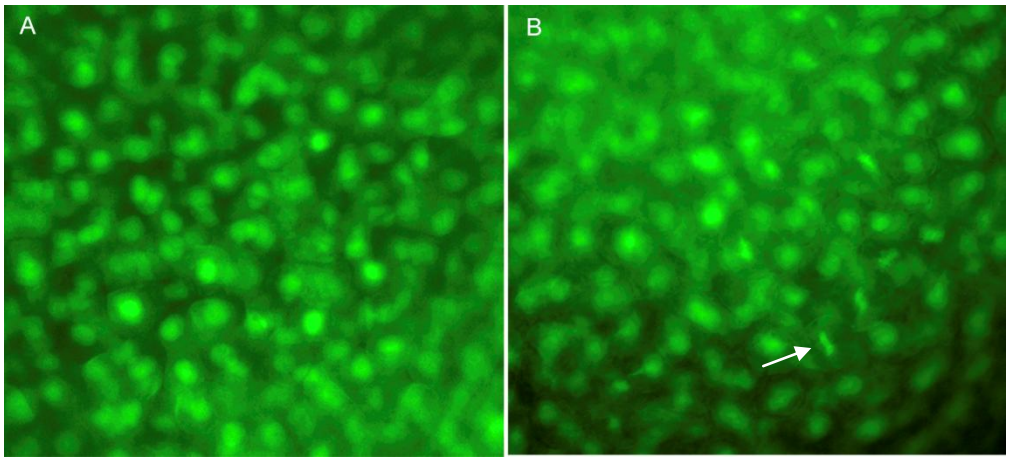


**Figure 3.16: β4b-GFP and chromatin are not exclusively co-localized**. Images taken at 400X of the dome stage of zebrafish gastrulation show the difference between (A) *Tg[β-actin:β4b-GFP]* and B) *Tg[H2A:GFP]* localization. H2A-GFP shows a strong association with the chromatin, which cannot be seen with β4b-GFP. Arrow marks the metaphase plate.

to the metaphase plate (Figure 3.16), suggesting it may not tightly associate with chromatin.

*CACNβ4b-GFP expression is seen in most heart cells and does not change over time*

L-type calcium channels in the heart are responsible for electrical excitement of the cell via calcium influx control (Obermair et al., 2008). Therefore we expected that at least some β4b-GFP in cardiomyocytes would localize to the plasma membrane. As the heart grows, the contractility gets stronger, and electrophysiology changes (Yelon, 2001). Subramayam et al. (2009) showed that in mice, nuclear targeting of β4b is regulated by electrical activity and calcium influx (Subramanyam et al., 2009). To determine whether change in cardiac physiology affected the localization of β4b-GFP, we examined cardiac cells in transgenic embryos from 36 hpf to 72 hpf (Figures 3.17-3.19). We performed heart presses (a technique involving mild compression of the cardiac tube) on transgenic embryos. We determined that most cells are expressing β4b, and this overall number of GFP positive cells, presumably both myocardium and endocardium, does not change drastically over time (Figure 3.17). Upon close examination of β4b cardiomyocytes at 72 hpf, we observed that β4b did indeed localize to the nuclei as well as the cell periphery in the cardiomyocytes (Figure 3.18). In terms of GFP nuclear expression, the electrical maturity of the cell does not appear to be a major influence in degree of nuclear localization of β4b during zebrafish development.

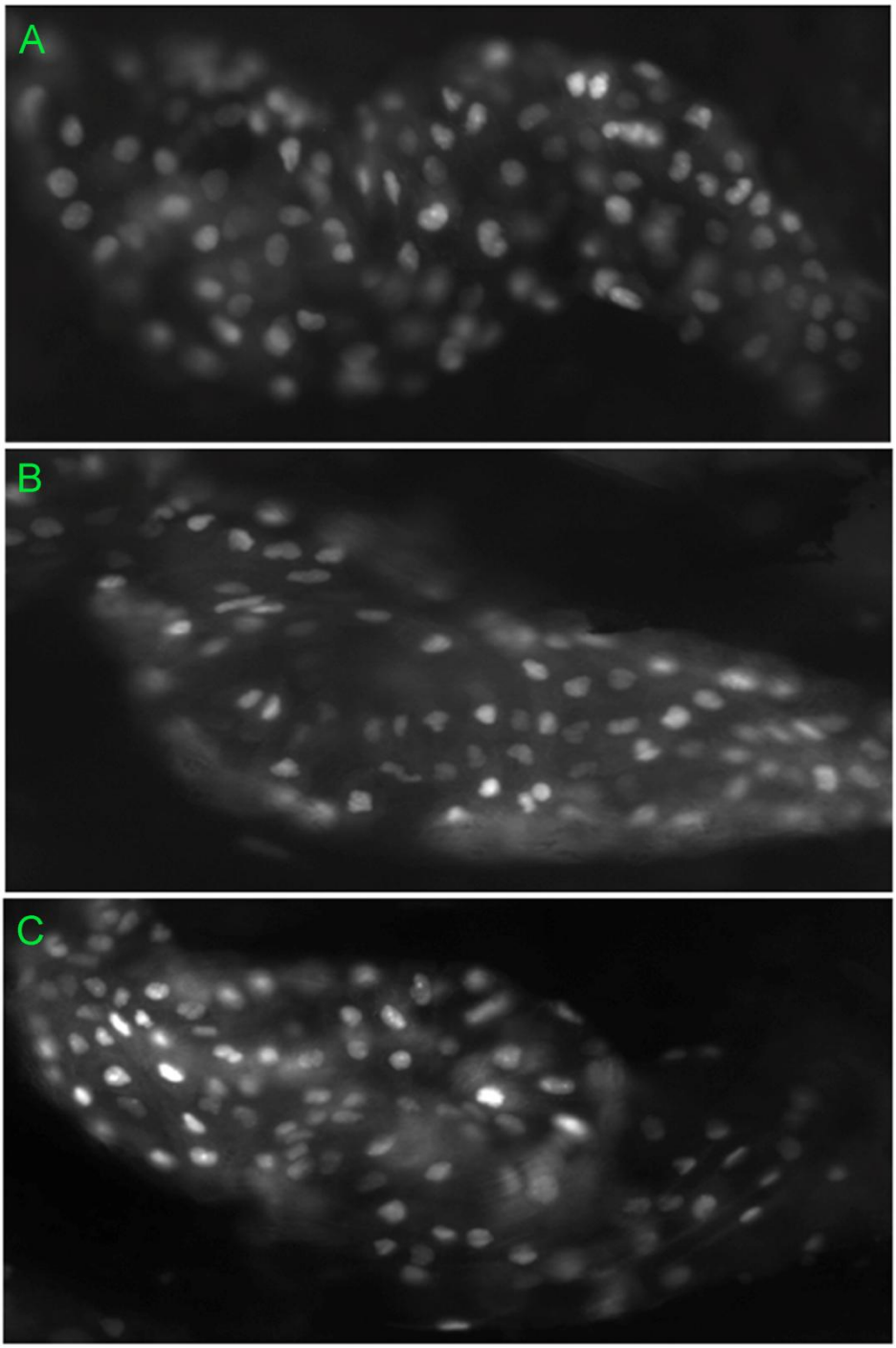


**Figure 3.17: Heart expression of β4b-GFP remains consistently nuclear over time**. Heart presses of *Tg[β-actin:β4b-GFP]* fish hearts at (A) 36 hpf, (B) 48 hpf and (C) 72 hpf reveal that GFP is localized in the nucleus of nearly all cells in the heart. The sub-cellular localization did not change significantly as heart morphology changed and as the hearts matured electrically. Images were taken at 400X magnification.

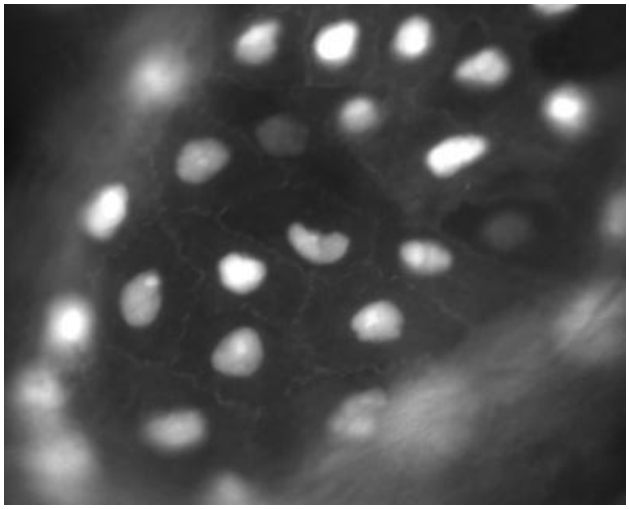

**Figure 3.18: β4b-GFP protein is localized near the membrane of 72 hpf zebrafish hearts**. Before the 72 hpf stage, β4b-GFP localization in the heart is limited to the nucleus, but by 72 hpf it is also associated with the membrane. Image was taken at 400X magnification.

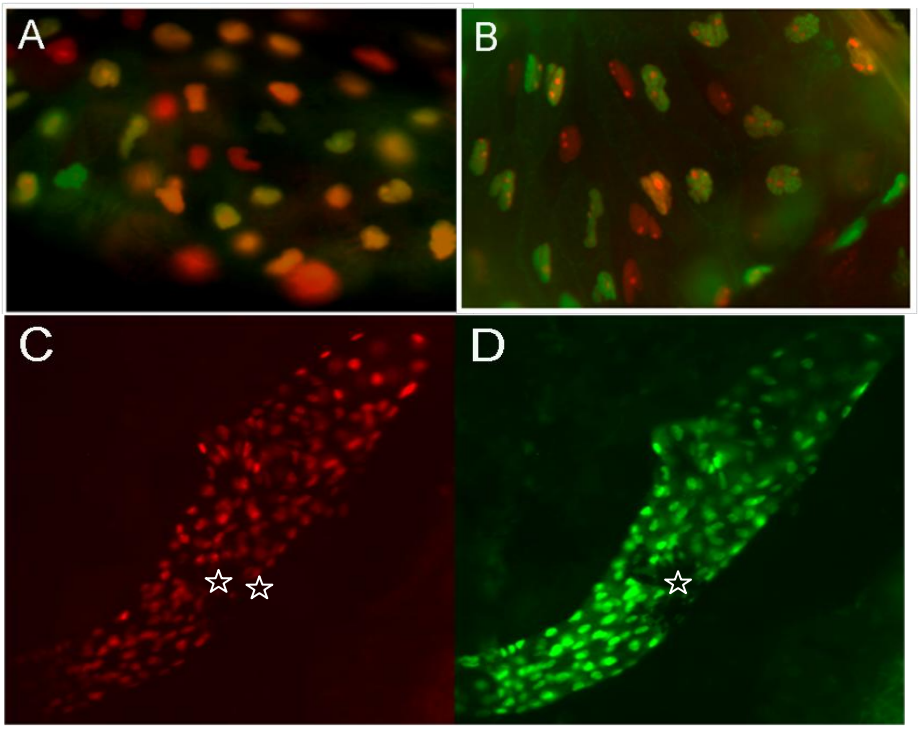


**Figure 3.19: β4b is expressed in most, but not all, nuclei in the heart**. (A and B) Overlayed images of Tg[β-actin:β4b-GFP,cmlc2:dsRed] fish at 72 hpf show red nuclei where β4b-GFP is not being expressed. Orange nuclei show co-localization, and nuclei that appear green are due to GFP intensity being greater than dsRed. Images A and B are of two different transgenic fish. Side by side comparison of these transgenics indicating (C) ds-Red (what is the nucleus designation here) localization (TRITC) and (D) GFP localization (FITC) also shows nuclear localization in most cells in the heart. White star marks a melanocyte blocking fluorescence. Images were taken at 400X.

The next question we wanted to address was whether or not β4b-GFP was expressed in every cell in the heart. The β-actin promoter is expected to actively drive transcription in all myocardial and endocardial cells. In practice, we observed that in *Tg[β-actin:β4b-GFP]* most cardiac cells expressed GFP, but possibly not all. To evaluate the nuclear localization in myocardial cells specifically, we bred *Tg[β-actin:β4b-GFP]* fish to Tg(cmcl2:dsRed) fish to create Tg[β-actin:β4b-GFP,cmlc2:dsRed] that have both green and red fluorescence in myocardial cell nuclei. We generated heart presses and imaged these fish at 72 hpf because cmcl2:dsRed expression cannot be detected until 72 hpf with our microscope. Overlayed images of these two proteins at 72 hpf show that β4b was expressed robustly in some cells while expression in others was absent or below detection (Figure 3.19). Some cells were green without apparent red expression which could represent nuclear expression in non-myocardial cells.

*N-terminus and CBE domains of CACNβ4.1 are necessary for epiboly function*

Now that we knew CACNβ4.1 is necessary for completion of epiboly, we wanted to determine which structural domains of the protein are required to perform its function during development. In order to answer this question, we performed a series of rescue experiments with different constructs in collaboration with Dr. William Horne's lab in Cornell, NY. We used two morpholinos that target the fifth exon splice site of CACNβ4.1 together for a synergistic effect. Morpholino injection caused lethality in about 75% of embryos as a result of CACNβ4.1 knockdown. Addition of 40 ng/µl of full length β4a RNA reduces the lethality to approximately 25% of injected embryos.

Embryo death due to failure of epiboly caused by the morpholino knockdown was rescued with wild-type β4a RNA, which demonstrated that this phenotype is specific to loss of the CACNβ4.1 proteins.

To analyze the protein domains necessary for its role in epiboly, Dr. Horne's lab created two RNA constructs encoding the truncated proteins ABC199 and ABC184. ABC199 contains the N-terminus, SH3, HOOK, and CBE domains, and upon injection also rescued the epiboly phenotype and reduced lethality to approximately 30% of injected embryos. We used a RNA concentration of 80 ng/µl to achieve rescue with the truncated constructs. For β4a rescue experiments, we used a concentration of 40 ng/µl, but equivalent rescue is also seen at a concentration of 80 ng/µl. The other truncated RNA construct, ABC184, ends at the 184$^{th}$ residue and contains the N-terminus, SH3 and HOOK domains, but not the CBE domain. Injection of this construct reduced lethality of injected embryos only to approximately 60%, which is not a significant difference between from morpholino injection alone (Figure 3.20). Although ABC184 can localize to the nucleus (Figure 3.9), it does not have the domain necessary to rescue epiboly. These experiments suggest that the chromoshadow binding element domain is needed for CACNβ4.1 to function in the embryo during epiboly.

In order to determine a potential binding partner for CACNβ4.1, we investigated whether any of several chromobox genes found in the genome are expressed in early development in zebrafish. The chromoshadow binding element is thought to bind chromobox proteins, which have two conserved domains, chromodomain and chromoshadow domain, which interact with histones and chromatin

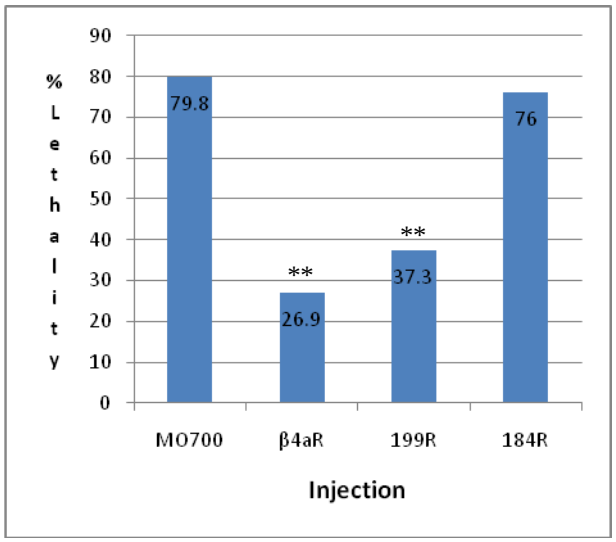


**Figure 3.20: Chromoshadow binding element (CBE) required for rescue of epiboly**. We injected embryos with β4.1 MOs alone or together with synthesized human full length or truncated CACNβ4a RNA. The Y axis indicates the percentage of death by 24 hpf due to embryo lysis from lethal disruption of epiboly. ANOVA analysis defines a p value of 1.3E-05, demonstrating significant differences among groups.

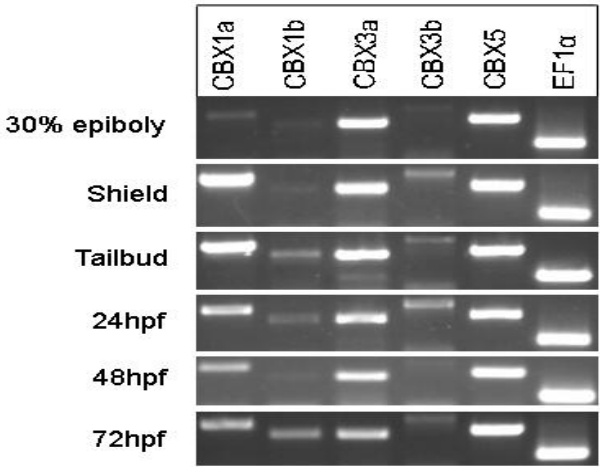


**Figure 3.21: Multiple chromobox family proteins are expressed in the early zebrafish embryo.** RT-PCR analysis on extracted RNA from different developmental stages reveals that multiple CBX genes are expressed during epiboly. EF1a is a ubuqitous control RNA. [Data from Maricarmen Perez].

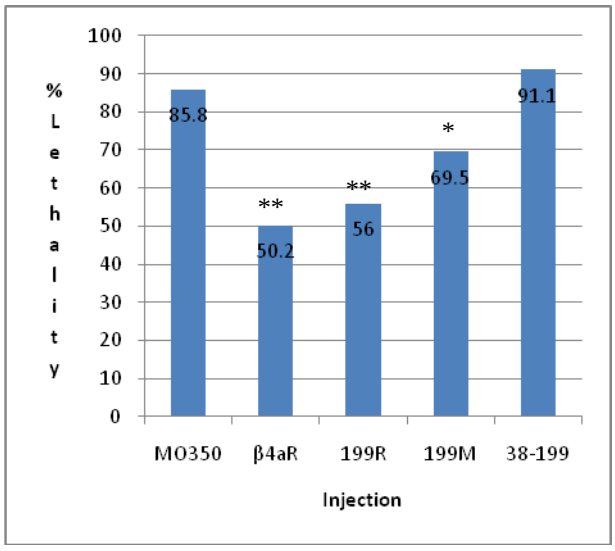


**Figure 3.22: Analysis of protein domains required for rescue of epiboly in β4.1 morphants.** We injected embryos with β4.1 MOs alone or together with human full length or truncated CACNβ4a RNA. Embryos counted as % lethality if they died prior to 24 hpf. ANOVA analysis defines a p value of 0.000515, indicating significant differences between the groups.

(Hibino et al., 2003; Jones et al., 2000; Ruddock-D'Cruz et al., 2008). In zebrafish, five chromobox proteins are presented in genomic databases [www.ncbi.org and genome.ucsc.edu], but their expression and functionality have not yet been studied. To analyze expression of these genes during zebrafish development, we extracted RNA from various stages of developing embryos and performed RT-PCR using primers specific to each of the five CBX genes. Maricarmen Perez, an REU student in summer 2009, found that two chromobox genes are expressed during early epiboly, and at least three of them are expressed after the mid-blastula transition at shield stage (Figure 3.21). Since several chromobox genes are expressed during zebrafish epiboly, it is possible that CACNβ4.1 interacts with one or more of these proteins in the nucleus.

In collaboration with William Horne we designed two constructs to test the functionality of the CBE domain. Chromobox proteins interact with specific sites of the CBE domain (Hibino et al., 2003; Jones et al., 2000; Ruddock-D'Cruz et al., 2008; Vendel et al., 2006). The first construct was a version of ABC199 RNA with two point mutations in two amino acids within the CBE ('199M') in putative binding sites. The second RNA construct only contained residues 38-199. In order to do these rescue experiments, we established a desired morpholino dose of 175 mM of each morpholino (new batch) was sufficient to obtain a high percentage of severe epiboly defective embryos. The control injection mix of each morpholino and rhodamine dye resulted in approximately 90% lethality (Figure 3.22). Co-injection of 40 or 80 ng/µl of β4a RNA reduced lethality to approximately 50% of injected embryos, and ABC199 rescue mix generated approximately 55% lethality. Injection of the 199M RNA with morpholino reduced the rescue effect by about half, generating approximately 75% lethality. The 38-

199 residue RNA injection mix resulted in approximately 90% lethality, showing no difference in injection of morpholinos alone. The 199M RNA injection data supported the hypothesis that CACNβ4.1 is interacting with chromobox proteins to perform its necessary function during epiboly. Rescue attempt with the 38-199 RNA, which contains the complete CBE domain but lacks the N-terminus shows that the N-terminus is critical for CACNβ4.1 to perform its epiboly function. Since the N-terminus contains a nuclear localization signal (Vendel et al., 2006), one possible explanation is that the encoded protein from amino acids 38-199 does not localize to the nucleus. Therefore our data suggests the hypothesis that during epiboly CACNβ4.1 interacts with other proteins via the CBE, and that its ability to localize to the nucleus is likely to be a critical aspect of its function.

# Chapter 4: Discussion

**Discussion**

The major findings of this study are that CACNβ4.1 localizes to the nucleus and requires the CBE domain to facilitate completion of epiboly in *Danio rerio*. Loss of CACNβ4.1 protein in zebrafish embryos disrupts the YSL, and embryos exhibit defects in later epiboly. These defects include irregular, lagging DEL cell migration and marginal EVL cells that do not constrict and elongate as occurs in WT embryos. Taken together, these results demonstrate a role for the CACNβ4.1 protein in proper cellular arrangement and completion of epiboly. Through analysis of β4a and β4b transgenics, we determined GFP sub-cellular localization in the nucleus in all cells, once the MBT has been completed. Nuclear localization still occurred consistently for truncated products lacking the CBE domain, GK domain, or the C-terminus, indicating these domains do not contain required nuclear localization signals. However, rescue of morpholino-induced defects in epiboly is only accomplished with RNA constructs containing the CBE domain, indicating this domain is essential for the normal function of β4 in promoting epiboly. Thus, our data support a role for β4 proteins involving interaction with chromoshadow domain-containing proteins in the nucleus, and substantiate our finding that β4 is required for early zebrafish development.

Our findings also suggest a requirement for the YSL cytoskeletal architecture during zebrafish epiboly. Trinkhaus discovered that YSL epiboly occurs in the absence of the blastoderm cap, via studies in the related teleost *Fundulus heteroclitus* (killifish) (TRINKAUS, 1963). Phenotypes of mutant or morphant embryos with microtubule, microfilament or E-cadherin disruption resemble CACNβ4 morphants (Cheng et al., 2004; Shimizu et al., 2005; Solnica-Krezel and Driever, 1994; Zalik et al., 1999).

Solnica-Kretzel and Driever (1994) described the microtubule networks that are established in accordance with the YSL and are required for epiboly (Solnica-Krezel and Driever, 1994). Nocodazole-induced disruption of the microtubule network blocks YSL migration, and causes failure of YSL epiboly, and slowed DEL/EVL epiboly. It is possible that the subsequent epiboly phenotypes in CACNβ4 morphants arise due to a disruption in the YSL microtubule networks.

Another possibility is that CACNβ4 regulates different processes involving actin or E-cadherin. Actin is recruited to cell margins of migrating EVL cells and two distinct rings of actin form between the DEL/YSL and EVL/YSL during late epiboly (Cheng et al., 2004). Disruption of the actin microfilaments via cytochalasin B leads to slowed or stopped epiboly, failure of yolk cell occlusion and eventual lysis of the embryo. E-cadherin is required for adhesion between deep cells. Zebrafish mutants of E-cadherin exhibit failed DEL migration and delayed EVL/YSL epiboly (Kane et al., 1996; Shimizu et al., 2005; Wagner et al., 2004). A recent study by Lachnit et al. (2009) uncovered a transcription factor *Pou5fl/Oct4* involved in maintaining cell pluripotency (Lachnit et al., 2008). Loss of this protein leads to severely slowed DEL epiboly, EVL cells that do not constrict properly, failure of epiboly and death of the embryo. It is possible that CACNβ4 is acting in a similar manner to regulate production of proteins required for epiboly, specifically in the establishment and maintenance of the YSL.

Recent findings present alternative roles for β proteins, including a role in gene regulation. Colecraft et al. (2002) showed nuclear localization of a β4-GFP fusion protein using adenovirus to transfect cultured adult rat heart cells (Colecraft et al., 2002). Our data of β4-GFP expression in *Danio rerio* presents nuclear localization in whole

organisms. Hibino et al. (2003) showed that β4c localized to the nucleus in transfected chick cochlear cells (Hibino et al., 2003). They also confirmed direct interaction of β4c with chromobox protein 2 (CHCB2) via a yeast two hybrid assay. Using the GAL4-CAT reporter assay, they determined that the protein interaction of β4c and CHCB2 decreases gene silencing activity. Our findings are consistent with these data in an alternative nuclear role for β4 in multiple vertebrate organisms. Future work remains to identify the downstream gene activation of β4 protein interactions with chromobox proteins, whether regulation is limited to a few genes or is more global.

Knowledge is rising in the scientific community about the protein domain interactions of nuclear proteins. To elucidate the nuclear function of CACNβ4, we wish to understand the protein domains required for β4 function, including nuclear import/export and protein interactions. Subramanyam et al. (2009) demonstrated that CACNβ4b is targeted to the nucleus via a NLS in the N-terminus, and localization is influenced by CACNα1 expression (Subramanyam et al., 2009). They expressed plasmids coding for C-terminally V5-tagged β4b in a mouse mutant line null for the CACNα1s gene, and observed β4b nuclear localization that is diminished by addition of a plasmid coding for the alpha subunit. Further studies of CACNβ4 in zebrafish should include morpholino knockdown of the α1 subunit in transgenic β4 embryos. Our previous data with the CACNβ4-3X mutant RNA morpholino rescue shows that interaction with the alpha subunit is not required for epiboly completion in zebrafish. A calcium channel independent role of developmental control could be determined via further information on the protein interaction domains of the CACNβ4 protein.

These findings raise some exciting new questions about the mechanisms of CACNβ4 function, including examination of β4 protein mobility. One hypothesis is that the β4 proteins are targeted specifically to two separate locations, the nucleus or the plamsa membrane (cortex), and once localized there, perform a particular function. Another possibility is that the β4 proteins dynamically shuttle from the plasma membrane to the nucleus (or vice versa), via specific nuclear localization sequences (NLS) and nuclear export sequences (NES) sequences, and function both in the nucleus and in the membrane. For example, Gao et al. recently (2008) described the Dapper (Drp) protein, which negatively influenced the Wnt/B-catenin pathway in transfected HeLa cells (Gao et al., 2008). Drp shuttles between the nucleus and the cytoplasm, and treatment with leptomycin B (which blocks nuclear export), caused Drp protein to accumulate in the nucleus. In another example, Bit-Avragime et al. (2008) identified two NLS and one NES in a tight junction MAGUK-family protein, Nagie Oko, which is required for cell polarity and epithelial cell integrity in zebrafish embryos (Bit-Avragim et al., 2008). In mammals, zona occulans proteins are scaffolding proteins that have dual roles in cell surface adhesion and gene regulation. These MAGUK family proteins have NES and NLS and shuttle to and from nucleus (Bauer et al., 2010). CACNβ4 is also a MAGUK family protein with dual roles in the membrane and in the nucleus. Subramanyam determined that electrical activity influenced nuclear shuttling of β4b (Subramanyam et al., 2009). Information about nuclear shuttling of proteins involved in gene regulation is useful for understanding the role of calcium channel beta proteins in vertebrate development.

A limitation to our study is determining the influence of the GFP protein on the cellular localization of our fusion proteins. Unmodified GFP protein is small (28 kDa), and localizes uniformly within the cytoplasm (Yang et al., 1996). Due to the small size of GFP it can localize to the nucleus without a NLS. In contrast, β4 localizes to two specific places by 24 hpf; the membrane and the nucleus. It remains unknown whether β4 proteins shuttle to and from the nucleus and the membrane. A future experiment to determine specific β4 cellular trafficking could involve blocking nuclear import of CACNβ4-GFP via a drug or mutation of NLS sequence. GFP alone would still diffuse to the nucleus if nuclear import is blocked, confirming that β4-GFP is targeted specifically to the nucleus, not influenced by the presence of GFP. Experimenting with nuclear export in addition could elucidate the concept of CACNβ4 nuclear shuttling.

Exciting new knowledge about multiple functions for CACNβ genes increases our understanding of the molecular complexity of channel auxiliary proteins. Mutations in CACNβ4 cause ataxia and epilepsy, as this gene plays an important role in neuronal function. Uncovering the precise cellular function of CACNβ4 in the nucleus would allow for development of drug targets to block the harmful effects of these mutations. Furthermore, our studies of CACNβ4 examine the function of chromobox proteins during development, which remains not well understood. Through developmental studies of CACNβ4 in zebrafish we can achieve a higher understanding of the intricate and vital processes that establish the vertebrate body plan.

# Chapter 5: Materials and Methods

## Materials and Methods

*Animal care*

All zebrafish were fed brine and flakes daily, and babies consumed Ziegler's liquid diet as well. Babies joined the fish facility in no-flow water at 6 days after fertilization. They were given slow flow at 10 days old and started eating brine and flakes at 2 weeks old. Fish became old enough for breeding between 3-4 months old. We replenished fish lines and humanely euthanized old fish aged 2 years, or when they stopped laying eggs. TL and WIK were the two wild-type lines used. The TL line produced all Tg[β-actin:β4.1-GFP] fish and wild-type fish used for microinjection. Transgenic fish purchased from the Zebrafish Model Organism Database (www.zfin.org), including Tg[H2A:dsRed], Tg[H2A:GFP], were created in a TL background and maintained by outcrosses in the WIK background. Our Tg[cmcl2:dsRed] and *p53* -/- mutant fish lines were bred in a WIK background. Therefore the Tg[H2A:dsRed, β-actin:β4b-GFP] fish had both a TL and WIK background, as did the Tg[cmlc2:dsRed, β-actin:β4b-GFP] embryos used for heart press imaging. Special thanks to Kristin Artinger for sending two adult *p53* -/- fish for use in morpholino injections, since these fish provided a decrease in non-specific death (Robu et al., 2007). In accordance with the Animal Care and Use Committee, we administered the anesthesia Mesab to all fish prior to certain procedures. These procedures included before fixation with PFA or Methanol, euthanization via ice bath and for certain experimental protocols such as heart presses.

*Screening transgenic lines*

After creation of CACNβ4.1 mosaic transgenic embryos for β4a-GFP, β4b-GFP, ABC184-GFP and ABC199-GFP under control of the β-actin promoter, we grew fish to 4 months old before they were screened for germline transgenesis. We screened adult fish by breeding them to each other and checking for any progeny with GFP fluorescence. To determine which parent was the transgenic one, we next bred them individually to wild type fish. From approximately 50 fish, we found one germline Tg[β-actin:β4b-GFP] female. We outcrossed this female to a wild type TL male and obtained 17 transgenic females and 3 transgenic males (which should all be heterozygous for the transgene). These fish were bred to each other to obtain a stable line homozygous for the transgene. Similarly, injected β4a-GFP mosaic transgenics were grown and from about 36 adults, we found a single germline Tg[β-actin:β4a-GFP] female. Her offspring were also bred to each other to create a homozygous line. We screened approximately 30 'BaG' fish (potential Tg[β-actin:GFP]) but we recovered no transgenic fish. Based on these results, the overall rate of transgenesis in our lab was less than 5% efficiency in contrast to 50% efficiency reported by Kawakami (2004) (Kawakami and Noda, 2004).

*Dechorionation and fixation of embryos*

Wild-type un-injected embryos can be dechorionated using pronase, and enzyme that degrades the proteins that make up the chorion. For this procedure, 2 ml of 20 μg/ml pronase (Roche, catalogue # 10165921001) was added to one petri dish of embryos and the dish swirled every thirty seconds until the first chorions started coming off (after about 5 minutes). We then immediately transferred the embryos into a 500 ml beaker

containing 200 ml of fresh embryo water. The embryos were swirled and allowed to settle to the bottom, then the water was decanted and fresh water added. This process was repeated about 5-7 more times until almost all the embryos had lost their chorions. Since pronase will damage embryos if they are directly exposed to it, any injected embryos must be dechorionated manually using tweezers. After dechorionation we then fixed them. For most protocols, embryos were fixed in 4% PFA overnight at 4°C or 2 hours at room temperature (note: we routinely fixed for 4 hours at room temperature for embryos aged less than 12 hpf), followed by three five minute washes in 1X PBT. Embryos can be stored in 1X PBT at 4°C for up to a week or put into cold 100% methanol and stored indefinitely at -20°C. Embryos can be fixed directly in methanol, but GFP or dsRed proteins cannot survive methanol fixation (note: the dsRed protein cannot survive PFA fixation, and thus experiments with this line were performed on freshly euthanized embryos). If embryos were fixed in methanol, for experiments such as *in situ hybridization*, they had to be rehydrated slowly using several methanol/PBT washes where methanol concentration is decreased in increments with each wash.

*Microinjection*

First, using the Narishige needle puller (heat:715, velocity: 80, pull: 60, time: 200) we created injection needles out of Kwik-Fil Borosilicate glass capillaries (World Precision Instruments, Inc.; item number TW100-6). In preparation for injection, we clipped the needle tip, loaded ~2 µl of liquid (morpholino, rhodamine dye, RNA, Hoechst stain, SYTOX green nucleic acid stain or 1X Danieu's buffer) into the back of the needle, and placed it into the Narishige Microinjector. We collected embryos just after

fertilization and aligned them in an injection plate (2% agarose dissolved in 1X TAE buffer), which had grooves in the agar that were used to position embryos. We microinjected using the Eppendorf FemtoJet so that each embryo received amount of liquid that filled approximately $1/6^{th}$ of the total volume of the embryo. The 4-cell stage was the oldest stage of embryo used for these experiments. To mark only YSL nuclei, we injected green Sytox dye into the yolk at the 1000 cell stage, since by this time blastomeres have become separated from the yolk by cell membranes (Solnica-Krezel and Driever, 1994). After injection, embryos were recovered in embryo water in a 29°C incubator, and later (around the beginning of epiboly) they were scored under fluorescent light and we removed any inadequately injected or unfertilized embryos.

*Morpholino/RNA injections*

For the morpholino injections to deplete CACNβ4.1 function in the embryo, we used two morpholinos in conjunction to increase knockdown efficiency, since single morpholino injections generated less than 20% severely affected embryos. Morpholino #14 targeted the CACNβ4.1 exon 5 donor site, and its sequence was: TCTCTATCTGCTTACCCTTGTACTC. Morpholino #16 targeted the CACNB4.1 exon 5 splice acceptor site, and its sequence was: AACTTCTGCATATGGAGAAGAAAGG. Experiments to examine dose response indicated that the dose of 350 nm of each morpholino (175nm of each morpholino from new stock) was optimal and therefore this dose was used in all subsequent experiments. We synthesized rescue RNA using DNA plasmid templates containing the human sequence for CACNβ4, which targets zebrafish CACNβ4.1 and CACNβ4.2, following the protocol found in the *RNA probe making*

section (see below). Dr. William Horne's lab in Cornell, NY created truncated RNA constructs used for rescue injections. Control embryos were injected with rhodamine dye diluted in 1X Danieu's buffer.

*Sytox injections*

We injected embryos with a 1:100 dilution of Sytox green dye (5 mM stock diluted in 1X Danieu's buffer) at the 1000 cell stage for visualization of YSL nuclei only, and imaged at the sphere stage. We injected embryos at the 1-cell stage to label all deep cell as well as YSL nuclei, allowing us to image migrating cell layers during epiboly.

*Fluorescent Microscopy*

Three different microscopes were used to take fluorescent images. In our lab (the lab of Dr. Deborah Garrity in the department of Biology at CSU) we used the Olympus SZX12 stereomicroscope with an Insight Digital CCD camera, magnification of 144X. In the lab of Dr. Steven Stack, also department of biology at CSU, we used the Leica DM5500B microscope under 400X magnification. In the Pathology building at CSU we used the Zeiss Axio Observer microscope with associated LSM 510 confocal equipment, magnifications of 200X and 400X. The FITC filter was used to visualize GFP (green spectrum), the TRITC filter was used to visualize dsRed (red spectrum), and the DAPI filter was used to visualize Hoechst (blue spectrum).

*Phalloidin staining and computer analysis*

For labeling the cell periphery, we used Alexa Fluor 488 phalloidin (Invitrogen, catalogue #A12379), eluted in 1.5 ml 100% methanol, which labeled the actin associated with cell membranes with green fluorescence. Embryos were dechorionated and fixed in 4% PFA, washed in PBT, then suspended into *in situ* block (composed of 49 ml 100% PBT, 1 ml Sheep serum, and 0.1 g BSA) overnight at 4°C. The next day they were suspended in the phalloidin solution for 1 hour in the dark (foil) at room temperature, washed in PBT, and imaged. The computer programs Adobe Photoshop and Image J provided the technology for analysis of the length and width of individual cells in the marginal EVL. The images were enlarged and brightened in Adobe Photoshop and cell width and length measurements were drawn on the images and analyzed in pixels using Image J software. Utilization of both the Sytox and phalloidin protocols allowed visualization of the cell nuclei and membranes, respectively.

*Hoechst Staining*

To visualize nuclei we first prepared a 0.1 mg/ml solution by dissolving dry Hoechst powder (Polysciences, Inc., catalogue #9460) into 1X PBT. A 1:100 dilution of this stock also worked adequately and stained quickly. Dechorionated embryos were fixed in 4% PFA (see *Dechorionation and fixation of embryos* section), washed with three five minute PBT washes, and suspended in Hoechst/PBT dilution. The tubes of embryos in Hoechst solution were wrapped in aluminum foil (since this staining must be done in the dark) and incubated for ten minutes at room temperature, followed by at least three five minute PBT washes, then imaged.

*Heart presses and imaging*

Mesab-treated embryos were placed individually on a glass slide, and the water absorbed with a KimWipe, careful not to touch the fish with the paper. Then embryos were gently crushed by laying a glass cover slip over them. We avoided directly pressing down or moving the cover slip once the fish had been pressed. Images were taken at a magnification of 10X and 40X on the Leica dissecting microscope in the Stack lab. Heart presses provided the highest quality pictures of transgenic fish hearts in terms of being able to see all nuclei in a single plane. Tg[β-actin:β4b-GFP] fish images were taken at 36 hpf and 48 hpf, and Tg[β –actin:β4b-GFP,cmcl2:dsRed] fish images were taken at 72 hpf.

*Other imaging techniques*

To get high-quality images of phalloidin-stained embryos at various epiboly stages, we mounted embryos in a small amount of 4% methyl cellulose to hold them in place. To position fish for photography of hearts at 36, 48 and 72 hpf, we created slices in a 1% agarose gel (made in diH20 and poured in a petri lid) and placing the fish ventral side up in the slices. In this way fish embryos were held in place by the agar with their hearts face-up, and imaged on the Stack microscope at a magnification of 400X.

*Gateway Cloning*

We used the Gateway Cloning technique to create several constructs used for injection for creation of mosaic transgenic embryos, and further breeding that created transgenic lines (see Tol2Kit Protocols online [c*hien.neuro.utah.edu/tol2kitwiki/index.php/Main_Page] for* further information) (Kwan

et al., 2007). All plasmids were derived from Dr. Koichi Kawakami's original plasmids, and were requested from Dr. Chi-Bin Chien at the University of Utah Medical Center in Salt Lake City, Utah. We received the plasmids on paper and eluted them into diH2O for storage at -80°C. All entry vectors were kanamycin/chloramphenicol resistant, and destination vectors were ampicillin/chloramphenicol resistant (for all plasmid sequences, see Tol2Kit website). Destination vectors and entry vectors used in the BP reaction contain a ccdb survival gene, which causes death when transcribed in standard chemically competent *E. coli* cell lines, but can be transformed into ccdb Survival cells (Invitrogen, catalogue #A10460). This ccdb survival gene and the chloramphenicol resistance gene lie between the recombination sites in both types of vectors. In order to ensure these vectors had not self-recombined, they were grown up on ampicillin/chloramphenicol plates.

To begin this project, Alicia Ebert designed primers with specific attenuation sites that matched with entry vector #218 for creation of five different constructs: full length β4a, full length β4b, ABC184, ABC199 and BCDE. The primer sequences are as follows: #211 Beta4a F: GGGGACAAGTTTGTACAAAAAAGCAGGCTCCATGTAT GACAATTTGTACCTGC, #212 Beta4 R: GGGGACCACTTTGTACAAGAAAGCTG GGTAAAGCCTATGTCGGGAGTCAT, #213 Beta4b F: GGGGACAAGTTTGTACA AAAAAGCAGGCTCGATGTCCTCCTCCTCCTA, #214 BCDE F: GGGGACAAGTT TGTACAAAAAAGCAGGCTTAGCATTTGCCGTGAAGAC, #215 ABC184 R: GGG GACCACTTTGTACAAGAAAGCTGGGTGAGGAATGTGCTCCGTCACT, and #216 ABC R: GGGGACCACTTTGTACAAGAAAGCTGGGTCCTCGTAACCTTTCAG

TGACG. She amplified the DNA via PCR and performed gel extraction and DNA clean-up to purify the DNA. She then used the BP reaction (via the BP reaction kit [Gateway, SKU#11789020] following included protocol) to insert the genes into entry vector #218 (pDONR221). We used the LR reaction to create the final plasmid constructs used for injection and creation of transgenic fish. For creation of four of the five β4.1 constructs (excluding BCDE), per 10 µl of LR reaction, the vectors used were: 10 fmoles of the 5' entry vector #299 containing the beta-actin promoter, 10 fmoles of #218 containing the gene of interest, 10 fmoles of the 3' entry vector #366 containing EGFP, and 20 fmoles of the destination vector #394 (using the LR reaction kit [Gateway, SKU#12538120] following included protocol). LR reactions were transformed in TOP 10 cells (Invitrogen, catalogue #C4040-03) for maximum transformation efficiency. For creation of a control plasmid, the gene specific entry vector #218 was replaced with a middle entry vector #383 that was EGFP, so this construct expressed GFP under the control of a β-actin promoter. For creation of a construct for co-localization data that had nucleus expression of a red fluorescence, a three-way LR reaction was performed. For this reaction we used 10 fmoles of #299, 10 fmoles of middle entry vector #233 which contained a nuclear-localized mCherry gene, and 20 fmoles of a destination vector from Lawson, #465. Programs Multalign (http://multalin.toulouse.inra.fr/multalin/multalin.html) and Reverse Compliment (www.bioinformatics.org/SMS/rev_comp.html) aided *in verification of the correct construct.* We injected the plasmid of choice along with 20 ng/µl transposase RNA (transcribed in vitro from vector #396). The transposase will incorporate the promoter:gene-tag fusion construct randomly into the zebrafish genome. Injection of

these constructs produced >50% mosaic transgenics. These potentially germline transgenic embryos were then grown up and bred, and their offspring screened for transgenesis.

*Transformation and Miniprep*

Plasmids were transformed into standard competent cells (Fisher, catalogue #BP4005-3) with the exception of Gateway cloning, for which we used ccdb Survival cells and TOP 10 competent cells (see above). We thawed bacterial cells and plasmids on ice, and then generally added 2 μl of the plasmid to the bacterial cells. We transformed no less than 50 ng and no more than 500 ng of DNA per reaction, but around 300 ng provides a field of colonies. Standard transformation reactions were performed. We inoculated 5 ml overnight cultures for plasmid DNA extraction (minipreps). For glycerol stocks, prior to miniprep we removed 250 μl of the culture and placed it in a 1.5 ml centrifuge tube along with 250 μl of glycerol, and the stock was kept in -80°C. We performed plasmid DNA extraction using the Wizard Plus SV Minipreps and DNA purification System (Promega, catalogue #A1460), following manufactor's instructions, which typically yielded about 2 μg of DNA.

*Primer design*

We used the Oligo Analyzer at the Integrated DNA Technologies website (www.idtdna.com/ANALYZER/Applications/OligoAnalyzer/Default.aspx) to design primers. For verification of constructs created via Gateway Cloning, we designed two unique primers. The first (#244) was a reverse primer designed to recognize the Tol2

destination vector #394 for diagnostic sequencing to verify the presence of EGFP. The second primer (#254) was a reverse primer that bound 97 base pairs upstream of from the base pair 730 in EGFP. We designed this primer in order to sequence across recombination sites and to verify that GFP was fused in frame with the beta4 gene. Both primers had a melting temperature of 60°C and a GC content of 50%. Primer sequences were as follows: #244 Tol2 R: CATGTCTGGATCATCATCGATGGTACCG, and #254 EGFP R: ACACGCTGAACTTGTGGCCGTTTA.

*PCR and RT-PCR*

For reverse transcription PCR, we used a reaction mixture containing 1 µl RNA sample (containing at least 50 ng of RNA, but typically around 200 ng), 1 µl dNTPs, 1 µl reverse primer and 11 µl diH2O for a final volume of 14 µl. The mixture was incubated in the thermocycler at 70°C for 10 minutes to denature the RNA and then held at 4°C for 5 minutes. We then added 4 µl AMV buffer, 1 µl RNase Inhibitor and 1 µl of AMV, then incubated in the thermocycler at 48°C for 45 minutes, 94°C for 2 minutes and 4°C ∞. A 'No RNA' sample in another tube served as a negative control. A program titled "CAS" was modified to fit the experimental parameters controlled the PCR reaction. The PCR reaction is as follows: 94°C for 5 minutes, [94°C for 45 seconds to denature, 60°C for 1 minute to anneal [note: this is just below melting temperature of most primers; 1.5 minutes was used for long primers], 72°C for 1 minute (per every thousand base pairs of sample) to extend] 39X, then 72°C for five minutes and 4°C ∞.

*Agarose Gel electrophoresis*

We separated the PCR products using agarose gel electrophoresis and viewed DNA samples under UV light. The molecular weight marker and positive control was Fermentas DNA Ladder Plus (catalogue #SM1331) ~6 µl per well). Fermentas Loading Dye (1 µl per 6 µl of DNA sample) was added to DNA samples that were not PCR products for proper loading. To each small well, we added 20 µl of sample (or, 50 µl in large wells) and the gels ran at 120V for 30 minutes.

*Restriction Digests*

To analyze plasmid DNA by restriction digestion, we typically set up reactions with 1 µg of plasmid (Note: typically, 5 µg of plasmid was used for probe making, gel extraction or DNA purification processes), 1 µl of restriction enzyme, 1/10 total volume of enzyme-specific buffer and nuclease-free water to a final volume of 20-50 µl. This reaction mixture was incubated at 37°C overnight (note: certain enzymes have star activity, and will begin random cleaving of DNA after 4 hours of incubation – see Fermentas Restriction Endonuclease chart). Digests were heat inactivated at 70°C and/or were stored at -20°C or for 20 minutes

*RNA probe making*

We linearized 5 µg of plasmid DNA for 2 hours at 37°C (see *Restriction Digests* section) using an appropriate restriction enzyme that cut once in the plasmid. We ethanol precipitated the DNA (see *Gel Extraction and DNA Clean-up* section) overnight at -80°C. After centrifugation, the DNA was resuspended in 20 µl diH20 for 1 hour at -20°C or

37°C. The DNA concentration was determined using a nano-spectrometer and/or gel electrophoresis. We synthesized the antisense RNA probe in a transcription mix consisting of: 1 μg linearized DNA, 1/5 total volume transcription 5X buffer, 2 μl NTP-DIG-RNA, 1 μl RNase inhibitor, 1 μl RNA polymerase (T7 or T3) and diH20, then incubated for 2 hours at 37°C (Thisse et. al, 1993). We then added 2 μl RNase free DNAse to digest the DNA template for 15 minutes at 37°C. The RNA was precipitated overnight at -80°C in a solution of 1 μl EDTA (0.5 M pH 8), 2.5 μl LiCl 4 M and 75 μl 100% cold ethanol. The precipitant was centrifuged for 30 minutes at 16 rpm followed by two 70% ethanol washes (5 minute spins). The pellet was then allowed to dry and resuspended in sterile DEPC water. The RNA concentration was brought up to 200 ng/ul using DEPC water.

*In Situ Hybridization*

Standard protocol was used for *in situ* hybridization (Thisse et al., 1993).

*Gel extraction and DNA Purification*

After gel electrophoresis, we used a razor blade to carefully excise the DNA band, visible under ultraviolet irradiation. We used the Zymoclean Gel DNA Recovery Kit (Zymo Research, catalogue #D4001) according to manufacturer's instructions in order to extract DNA from the gel slice. We used one of two methods to purify the DNA; Phenol/Chloroform extraction and/or ethanol precipitation. For Phenol/Chloroform extraction, we routinely brought solutions to a starting volume of 100 μl minimum in diH20. Ethanol precipitation followed this protocol, but was sometimes used alone for

DNA purification. The DNA precipitated overnight at -80°C in a solution of 3 µl GlycoBlue carrier, 1/10 total volume 3 M sodium acetate, and 2.5 total volume cold 100% ethanol added to at least 100 µl of sample. The DNA was centrifuged for 30 minutes at 12-16 rpm, washed twice with 70% ethanol in 5 minute spin cycles and the pellet allowed to dry. Pellets were resuspended in 20 µl diH20 at -20°C for at least an hour.

Reference List

**Barclay,J., Balaguero,N., Mione,M., Ackerman,S.L., Letts,V.A., Brodbeck,J., Canti,C., Meir,A., Page,K.M., Kusumi,K. et al.** (2001). Ducky mouse phenotype of epilepsy and ataxia is associated with mutations in the Cacna2d2 gene and decreased calcium channel current in cerebellar Purkinje cells. *J. Neurosci.* **21,** 6095-6104.

**Bauer,H., Zweimueller-Mayer,J., Steinbacher,P., Lametschwandtner,A., and Bauer,H.C.** (2010). The dual role of zonula occludens (ZO) proteins. *J. Biomed. Biotechnol.* **2010,** 402593.

**Bit-Avragim,N., Rohr,S., Rudolph,F., Van,d., V, Furst,D., Eichhorst,J., Wiesner,B., and bdelilah-Seyfried,S.** (2008). Nuclear localization of the zebrafish tight junction protein nagie oko. *Dev. Dyn.* **237,** 83-90.

**Bruce,A.E., Howley,C., Dixon,F.M., and Ho,R.K.** (2005). T-box gene eomesodermin and the homeobox-containing Mix/Bix gene mtx2 regulate epiboly movements in the zebrafish. *Dev. Dyn.* **233,** 105-114.

**Burgess,D.L., Jones,J.M., Meisler,M.H., and Noebels,J.L.** (1997). Mutation of the Ca2+ channel beta subunit gene Cchb4 is associated with ataxia and seizures in the lethargic (lh) mouse. *Cell* **88,** 385-392.

**Carvalho,L., Stuhmer,J., Bois,J.S., Kalaidzidis,Y., Lecaudey,V., and Heisenberg,C.P.** (2009). Control of convergent yolk syncytial layer nuclear movement in zebrafish. *Development* **136,** 1305-1315.

**Castellano,A., Wei,X., Birnbaumer,L., and Perez-Reyes,E.** (1993). Cloning and expression of a neuronal calcium channel beta subunit. *J. Biol. Chem.* **268,** 12359-12366.

**Catterall,W.A.** (2000). Structure and regulation of voltage-gated Ca2+ channels. *Annu. Rev. Cell Dev. Biol.* **16,** 521-555.

**Cheng,J.C., Miller,A.L., and Webb,S.E.** (2004). Organization and function of microfilaments during late epiboly in zebrafish embryos. *Dev. Dyn.* **231,** 313-323.

**Colecraft,H.M., Alseikhan,B., Takahashi,S.X., Chaudhuri,D., Mittman,S., Yegnasubramanian,V., Alvania,R.S., Johns,D.C., Marban,E., and Yue,D.T.** (2002). Novel functional properties of Ca(2+) channel beta subunits revealed by their expression in adult rat heart cells. *J. Physiol* **541,** 435-452.

**Dai,S., Hall,D.D., and Hell,J.W.** (2009). Supramolecular assemblies and localized regulation of voltage-gated ion channels. *Physiol Rev.* **89,** 411-452.

**Dolphin,A.C.** (2003). Beta subunits of voltage-gated calcium channels. *J. Bioenerg. Biomembr.* **35,** 599-620.

**Dolphin,A.C.** (2006). A short history of voltage-gated calcium channels. *Br. J. Pharmacol.* **147 Suppl 1,** S56-S62.

**Doyle,J., Ren,X., Lennon,G., and Stubbs,L.** (1997). Mutations in the Cacnl1a4 calcium channel gene are associated with seizures, cerebellar degeneration, and ataxia in tottering and leaner mutant mice. *Mamm. Genome* **8,** 113-120.

**Dunlap,K., Luebke,J.I., and Turner,T.J.** (1995). Exocytotic Ca2+ channels in mammalian central neurons. *Trends Neurosci.* **18,** 89-98.

**Ebert,A.M., McAnelly,C.A., Handschy,A.V., Mueller,R.L., Horne,W.A., and Garrity,D.M.** (2008a). Genomic organization, expression, and phylogenetic analysis of Ca2+ channel beta4 genes in 13 vertebrate species. *Physiol Genomics* **35,** 133-144.

**Ebert,A.M., McAnelly,C.A., Srinivasan,A., Linker,J.L., Horne,W.A., and Garrity,D.M.** (2008b). Ca2+ channel-independent requirement for MAGUK family CACNB4 genes in initiation of zebrafish epiboly. *Proc. Natl. Acad. Sci. U. S. A* **105,** 198-203.

**Ebert,A.M., McAnelly,C.A., Srinivasan,A., Mueller,R.L., Garrity,D.B., and Garrity,D.M.** (2008c). The calcium channel beta2 (CACNB2) subunit repertoire in teleosts. *BMC. Mol. Biol.* **9,** 38.

**Fletcher,C.F., Lutz,C.M., O'Sullivan,T.N., Shaughnessy,J.D., Jr., Hawkes,R., Frankel,W.N., Copeland,N.G., and Jenkins,N.A.** (1996). Absence epilepsy in tottering mutant mice is associated with calcium channel defects. *Cell* **87,** 607-617.

**Franzini-Armstrong,C., Protasi,F., and Ramesh,V.** (1998). Comparative ultrastructure of Ca2+ release units in skeletal and cardiac muscle. *Ann. N. Y. Acad. Sci.* **853,** 20-30.

**Gao,X., Wen,J., Zhang,L., Li,X., Ning,Y., Meng,A., and Chen,Y.G.** (2008). Dapper1 is a nucleocytoplasmic shuttling protein that negatively modulates Wnt signaling in the nucleus. *J. Biol. Chem.* **283,** 35679-35688.

**Gilbert,S.F. and Sarkar,S.** (2000). Embracing complexity: organicism for the 21st century. *Dev. Dyn.* **219,** 1-9.

**Gonzalez-Gutierrez,G., Miranda-Laferte,E., Neely,A., and Hidalgo,P.** (2007). The Src homology 3 domain of the beta-subunit of voltage-gated calcium channels promotes endocytosis via dynamin interaction. *J. Biol. Chem.* **282,** 2156-2162.

**Gu,X., Wang,Y., and Gu,J.** (2002). Age distribution of human gene families shows significant roles of both large- and small-scale duplications in vertebrate evolution. *Nat. Genet.* **31,** 205-209.

**Hibino,H., Pironkova,R., Onwumere,O., Rousset,M., Charnet,P., Hudspeth,A.J., and Lesage,F.** (2003). Direct interaction with a nuclear protein and regulation of gene

silencing by a variant of the Ca2+-channel beta 4 subunit. *Proc. Natl. Acad. Sci. U. S. A* **100,** 307-312.

**Holloway,B.A., Gomez de la Torre Canny, Ye,Y., Slusarski,D.C., Freisinger,C.M., Dosch,R., Chou,M.M., Wagner,D.S., and Mullins,M.C.** (2009). A novel role for MAPKAPK2 in morphogenesis during zebrafish development. *PLoS. Genet.* **5,** e1000413.

**Hsu,H.J., Liang,M.R., Chen,C.T., and Chung,B.C.** (2006). Pregnenolone stabilizes microtubules and promotes zebrafish embryonic cell movement. *Nature* **439,** 480-483.

**Jeziorski,M.C. and Greenberg,R.M.** (2006). Voltage-gated calcium channel subunits from platyhelminths: potential role in praziquantel action. *Int. J. Parasitol.* **36,** 625-632.

**Jones,D.O., Cowell,I.G., and Singh,P.B.** (2000). Mammalian chromodomain proteins: their role in genome organisation and expression. *Bioessays* **22,** 124-137.

**Kane,D.A., Hammerschmidt,M., Mullins,M.C., Maischein,H.M., Brand,M., van Eeden,F.J., Furutani-Seiki,M., Granato,M., Haffter,P., Heisenberg,C.P. et al.** (1996). The zebrafish epiboly mutants. *Development* **123,** 47-55.

**Kane,D.A. and Kimmel,C.B.** (1993). The zebrafish midblastula transition. *Development* **119,** 447-456.

**Kane,D.A., McFarland,K.N., and Warga,R.M.** (2005). Mutations in half baked/E-cadherin block cell behaviors that are necessary for teleost epiboly. *Development* **132,** 1105-1116.

**Kawakami,K. and Noda,T.** (2004). Transposition of the Tol2 element, an Ac-like element from the Japanese medaka fish Oryzias latipes, in mouse embryonic stem cells. *Genetics* **166,** 895-899.

**Koppen,M., Fernandez,B.G., Carvalho,L., Jacinto,A., and Heisenberg,C.P.** (2006). Coordinated cell-shape changes control epithelial movement in zebrafish and Drosophila. *Development* **133,** 2671-2681.

**Kwan,K.M., Fujimoto,E., Grabher,C., Mangum,B.D., Hardy,M.E., Campbell,D.S., Parant,J.M., Yost,H.J., Kanki,J.P., and Chien,C.B.** (2007). The Tol2kit: a multisite gateway-based construction kit for Tol2 transposon transgenesis constructs. *Dev. Dyn.* **236,** 3088-3099.

**Lachnit,M., Kur,E., and Driever,W.** (2008). Alterations of the cytoskeleton in all three embryonic lineages contribute to the epiboly defect of Pou5f1/Oct4 deficient MZspg zebrafish embryos. *Dev. Biol.* **315,** 1-17.

**Mizoguchi,T., Verkade,H., Heath,J.K., Kuroiwa,A., and Kikuchi,Y.** (2008). Sdf1/Cxcr4 signaling controls the dorsal migration of endodermal cells during zebrafish gastrulation. *Development* **135,** 2521-2529.

**Obermair,G.J., Tuluc,P., and Flucher,B.E.** (2008). Auxiliary Ca(2+) channel subunits: lessons learned from muscle. *Curr. Opin. Pharmacol.* **8,** 311-318.

**Robu,M.E., Larson,J.D., Nasevicius,A., Beiraghi,S., Brenner,C., Farber,S.A., and Ekker,S.C.** (2007). p53 activation by knockdown technologies. *PLoS. Genet.* **3,** e78.

**Rottbauer,W., Baker,K., Wo,Z.G., Mohideen,M.A., Cantiello,H.F., and Fishman,M.C.** (2001). Growth and function of the embryonic heart depend upon the cardiac-specific L-type calcium channel alpha1 subunit. *Dev. Cell* **1,** 265-275.

**Ruddock-D'Cruz,N.T., Prashadkumar,S., Wilson,K.J., Heffernan,C., Cooney,M.A., French,A.J., Jans,D.A., Verma,P.J., and Holland,M.K.** (2008). Dynamic changes in localization of Chromobox (Cbx) family members during the maternal to embryonic transition. *Mol. Reprod. Dev.* **75,** 477-488.

**Sakaguchi,T., Kikuchi,Y., Kuroiwa,A., Takeda,H., and Stainier,D.Y.** (2006). The yolk syncytial layer regulates myocardial migration by influencing extracellular matrix assembly in zebrafish. *Development* **133,** 4063-4072.

**SANDOW,A.** (1952). Excitation-contraction coupling in muscular response. *Yale J. Biol. Med.* **25,** 176-201.

**Schier,A.F. and Talbot,W.S.** (2005). Molecular genetics of axis formation in zebrafish. *Annu. Rev. Genet.* **39,** 561-613.

**Shimizu,T., Yabe,T., Muraoka,O., Yonemura,S., Aramaki,S., Hatta,K., Bae,Y.K., Nojima,H., and Hibi,M.** (2005). E-cadherin is required for gastrulation cell movements in zebrafish. *Mech. Dev.* **122,** 747-763.

**Solnica-Krezel,L.** (2006). Gastrulation in zebrafish -- all just about adhesion? *Curr. Opin. Genet. Dev.* **16,** 433-441.

**Solnica-Krezel,L. and Driever,W.** (1994). Microtubule arrays of the zebrafish yolk cell: organization and function during epiboly. *Development* **120,** 2443-2455.

**Subramanyam,P., Obermair,G.J., Baumgartner,S., Gebhart,M., Striessnig,J., Kaufmann,W.A., Geley,S., and Flucher,B.E.** (2009). Activity and calcium regulate nuclear targeting of the calcium channel beta4b subunit in nerve and muscle cells. *Channels (Austin. )* **3,** 343-355.

**Sumanas,S. and Larson,J.D.** (2002). Morpholino phosphorodiamidate oligonucleotides in zebrafish: a recipe for functional genomics? *Brief. Funct. Genomic. Proteomic.* **1,** 239-256.

**Thisse,C., Thisse,B., Schilling,T.F., and Postlethwait,J.H.** (1993). Structure of the zebrafish snail1 gene and its expression in wild-type, spadetail and no tail mutant embryos. *Development* **119,** 1203-1215.

**TRINKAUS,J.P.** (1963). The cellular basis of Fundulus epiboly. Adhesivity of blastula and gastrula cells in culture. *Dev. Biol.* **7,** 513-532.

**Vendel,A.C., Rithner,C.D., Lyons,B.A., and Horne,W.A.** (2006). Solution structure of the N-terminal A domain of the human voltage-gated Ca2+channel beta4a subunit. *Protein Sci.* **15,** 378-383.

**Wagner,D.S., Dosch,R., Mintzer,K.A., Wiemelt,A.P., and Mullins,M.C.** (2004). Maternal control of development at the midblastula transition and beyond: mutants from the zebrafish II. *Dev. Cell* **6,** 781-790.

**Webb,S.E. and Miller,A.L.** (2003). Calcium signalling during embryonic development. *Nat. Rev. Mol. Cell Biol.* **4,** 539-551.

**Wilkins,S.J., Yoong,S., Verkade,H., Mizoguchi,T., Plowman,S.J., Hancock,J.F., Kikuchi,Y., Heath,J.K., and Perkins,A.C.** (2008). Mtx2 directs zebrafish morphogenetic movements during epiboly by regulating microfilament formation. *Dev. Biol.* **314,** 12-22.

**Yang,F., Moss,L.G., and Phillips,G.N., Jr.** (1996). The molecular structure of green fluorescent protein. *Nat. Biotechnol.* **14,** 1246-1251.

**Yelon,D.** (2001). Cardiac patterning and morphogenesis in zebrafish. *Dev. Dyn.* **222,** 552-563.

**Zalik,S.E., Lewandowski,E., Kam,Z., and Geiger,B.** (1999). Cell adhesion and the actin cytoskeleton of the enveloping layer in the zebrafish embryo during epiboly. *Biochem. Cell Biol.* **77,** 527-542.

**Zhou,W., Horstick,E.J., Hirata,H., and Kuwada,J.Y.** (2008). Identification and expression of voltage-gated calcium channel beta subunits in Zebrafish. *Dev. Dyn.* **237,** 3842-3852.

**Zhou,W., Saint-Amant,L., Hirata,H., Cui,W.W., Sprague,S.M., and Kuwada,J.Y.** (2006). Non-sense mutations in the dihydropyridine receptor beta1 gene, CACNB1, paralyze zebrafish relaxed mutants. *Cell Calcium* **39,** 227-236.